arXiv:1404.7035v2 [hep-ex] 7 Aug 2014

Measurement of χ_{c1} and χ_{c2} production with $\sqrt{s} = 7$ TeV pp collisions at ATLAS

The ATLAS Collaboration

Abstract

The prompt and non-prompt production cross-sections for the χ_{c1} and χ_{c2} charmonium states are measured in pp collisions at $\sqrt{s} = 7$ TeV with the ATLAS detector at the LHC using $4.5\,\mathrm{fb}^{-1}$ of integrated luminosity. The χ_c states are reconstructed through the radiative decay $\chi_c \to J/\psi\,\gamma$ (with $J/\psi \to \mu^+\mu^-$) where photons are reconstructed from $\gamma \to e^+e^-$ conversions. The production rate of the χ_{c2} state relative to the χ_{c1} state is measured for prompt and non-prompt χ_c as a function of J/ψ transverse momentum. The prompt χ_c cross-sections are combined with existing measurements of prompt J/ψ production to derive the fraction of prompt J/ψ produced in feed-down from χ_c decays. The fractions of χ_{c1} and χ_{c2} produced in b-hadron decays are also measured.

Measurement of χ_{c1} and χ_{c2} production with $\sqrt{s} = 7$ TeV pp collisions at ATLAS

The ATLAS Collaboration

ABSTRACT: The prompt and non-prompt production cross-sections for the χ_{c1} and χ_{c2} charmonium states are measured in pp collisions at $\sqrt{s} = 7$ TeV with the ATLAS detector at the LHC using $4.5\,\text{fb}^{-1}$ of integrated luminosity. The χ_c states are reconstructed through the radiative decay $\chi_c \to J/\psi\,\gamma$ (with $J/\psi \to \mu^+\mu^-$) where photons are reconstructed from $\gamma \to e^+e^-$ conversions. The production rate of the χ_{c2} state relative to the χ_{c1} state is measured for prompt and non-prompt χ_c as a function of J/ψ transverse momentum. The prompt χ_c cross-sections are combined with existing measurements of prompt J/ψ production to derive the fraction of prompt J/ψ produced in feed-down from χ_c decays. The fractions of χ_{c1} and χ_{c2} produced in b-hadron decays are also measured.

Contents

1   Introduction

The study of heavy quarkonium production in hadronic collisions offers a unique insight into the dynamics of the strong interaction. Understanding the hadronic production of quarkonium states within quantum chromodynamics (QCD) has been a long-standing challenge, complicated by the presence of several important energy scales [1]. While the production of a heavy quark pair is generally a high-energy process that can be well described perturbatively, the energy scale associated with the evolution of a heavy quark pair into a physical bound state introduces large uncertainties to theoretical predictions.

Understanding the hadronic production of the charmonium states is particularly challenging as the mass of the charm quark is such that the modelling of the bound state as a simple non-relativistic system is less well motivated than for the heavier bottomonium system. Several theoretical approaches have been developed to describe hadronic charmonium production, though the wealth of production and polarisation measurements that now exist are not comprehensively described by any single theoretical approach [2]. However, progress is being made in the calculation of colour-singlet (CS) and colour-octet (CO) production processes at higher perturbative orders and recent calculations provide a good description of the world data on prompt J/ψ production cross-sections [3].

The $\chi_{cJ}(1P)$ states (with $J = 0, 1, 2$) are the only triplet of P-wave states below the open-charm threshold. The spectroscopy of these states is characterised by small hyperfine mass splittings and the branching fractions for the decays $\chi_{cJ} \to J/\psi\,\gamma$ are large for the

$J = 1, 2$ states (34.4% and 19.5%, respectively), while the corresponding branching fraction for the $J = 0$ state is significantly lower (1.3%) [4]. The χ_{cJ} states may be produced directly in hadronic collisions or through the decay of higher-mass quarkonium states; these production modes are referred to as prompt. In addition to prompt production, the decay chains of b-hadrons can also produce χ_{cJ} states; these production modes are referred to as non-prompt.

The large cross-section for inclusive charmonium production and extensive data samples available at the Large Hadron Collider (LHC) allow the hadronic production of charmonium to be studied in detail. The inclusive production rate of prompt J/ψ is the most experimentally accessible charmonium production observable at the LHC, with reconstruction of the decay $J/\psi \to \mu^+\mu^-$ being well suited to the hadronic environment. However, the comparison of experimental measurements with theoretical predictions is complicated by the large feed-down contributions from χ_c and $\psi(2S)$ decays. The direct component of the inclusive J/ψ cross-section, produced in the pp interaction, can be obtained only if these feed-down contributions are precisely quantified. Existing measurements suggest that the contribution to prompt J/ψ production from χ_c decays is around 25% [5]. An understanding of χ_c production is therefore a crucial component of any general description of charmonium production at the LHC. Furthermore, χ_c production observables, such as the relative production rates of the χ_{c1} and χ_{c2} states, represent sensitive probes of the prompt charmonium production mechanism that can provide information complementary to the study of the S-wave states.

The production of charmonium states in b-hadron decays can be used as a proxy observable for studying b-quark production at the LHC. Theoretical predictions of b-quark production can be combined with fragmentation functions and momentum spectra from $H_b \to (c\bar{c}) X$ decays (where H_b denotes a b-hadron and $(c\bar{c})$ denotes a charmonium state) extracted from e^+e^- collision data to provide direct predictions for non-prompt charmonium production [6, 7]. Such predictions have had much success in describing the measurements of non-prompt J/ψ and $\psi(2S)$ production performed by the LHC experiments [8–12].

Various aspects of the production of χ_c states have been studied at the LHC [13–16] and at the Tevatron [17, 18]; however, measurements of the absolute production cross-sections for prompt χ_c and studies of non-prompt χ_c production have not been performed previously at the LHC.

This paper presents measurements of the inclusive production of the χ_{c1} and χ_{c2} states in pp collisions at a centre-of-mass energy $\sqrt{s} = 7$ TeV at the LHC. The χ_c states are reconstructed through the radiative decays $\chi_{cJ} \to J/\psi\,\gamma$ (with $J/\psi \to \mu^+\mu^-$), where the photon is reconstructed through its conversion into a positron–electron (e^+e^-) pair. Photon conversions reconstructed in the ATLAS inner tracking detector offer the very good mass resolution needed to resolve the χ_{c1} and χ_{c2} states individually. The χ_{c0} production rate is not measured explicitly because the inclusive yield of χ_{c0} in the data sample used in this analysis is considered to be too small to perform a reliable measurement.

The inclusive production of the χ_{c1} and χ_{c2} states is separated experimentally into prompt and non-prompt components and measured differentially in both χ_c transverse momentum $p_T^{\chi_c}$ and J/ψ transverse momentum $p_T^{J/\psi}$, within the rapidity region $|y^{J/\psi}| < 0.75$.

The results obtained as a function of $p_\mathrm{T}^{J/\psi}$ and $p_\mathrm{T}^{\chi_c}$ are presented within the regions $10 \leq p_\mathrm{T}^{J/\psi} < 30$ GeV and $12 \leq p_\mathrm{T}^{\chi_c} < 30$ GeV respectively. These new measurements are combined with existing measurements of inclusive J/ψ production [8] to determine the fraction of prompt J/ψ produced in feed-down from χ_c decays. The ratio $\sigma\left(\chi_{c2}\right)/\sigma\left(\chi_{c1}\right)$ is a useful theoretical quantity as it is sensitive to the presence of possible colour-octet contributions to χ_c production [19]. This cross-section ratio is measured as a function of $p_\mathrm{T}^{J/\psi}$ for prompt χ_{c1} and χ_{c2} production. These measurements are compared to theoretical predictions and to the measurements by other experiments. The branching fraction $\mathcal{B}(B^\pm \to \chi_{c1}K^\pm)$ is also measured with the same data sample and event selection.

2   The ATLAS detector, data and Monte Carlo samples

The ATLAS detector [20] is a general-purpose particle physics detector with a cylindrical geometry[1] with forward-backward symmetric coverage in pseudorapidity η. The detector consists of inner tracking detectors, calorimeters and a muon spectrometer, and has a three-level trigger system.

The inner tracking detector (ID) is composed of a silicon pixel detector, a semiconductor microstrip detector (SCT) and a transition radiation tracker, which together cover the pseudorapidity range $|\eta| < 2.5$. The ID directly surrounds the beam pipe and is immersed in a 2 T axial magnetic field generated by a superconducting solenoid. The calorimeter system surrounds the solenoid and consists of a highly granular liquid-argon electromagnetic calorimeter and an iron/scintillator tile hadronic calorimeter. The muon spectrometer (MS) surrounds the calorimeters and consists of three large air-core superconducting magnets (each with eight coils), which generate a toroidal magnetic field. The MS is instrumented in three layers with precision detectors (monitored drift tubes and cathode strip chambers) that provide precision muon tracking covering $|\eta| < 2.7$ and fast trigger detectors (resistive plate chambers and thin gap chambers) covering the range $|\eta| < 2.4$.

The ATLAS trigger is a three-level system consisting of a level-1 trigger implemented in hardware and a software-based two-stage high level trigger (HLT). The data sample used in this analysis is collected with a dimuon trigger. The level-1 muon trigger system identifies regions of interest (RoI) by searching for coincidences between hits in different trigger detector layers within predefined geometrical windows enclosing the paths of muons with a given set of transverse momentum thresholds. The level-1 system also provides a rough measurement of muon position with a spatial granularity of $\Delta\phi \times \Delta\eta \approx 0.1 \times 0.1$. The level-1 RoI then serves as a seed for HLT algorithms that use higher precision MS and ID measurements to reconstruct muon trigger objects. The selection performed by the HLT algorithms is discussed in section 3.

---

[1]ATLAS uses a right-handed coordinate system with its origin at the nominal interaction point (IP) in the centre of the detector and the z-axis along the beam pipe. The x-axis points from the IP to the centre of the LHC ring, and the y-axis points upward. Cylindrical coordinates (r, ϕ) are used in the transverse plane, ϕ being the azimuthal angle around the beam pipe. The pseudorapidity is defined in terms of the polar angle θ as $\eta = -\ln\tan(\theta/2)$.

The measurements presented in this paper are performed with a data sample corresponding to an integrated luminosity of $4.5\,\text{fb}^{-1}$ collected during the 2011 LHC proton–proton run at a centre-of-mass energy $\sqrt{s} = 7$ TeV. The selected events were collected under stable LHC beam conditions with the detector in a fully operational state.

Four Monte Carlo (MC) simulation samples are used to estimate the photon conversion reconstruction efficiency and to characterise the modelling of the χ_c signal components used in the fitting procedure. The samples consist of simulated $\chi_{c1} \to J/\psi\,\gamma \to \mu^+\mu^-\gamma$ and $\chi_{c2} \to J/\psi\,\gamma \to \mu^+\mu^-\gamma$ decays produced either directly in pp interactions or through the process $pp \to b\bar{b}X \to \chi_c X'$. All samples are generated with PYTHIA 6 [21] and use the ATLAS 2011 MC underlying event and hadronisation model tuning [22]. The response of the ATLAS detector is simulated using GEANT4 [23, 24]. The events are reconstructed using the same algorithms used to process the data. Each χ_c event is overlaid with a number of minimum-bias pp events such that the overall distribution of additional pp interactions due to pile-up in data events is accurately described by the simulated samples.

3 Event and χ_c candidate selection

The selected events passed a dimuon trigger in which the HLT identified two oppositely charged muons, each with transverse momentum $p_\mathrm{T} > 4$ GeV. The HLT fits the two candidate muon tracks to a common vertex and a very loose requirement on the vertex χ^2 is imposed. Finally, a broad dimuon invariant mass cut $(2.5 < m\,(\mu^+\mu^-) < 4.0$ GeV$)$ is applied to select dimuon candidates consistent with $J/\psi \to \mu^+\mu^-$ decays. Each event passing the trigger selection is required to contain at least one reconstructed pp collision vertex formed from at least three reconstructed tracks with $p_\mathrm{T} > 400$ MeV.

In the offline analysis, muon candidates are formed from reconstructed ID tracks matched to tracks reconstructed in the MS. Each muon track is required to be reconstructed from at least six SCT hits and at least one pixel detector hit. For the low-p_T muons (typically below 20 GeV) produced in $J/\psi \to \mu^+\mu^-$ decays, the track parameters measured in the ID provide more accurate measurements than the MS as they are not affected by muon energy loss in the calorimeters. Therefore, the ID measurements alone are used to reconstruct the momentum of muon candidates. Events are required to contain at least one pair of oppositely charged muons, each with transverse momentum $p_\mathrm{T}^\mu > 4$ GeV and $|\eta^\mu| < 2.3$ (the region where the trigger and reconstruction efficiencies are optimal). Each muon pair is fitted to a common vertex and a very loose vertex quality requirement (fully efficient for genuine $J/\psi \to \mu^+\mu^-$ decays) is imposed. The dimuon pair is considered a $J/\psi \to \mu^+\mu^-$ candidate if the invariant mass of the pair, calculated from the track parameters recalculated by the vertex fit, satisfies $2.95 < m\,(\mu^+\mu^-) < 3.25$ GeV. The event and $J/\psi \to \mu^+\mu^-$ candidate are retained for further analysis if the two muon candidates reconstructed offline are consistent with the objects reconstructed by the HLT (matched within $\Delta R = \sqrt{(\Delta\phi)^2 + (\Delta\eta)^2} < 0.01$). The rapidity of the J/ψ candidate reconstructed offline is required to satisfy $|y^{J/\psi}| < 0.75$. This selection retains only the candidates reconstructed within the region of the detector with the optimal dimuon mass resolution, which is necessary to reliably resolve the individual χ_{cJ} states.

Photon conversions are reconstructed from pairs of oppositely charged ID tracks whose helices touch when projected onto the transverse plane. Tracks must be reconstructed with transverse momentum $p_T > 400$ MeV and $|\eta| < 2.3$ and contain at least six SCT hits. Track pairs consistent with the photon conversion hypothesis are fitted to a common vertex with their opening angle constrained to be zero. The vertex fit is required to converge with χ^2 per degree of freedom less than five. To reject fake conversions from $\pi^0 \to e^+e^-\gamma$ decays and other promptly produced track pairs, the radial displacement r of the reconstructed conversion vertex with respect to the z-axis is required to satisfy $40 < r < 150$ mm. This fiducial region includes the three layers of silicon pixels in the ID, and so selects conversions occurring within these silicon pixel layers and their associated service structures. The efficiency for reconstructing converted photons from only ID tracks decreases significantly beyond the upper limit of 150 mm. In this analysis, no information from the calorimeters is used in the reconstruction of photon conversions. The reconstructed momentum of the converted photon is calculated from e^+e^- track parameters recalculated by the vertex fit with the invariant mass constrained to be zero. Reconstructed converted photons are required to have transverse momentum $p_T^\gamma > 1.5$ GeV and $|\eta^\gamma| < 2.0$.

Candidate $\chi_c \to J/\psi\,\gamma \to \mu^+\mu^-\gamma$ decays are selected by associating a reconstructed photon conversion with a candidate $J/\psi \to \mu^+\mu^-$ decay. To reject combinations of $J/\psi \to \mu^+\mu^-$ decays and photons not consistent with a χ_c decay, the impact parameter of the converted photon with respect to the dimuon vertex is required to be less than 5 mm. This requirement has a negligible inefficiency for genuine χ_c decays.

4 Cross-section determination

The distribution of mass difference $\Delta m = m\left(\mu^+\mu^-\gamma\right) - m\left(\mu^+\mu^-\right)$ is used to distinguish the χ_{c1} and χ_{c2} states. This distribution is used in place of the three-body invariant mass as some partial cancellation of contributions from the dimuon mass resolution is achieved, resulting in improved overall mass resolution. Non-prompt χ_c candidates produced in the decays of b-hadrons can be distinguished experimentally from prompt χ_c candidates (produced in the primary pp interaction) with the pseudo-proper decay time distribution τ. The pseudo-proper decay time τ is defined as

$$\tau = \frac{L_{xy} \cdot m_{J/\psi}}{p_T},$$

where $m_{J/\psi}$ is the world-average J/ψ mass, p_T is the transverse momentum of the J/ψ candidate and L_{xy} is the distance between the primary pp interaction vertex and the $J/\psi \to \mu^+\mu^-$ decay vertex in the transverse plane. The primary pp interaction vertex, defined as the vertex with the highest track $\sum p_T^2$, is used to calculate L_{xy} on a per-candidate basis.

The differential χ_{c1} and χ_{c2} cross-sections for prompt and non-prompt production in a given bin of $p_T^{\chi_c}$ are measured from,

$$\frac{\mathrm{d}\sigma\left(\chi_{cJ}\right)}{\mathrm{d}p_T^{\chi_c}} \cdot \mathcal{B}\left(\chi_{cJ} \to J/\psi\,\gamma\right) \cdot \mathcal{B}\left(J/\psi \to \mu^+\mu^-\right) = \frac{N_J}{\mathcal{L} \cdot \Delta p_T^{\chi_c}},$$

where $\mathcal{L}$ is the integrated luminosity, $\Delta p_{\mathrm{T}}^{\chi_c}$ is the bin width in $p_{\mathrm{T}}^{\chi_c}$ and N_J is the acceptance-and efficiency-corrected fitted χ_{cJ} signal yield for a given bin in $p_{\mathrm{T}}^{\chi_c}$. The same formula is also used to deduce the differential cross-sections measured as a function of J/ψ transverse momentum with $p_{\mathrm{T}}^{\chi_c}$ replaced by $p_{\mathrm{T}}^{J/\psi}$.

To obtain corrected prompt and non-prompt χ_{c1} and χ_{c2} yields, a weight is first determined for each χ_c candidate to correct for experimental efficiency and detector acceptance. Corrected yields are then extracted from a simultaneous two-dimensional unbinned maximum likelihood fit to the weighted mass difference Δm and pseudo-proper decay time τ distributions in bins of $p_{\mathrm{T}}^{\chi_c}$ and $p_{\mathrm{T}}^{J/\psi}$. The differing production kinematics for prompt and non-prompt χ_{c1} and χ_{c2} result in a different detector acceptance for each yield. To account for these differences, the fit procedure is performed once for each measured yield, with the data weighted differently each time to accurately correct that particular yield. The correction weight w for each χ_c candidate is calculated as

$$ w^{-1} = \mathcal{A} \cdot \epsilon_{\mathrm{trig}} \cdot \epsilon_{\mathrm{dimuon}} \cdot \epsilon_\gamma \, , $$

where $\mathcal{A}$ is the detector acceptance, ϵ_{trig} is the trigger efficiency, $\epsilon_{\mathrm{dimuon}}$ is the dimuon reconstruction efficiency and ϵ_γ is the photon conversion reconstruction efficiency.

4.1 Acceptance

The detector acceptance $\mathcal{A}$ is defined as the probability that final-state decay products in a $\chi_c \to J/\psi\,\gamma \to \mu^+\mu^-\gamma$ decay fall within the fiducial region defined by $p_{\mathrm{T}}^\mu > 4$ GeV and $|\eta^\mu| < 2.3$ for muons and $p_{\mathrm{T}}^\gamma > 1.5$ GeV and $|\eta^\gamma| < 2.0$ for photons. The acceptance depends strongly on the angular distributions of the decay products in their respective decay frames. The form of these angular distributions is a function of the spin-alignment of the χ_{cJ} with respect to a given axis.

The angular distribution of the μ^+ in the J/ψ rest frame for inclusive production is described by

$$ \frac{\mathrm{d}^2 N}{\mathrm{d}\cos\theta d\phi} \propto \frac{1}{3 + \lambda_\theta} \left[1 + \lambda_\theta \cos^2\theta + \lambda_\phi \sin^2\theta \cos 2\phi + \lambda_{\theta\phi} \sin 2\theta \cos\phi \right] , \qquad (4.1) $$

where θ and ϕ are the polar and azimuthal angles, respectively, between the μ^+ and the chosen spin-alignment axis [25]. Similarly, the angular distribution of the J/ψ in the χ_{cJ} rest frame is described by

$$ \frac{\mathrm{d}^2 N}{\mathrm{d}\cos\Theta d\Phi} \propto \frac{1}{3 + \lambda_\Theta} \left[1 + \lambda_\Theta \cos^2\Theta + \lambda_\Phi \sin^2\Theta \cos 2\Phi + \lambda_{\Theta\Phi} \sin 2\Theta \cos\Phi \right] , \qquad (4.2) $$

where Θ and Φ are the polar and azimuthal angles, respectively, between the J/ψ and the chosen spin-alignment axis. This distribution is valid for χ_{c1}, and is also valid for χ_{c2} if contributions from higher-order multipoles to the radiative transition $\chi_{c2} \to J/\psi\,\gamma$ are neglected (the E1 approximation). This approximation is motivated by the fact that the current experimental data suggest that higher-order multipoles in both $J = 1$ and $J = 2$ radiative decays represent less than 10% of the total amplitude [4]. The values of the λ

parameters in equations (4.1) and (4.2) are determined by the J/ψ and χ_c spin-alignments, respectively.

For the radiative decay $\chi_c \to J/\psi\,\gamma$, it has been shown that the angular distribution of the μ^+ in the J/ψ rest frame and the J/ψ in the χ_c rest frame are identical (i.e. $\lambda_\Theta = \lambda_\theta$, $\lambda_\Phi = \lambda_\phi$, $\lambda_{\Theta\Phi} = \lambda_{\theta\phi}$) if one measures the angles Θ, Φ and θ, ϕ with respect to parallel spin-alignment axes [25]. Furthermore, this choice of axes reduces the dependence of the λ parameters in equation (4.1) on the higher-order multipole contributions to the radiative transitions [25]. In this analysis, the helicity frame is used and the spin-alignment axis is defined as the χ_{cJ} line of flight in the laboratory frame.

Scenarios are identified (four for χ_{c1} and five for χ_{c2}) that span the allowed λ parameter space and give rise to the most extreme variations in the acceptance. These are detailed in table 1. The scenarios correspond to the pure helicity eigenstates of the χ_{c1} and χ_{c2} states along with two scenarios with an azimuthal anisotropy (AZ+ and AZ−). These scenarios are used to calculate the uncertainty envelope associated with spin-alignment effects. The central value for the acceptance is calculated by assuming that the χ_{cJ} are unpolarised, with isotropic angular distributions for the χ_c and J/ψ decays ($\lambda_\theta = \lambda_\phi = \lambda_{\theta\phi} = 0$). Spin-alignment scenarios with non-zero values for $\lambda_{\theta\phi}$ are found to result in relative changes in the acceptance below any of the other scenarios considered.

	Label	λ_θ	λ_ϕ	$\lambda_{\theta\phi}$
χ_{c1}	Isotropic	0	0	0
	Helicity 0	$+1$	0	0
	Helicity ± 1	$-1/3$	0	0
	AZ+	$-1/3$	$+1/3$	0
	AZ−	$-1/3$	$-1/3$	0
χ_{c2}	Isotropic	0	0	0
	Helicity 0	$-3/5$	0	0
	Helicity ± 1	$-1/3$	0	0
	Helicity ± 2	$+1$	0	0
	AZ+	$+1/5$	$+1/\sqrt{5}$	0
	AZ−	$+1/5$	$-1/\sqrt{5}$	0

Table 1. The set of χ_{c1} and χ_{c2} spin-alignment scenarios studied.

Two-dimensional acceptance maps binned in $p_{\rm T}^{\chi_c}$ and $|y^{\chi_c}|$ are derived for each spin-alignment scenario using a large sample of generator-level MC events. The angular distributions of the decays $\chi_c \to J/\psi\,\gamma$ and $J/\psi \to \mu^+\mu^-$ are generated according to Equations 4.1 and 4.2 with the λ parameters shown in table 1. Figure 1 shows the acceptance map for $\chi_{c1} \to J/\psi\,\gamma \to \mu^+\mu^-\gamma$ decays calculated with isotropic decay angular distributions (consistent with unpolarised χ_c production). The acceptance is significantly reduced at high rapidity due to the fiducial cut $|\eta^\gamma| < 2.0$. Since $J/\psi \to \mu^+\mu^-$ candidates are only reconstructed within $|y^{J/\psi}| < 0.75$, none of the converted photons associated with the reconstructed χ_c candidates approaches $|\eta^\gamma| \approx 2.0$ and the analysis is not sensitive to reduced
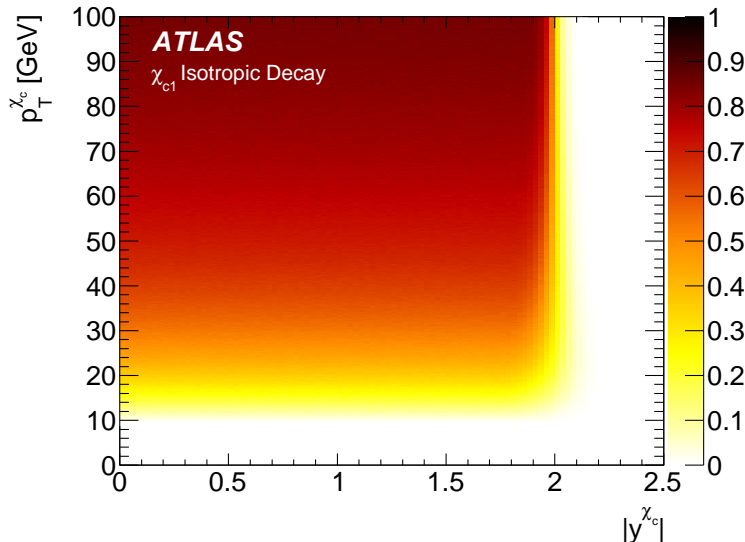
Figure 1. The acceptance for $\chi_{c1} \to J/\psi\,\gamma \to \mu^+\mu^-\gamma$ decays as a function of $p_T^{\chi_c}$ and $|y^{\chi_c}|$.

acceptance in this region. The acceptance also decreases significantly towards low $p_T^{\chi_c}$ and is negligible for $p_T^{\chi_c} < 10$ GeV.

The cross-section measurements binned in $p_T^{\chi_c}$ are corrected directly with acceptance maps as described above. The acceptance correction for the measurements binned in $p_T^{J/\psi}$ is sensitive to the $p_T^{\chi_c}$ spectrum used as input to the simulation and must be calculated with an alternative approach. Acceptance corrections are derived for each measured $p_T^{J/\psi}$ bin with the same simulation used to generate the acceptance maps, but with the χ_c decays generated with a transverse momentum spectrum taken from a fitted parameterisation of the differential cross-sections measured as a function of $p_T^{\chi_c}$ and presented in this paper.

4.2 Trigger efficiency

The dimuon trigger efficiency is determined from $J/\psi \to \mu^+\mu^-$ and $\Upsilon \to \mu^+\mu^-$ decays in data using the method described in ref. [26]. The dimuon trigger efficiency ϵ_{trig} is defined as the efficiency with which the trigger system can select events that pass the full offline dimuon selection. The method factorises the total efficiency into three parts,

$$\epsilon_{\text{trig}} = \epsilon_{\text{RoI}}\left(p_{T1}^\mu, q_1 \cdot \eta_1^\mu\right) \cdot \epsilon_{\text{RoI}}\left(p_{T2}^\mu, q_2 \cdot \eta_2^\mu\right) \cdot c_{\mu^+\mu^-}\left(\Delta R, |y(\mu^+\mu^-)|\right) ,$$

where ϵ_{RoI} is the efficiency with which the trigger system can identify a single muon with transverse momentum p_T^μ and charge-signed pseudorapidity $q \cdot \eta^\mu$ as an RoI. Charge-signed pseudorapidity is used to account for the charge asymmetry in single-muon triggering due to the toroidal magnetic field. The factor $c_{\mu^+\mu^-}$ is present to correct for inefficiencies associated with the dimuon selection of the trigger. These include vertexing and dimuon charge requirements and effects associated with the finite size of the muon RoI. The factor $c_{\mu^+\mu^-}$ and the single-muon efficiency ϵ_{RoI} are determined using a sample of $J/\psi \to \mu^+\mu^-$

decays selected with a single-muon trigger with an 18 GeV transverse momentum threshold. The efficiency ϵ_{RoI} is derived in two-dimensional bins of p_{T}^{μ} and $q \cdot \eta^{\mu}$ from the fraction of fitted $J/\psi \to \mu^+\mu^-$ decays that pass the high-p_{T} single-muon trigger and that also pass the dimuon trigger selection (corrected for dimuon effects with $c_{\mu^+\mu^-}$). The average dimuon trigger efficiency for $J/\psi \to \mu^+\mu^-$ decays with $10 \leq p_{\text{T}}^{J/\psi} < 30$ GeV is between 50% to 60% for the fiducial region studied.

4.3 Muon reconstruction efficiency

The efficiency to reconstruct and identify both muons from the decay $J/\psi \to \mu^+\mu^-$ is described by the equation

$$\epsilon_{\text{dimuon}} = \epsilon_{\text{trk}}\left(p_{\text{T1}}^{\mu}, \eta_1^{\mu}\right) \cdot \epsilon_{\text{trk}}\left(p_{\text{T2}}^{\mu}, \eta_2^{\mu}\right) \cdot \epsilon_{\mu}\left(p_{\text{T1}}^{\mu}, q_1 \cdot \eta_1^{\mu}\right) \cdot \epsilon_{\mu}\left(p_{\text{T2}}^{\mu}, q_2 \cdot \eta_2^{\mu}\right) .$$

The quantity ϵ_{trk} is the reconstruction efficiency for muon tracks subject to the ID track selection described in section 3 and is determined to be $(99 \pm 1)\%$ over the full kinematic region studied [26]. The single-muon identification efficiency ϵ_{μ} is derived from an analysis of a sample of $J/\psi \to \mu^+\mu^-$ decays in data, unbiased by any muon selection criteria as described in ref. [26]. The muon identification efficiency reaches a plateau of around 98% for muons with $p_{\text{T}}^{\mu} > 8$ GeV.

The efficiency of the dimuon invariant mass requirement $2.95 < m\left(\mu^+\mu^-\right) < 3.25$ GeV discussed in section 3 is estimated to be $(99.0 \pm 0.5)\%$ by performing fits to the $m\left(\mu^+\mu^-\right)$ distribution of an inclusive sample of $J/\psi \to \mu^+\mu^-$ decays reconstructed within the same fiducial region used in the analysis.

4.4 Photon conversion reconstruction efficiency

The total photon conversion reconstruction efficiency ϵ_{γ} is determined from the MC-simulated $\chi_c \to J/\psi\,\gamma$ event samples described in section 2. The decay products in the simulated samples of radiative χ_c decays are propagated through the ATLAS detector simulation. The description of the ID material distribution in the MC simulation samples is checked by comparing the distributions of various conversion observables (including conversion vertex fit χ^2, vertex position and kinematic variables) measured in data and MC simulation. The distributions are found to agree well and no significant discrepancies are observed. Studies of the ID material description in the MC simulation with secondary hadronic interactions also agree well with data [27].

The total photon conversion reconstruction efficiency ϵ_{γ} is factorised into two parts,

$$\epsilon_{\gamma} = P_{\text{conv}}\left(\eta^{\gamma}\right) \cdot \epsilon_{\text{conv}}\left(p_{\text{T}}^{\gamma}, |\eta^{\gamma}|\right) ,$$

where P_{conv} is the probability that a photon converts within the fiducial region for conversions ($40 < r < 150$ mm) and ϵ_{conv} is the converted-photon reconstruction efficiency. The conversion probability P_{conv} is derived from the ratio of the number of generated photons from radiative χ_c decays that convert in the fiducial region of the ID to the total number of photons from radiative χ_c decays. The calculation of P_{conv} is performed in bins of η^{γ} to

account for changes in the detector material traversed for photons of different pseudorapidity. No significant dependence of P_{conv} on photon energy is observed for photons within the kinematic fiducial region ($p_{\text{T}}^{\gamma} > 1.5$ GeV). The conversion probability varies from around 7% to 11% within the fiducial region studied.

The reconstruction efficiency for converted photons, ϵ_{conv}, is determined from the equation

$$\epsilon_{\text{conv}} = N_{\text{reco}}^{\gamma}/N_{\text{conv}}^{\gamma} \ ,$$

where N_{conv}^{γ} is the number of simulated photons from radiative χ_c decays that convert in the fiducial region of the ID and N_{reco}^{γ} is the number of reconstructed photon conversions. This ratio is calculated in bins of p_{T}^{γ} and $|\eta^{\gamma}|$ (no significant asymmetry in photon pseudorapidity is observed) with a method that is verified to account correctly for experimental resolution in p_{T}^{γ}. The conversion reconstruction efficiency is around 15% at $p_{\text{T}}^{\gamma} = 1.5$ GeV and approaches a plateau of approximately 45% for $p_{\text{T}}^{\gamma} > 5.0$ GeV.

4.5 Extraction of corrected yields

Corrected χ_{cJ} yields are extracted by performing a simultaneous fit to the mass difference $\Delta m = m\left(\mu^{+}\mu^{-}\gamma\right) - m\left(\mu^{+}\mu^{-}\right)$ and pseudo-proper decay time τ distributions of weighted χ_c candidates. Separate unbinned maximum likelihood fits are performed in bins of both J/ψ candidate transverse momentum $p_{\text{T}}^{J/\psi}$ and χ_c candidate transverse momentum $p_{\text{T}}^{\chi_c}$. The fits are performed within the χ_c signal region of $0.2 < \Delta m < 0.7$ GeV and no restriction on τ is applied. The full probability density function (pdf) used to perform the fits has the form,

$$F\left(\Delta m, \tau, \delta\tau\right) = f_{\text{sig}} \cdot F_{\text{sig}}\left(\Delta m, \tau, \delta\tau\right) + \left(1 - f_{\text{sig}}\right) \cdot F_{\text{bkgd}}\left(\Delta m, \tau, \delta\tau\right) \ ,$$

where f_{sig} is the fraction of χ_c signal candidates determined by the fit, while F_{sig} and F_{bkgd} are pdfs that respectively model the signal and background components of the mass difference and pseudo-proper decay time distributions. The quantity $\delta\tau$ is the per-candidate uncertainty on the pseudo-proper decay time calculated from the covariance matrix of the vertex fit to the dimuon tracks. The distributions of the pseudo-proper decay time uncertainty $\delta\tau$ observed in the background ($\Delta m < 0.3$ GeV or $\Delta m > 0.48$ GeV) and signal (background subtracted within $0.3 < \Delta m < 0.48$ GeV) regions are found to be consistent within their uncertainties. Consequently, terms for the distribution of $\delta\tau$ factorise in the likelihood and are not included [28].

The signal pdf F_{sig} is composed of several components,

$$
\begin{aligned}
F_{\text{sig}}\left(\Delta m, \tau, \delta\tau\right) = & f_{\text{sig}}^{\text{P}} \cdot \left[f_0^{\text{P}} \cdot M_0\left(\Delta m\right) + \left(1 - f_0^{\text{P}}\right) \cdot \left(f_1^{\text{P}} \cdot M_1\left(\Delta m\right)\right.\right. \\
& \left.\left. + \left(1 - f_1^{\text{P}}\right) \cdot M_2\left(\Delta m\right)\right)\right] \cdot T_{\text{sig}}^{\text{P}}\left(\tau, \delta\tau\right) \\
& + \left(1 - f_{\text{sig}}^{\text{P}}\right) \cdot \left[f_0^{\text{NP}} \cdot M_0\left(\Delta m\right) + \left(1 - f_0^{\text{NP}}\right) \cdot \left(f_1^{\text{NP}} \cdot M_1\left(\Delta m\right)\right.\right. \\
& \left.\left. + \left(1 - f_1^{\text{NP}}\right) \cdot M_2\left(\Delta m\right)\right)\right] \cdot T_{\text{sig}}^{\text{NP}}\left(\tau, \delta\tau\right) \ ,
\end{aligned}
$$

where the pdfs $M_J(\Delta m)$ model the χ_{cJ} signal components of the Δm distribution and $T_{\text{sig}}^{\text{(N)P}}$ model the (non-)prompt χ_c signal contributions to the pseudo-proper decay time distribution. The parameter $f_{\text{sig}}^{\text{P}}$ is the fraction of the total χ_c signal that is promptly produced, $f_0^{\text{(N)P}}$ is the fraction of (non-)prompt signal identified as χ_{c0} and $f_1^{\text{(N)P}}$ is the fraction of (non-)prompt signal (excluding χ_{c0} contributions) identified as χ_{c1}.

The χ_{c1} and χ_{c2} signal pdfs $M_{1,2}(\Delta m)$ are each described by a Crystal Ball (CB) function [29]. The CB function is characterised by a Gaussian core with a width σ_i (associated with the pdf $M_i(\Delta m)$) and a power law low-mass tail described by the parameter n. The transition between the core and tail is described by the threshold parameter α. The mass resolutions of prompt and non-prompt χ_c are found to be consistent from MC simulation studies. The natural widths of the χ_{c1} and χ_{c2} states are sufficiently small (below 2 MeV [4]) relative to the detector mass resolution (around 10 MeV) that their effects can be neglected. The peak positions of both the χ_{c1} and χ_{c2} CB functions are fixed to the world average values of their respective masses [4] multiplied by a common scale factor κ. The factor κ is a free parameter in the fit and is present to account for electron energy losses that result in a small momentum scale shift. The fitted values are typically around $\kappa = 0.98$. The two parameters α and n of the CB functions are found to be consistent for both states and are fixed to values determined from fits to MC simulation samples. The resolution parameter σ_1 is determined by the fit with the constraint $\sigma_2 = 1.07 \times \sigma_1$ applied, where the value of the scale factor is extracted from MC simulation studies. The χ_{c0} signal pdf, $M_0(\Delta m)$, is modelled by the sum of a CB function and a Gaussian pdf; all parameters describing the shape of the χ_{c0} signal are fixed to values determined from MC simulation (including a natural width of (10.3 ± 0.6) MeV [4]), while the peak position of the χ_{c0} signal is a free parameter in the fit. The χ_{c0} peak is clearly visible in the Δm distribution shown in figure 2. However, the χ_{c0} yield is not reported because the statistical significance of the signal is marginal when the data are fitted in separate bins of $p_{\text{T}}^{J/\psi}$ and $p_{\text{T}}^{\chi_c}$.

The pdfs $T_{\text{sig}}^{\text{P}}$ and $T_{\text{sig}}^{\text{NP}}$ describing the prompt and non-prompt χ_c signal contributions to the pseudo-proper decay time distributions are modelled by a delta function $\delta(\tau)$ and an exponential function $\exp(-\tau/\tau_{\text{sig}})$, where τ_{sig} is a free parameter in the fit. Both χ_c signal pseudo-proper decay time pdfs are convolved with the function $R(\tau' - \tau, \delta\tau)$ describing the experimental resolution in pseudo-proper decay time. The resolution function R is described by a Gaussian function with a mean value of zero and width $S \cdot \delta\tau$ where S is a scale factor that is determined by the fit, while $\delta\tau$ is the per-candidate uncertainty on the pseudo-proper decay time τ.

The background pdf F_{bkgd} is composed of two components,

$$
\begin{aligned}
F_{\text{bkgd}}(\Delta m, \tau, \delta\tau) = & f_{\text{bkgd}}^{\text{P}} \cdot M_{\text{bkgd}}^{\text{P}}(\Delta m) \cdot T_{\text{bkgd}}^{\text{P}}(\tau, \delta\tau) \\
& + \left(1 - f_{\text{bkgd}}^{\text{P}}\right) \cdot M_{\text{bkgd}}^{\text{NP}}(\Delta m) \cdot T_{\text{bkgd}}^{\text{NP}}(\tau, \delta\tau) ,
\end{aligned}
$$

where $M_{\text{bkgd}}^{\text{(N)P}}$ describes the (non-)prompt background contributions to the Δm distribution and $T_{\text{bkgd}}^{\text{(N)P}}$ describes the (non-)prompt background contributions to the pseudo-proper decay

time distribution. The parameter $f_{\text{bkgd}}^{\text{P}}$ is the fraction of the background that is promptly produced. The functions $M_{\text{bkgd}}^{\text{(N)P}}$ are both modelled by the function

$$M_{\text{bkgd}}\left(\Delta m\right) = \text{erf}\left(A \cdot (\Delta m - m_0)\right) \cdot \exp\left(B \cdot (\Delta m - m_0)\right) + C \cdot (\Delta m - m_0)^2 \; ,$$

where all four parameters (A, B, C and m_0) in the pdf are determined by the fit. The shape of the background pdf is motivated by studies with MC simulation samples and a sample of $\mu^+\mu^-\gamma$ candidates in data with dimuon invariant masses in the sidebands of the J/ψ peak. The prompt and non-prompt background pdfs each use an independent set of four parameters. Endowing both background pdfs with an independent set of parameters is motivated by the observation that the shape of the background contribution to the Δm distribution in data varies significantly as a function of pseudo-proper decay time. The pdf $T_{\text{bkgd}}^{\text{P}}\left(\tau, \delta\tau\right)$ is modelled with a delta function convolved with the pseudo-proper decay time resolution function R. The pdf $T_{\text{bkgd}}^{\text{NP}}\left(\tau, \delta\tau\right)$ consists of two components,

$$T_{\text{bkgd}}^{\text{NP}}\left(\tau, \delta\tau\right) = \left[\frac{g_{\text{bkgd}}}{\tau_{\text{bkgd}}} \cdot \exp\left(-\tau'/\tau_{\text{bkgd}}\right) \right.$$
$$\left. + \frac{(1 - g_{\text{bkgd}})}{2\tau_{\text{sym}}} \cdot \exp\left(-|\tau'|/\tau_{\text{sym}}\right)\right] \otimes R\left(\tau' - \tau, \delta\tau\right) \; ,$$

where g_{bkgd} determines the relative mixture of the single- and double-sided exponential components. The parameters τ_{bkgd} and τ_{sym} determine the shapes of the single- and double-sided exponential components, respectively. The result of the fit described above to the inclusive data sample with $10 \leq p_{\text{T}}^{J/\psi} < 30$ GeV is shown by the projections onto the mass difference and pseudo-proper decay time axes as shown in figure 2. The purity of the selected J/ψ candidates is around 90%, with no strong dependence on pseudo-proper decay time. A larger background contribution to the $m\left(\mu^+\mu^-\gamma\right) - m\left(\mu^+\mu^-\right)$ distribution, relative to the χ_c signal, is observed for $\mu^+\mu^-\gamma$ candidates with longer pseudo-proper decay times. This behaviour is consistent with the expectation from MC simulation and is due to the presence of additional charged particles and photons produced close to the dimuon system in the decays of b-hadrons.

Bin migrations in the measured $p_{\text{T}}^{\chi_c}$ and $p_{\text{T}}^{J/\psi}$ distributions are corrected with the method described in refs [8, 26]. The approach involves fitting the measured $p_{\text{T}}^{\chi_c}$ and $p_{\text{T}}^{J/\psi}$ distributions with a smooth analytic function that is convolved with a resolution function determined from MC simulation. The ratio of the functions with and without convolution is used to deduce a correction factor for each measured bin in $p_{\text{T}}^{\chi_c}$ and $p_{\text{T}}^{J/\psi}$. The average corrections for the cross-sections measured as a function of $p_{\text{T}}^{J/\psi}$ is 0.5%. Corrections to the cross-sections measured as a function of $p_{\text{T}}^{\chi_c}$ are significantly larger, around 4% on average, due to an asymmetric experimental resolution in $p_{\text{T}}^{\chi_c}$ caused by electron energy loss through bremsstrahlung.
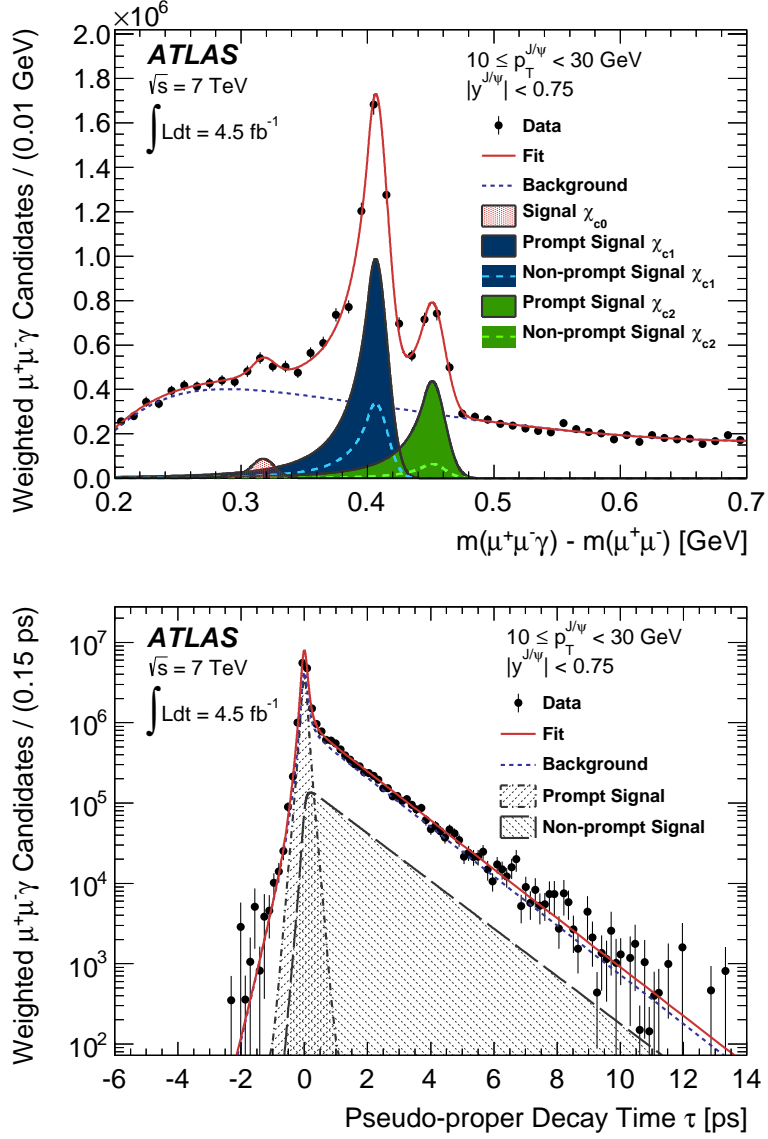
Figure 2. The mass difference $\Delta m = m\left(\mu^+\mu^-\gamma\right) - m\left(\mu^+\mu^-\right)$ distribution (top) for χ_c candidates reconstructed within $10 \le p_T^{J/\psi} < 30$ GeV and $|y^{J/\psi}| < 0.75$. The pseudo-proper decay time τ distribution of the same sample of χ_c candidates is also shown (bottom). Both distributions are corrected for acceptance and experimental efficiency (the prompt χ_{c1} acceptance correction is shown here for demonstration). The result of the simultaneous fit to both distributions is shown by the overlaid solid red lines. The fitted χ_{cJ} signals are shown by the shaded regions while the fitted background distributions are shown by the dashed blue lines.

5 Systematic uncertainties

The relevant sources of systematic uncertainty on the prompt and non-prompt χ_{c1} and χ_{c2} cross-section measurements have been identified and their effects are discussed and quantified below.

Statistical uncertainties in efficiency corrections

One component of the systematic uncertainty in the efficiency corrections is statistical in nature due to the finite size of the MC and data control samples used to derive the efficiencies. The corresponding uncertainty in the χ_c yields is quantified by repeatedly varying the values of the efficiencies within their statistical uncertainties by a random amount and recalculating the weights used to extract the corrected χ_c yields. The systematic uncertainty is estimated from the RMS of the distribution of the average weight in each $p_{\mathrm{T}}^{\chi_c}$ and $p_{\mathrm{T}}^{J/\psi}$ bin.

Conversion probability

The conversion probability P_{conv} derived using MC simulation samples is sensitive to the modelling of the ID material distribution in the ATLAS detector simulation. As discussed in section 4.4, the description of the ID material distribution in MC simulation is found to agree with the distribution observed in data [27]. The uncertainties in the modelling of the mass distribution are used to define an alternative ATLAS detector model with a larger amount of material in the conversion fiducial region. Samples of $\chi_c \to J/\psi\,\gamma$ events are generated with both the nominal and the alternative detector model, using the same method as described in ref. [30]. The difference in the simulated conversion probabilities is taken as an estimate of the corresponding systematic uncertainty.

Converted-photon reconstruction efficiency

The converted-photon reconstruction efficiency ϵ_{conv} derived using MC simulation samples is sensitive to any potential differences in the behaviour of the photon conversion reconstruction algorithm in data and simulation. These effects are studied by comparing several sensitive distributions (including conversion vertex position, vertex fit quality and e^+e^- track hits) of a sample of photon conversions in data and simulation. The systematic uncertainty in ϵ_{conv} due to residual simulation mis-modelling effects is estimated to be $\pm 9\%$. The systematic uncertainty on the determination of ϵ_{conv} due to potential residual mismodelling of bin migrations in p_{T}^{γ} is estimated to be $\pm 5\%$ from several self consistency tests performed with MC simulation samples.

Acceptance

The per-candidate acceptance correction for the measurements binned in $p_{\mathrm{T}}^{\chi_c}$ is calculated from the reconstructed value of $p_{\mathrm{T}}^{\chi_c}$ for each χ_c candidate. This reconstructed value of $p_{\mathrm{T}}^{\chi_c}$ is scaled by around $+0.5\%$ to avoid an over-correction due to the asymmetric experimental resolution in $p_{\mathrm{T}}^{\chi_c}$. The correction procedure is verified with simulation studies and has a systematic uncertainty of $\pm 2\%$. The acceptance corrections for the measurements binned in $p_{\mathrm{T}}^{J/\psi}$ are sensitive to the $p_{\mathrm{T}}^{\chi_c}$ distribution used as an

input to the acceptance simulation. This sensitivity is studied by varying the analytic function used to fit the measured $p_{\mathrm{T}}^{\chi_c}$ distribution. The systematic uncertainty in the acceptance corrections due to the fitted parametrisation of the measured $p_{\mathrm{T}}^{\chi_c}$ distributions is estimated to be between 4-8%, depending on the individual χ_{cJ} yield. The systematic uncertainty in the acceptance correction, due to the unknown χ_c spin-alignment, is evaluated by comparing the acceptance calculated assuming isotropic decay angular distributions to that calculated with the angular distributions corresponding to the spin-alignment scenarios shown in Table 1. This comparison is used to derive an uncertainty envelope associated with the unknown χ_c spin-alignment. The spin-alignment envelope is treated as a separate uncertainty and is discussed in more detail in section 6.

Fit model

The systematic uncertainty on the χ_{cJ} yields due to the fit model is quantified with a MC pseudo-experiment approach. Pseudo-data samples are generated from the nominal fit result in individual bins of $p_{\mathrm{T}}^{\chi_c}$ and $p_{\mathrm{T}}^{J/\psi}$. Each pseudo-data sample is fitted with the nominal fit model and five alternative fit models that include a variety of alterations as discussed below.

- Each of the fixed α and n parameters in the χ_{c1} and χ_{c2} signal CB functions is individually released to be determined by the fit.
- The scaling of the χ_{c1} and χ_{c2} Δm resolution parameters σ_1 and σ_2 is removed and both parameters are independently determined by the fit.
- The fit is repeated with the χ_{c0} signal component of the pdf removed. This test is motivated by the fact that the χ_{c0} signal is insignificant in some of the p_{T} bins studied.
- An alternative background pdf (with four free parameters) for the mass difference distribution is tested.

The systematic uncertainty due to the fit model is then estimated from the mean of the distribution of the relative changes in the yield between the nominal and alternative models. The systematic uncertainty due to the fit model for the prompt and non-prompt cross-section ratios and non-prompt fractions is evaluated in the same way to ensure correlations between the signal components in the evaluation of the systematic uncertainty are taken into account.

Integrated luminosity

The uncertainty in the integrated luminosity of the data sample used is estimated to be 1.8%. The methods used to determine this uncertainty are described in detail in ref. [31]. This systematic uncertainty does not affect the cross-section ratios or non-prompt fractions.

The individual sources of systematic uncertainty are summarised in tables 2 and 3. The largest sources of systematic uncertainty are associated with the photon conversion reconstruction efficiency, the fit model and the acceptance. The individual sources of systematic

uncertainty studied are not strongly correlated and the total systematic uncertainty on the measurements is obtained by adding the individual systematic uncertainties in quadrature. These uncertainties are generally much smaller than the uncertainty associated with the unknown χ_c spin-alignment.

Binning: $p_{\mathrm{T}}^{J/\psi}$	Fractional Uncertainty [%]			
	Prompt		Non-prompt	
	χ_{c1}	χ_{c2}	χ_{c1}	χ_{c2}
Muon reco. efficiency	1	1	1	1
Trigger efficiency	4	4	4	4
Converted-photon reco. efficiency	11	11	11	11
Conversion probability	4	4	4	4
Acceptance	4	4	5	8
Fit model	2	3	3	9
Total systematic	13	13	13	17
Spin-alignment envelope (upper)	34	36	32	36
Spin-alignment envelope (lower)	13	23	13	23

Table 2. The individual contributions to the systematic uncertainty on the cross-section measurements binned in $p_{\mathrm{T}}^{J/\psi}$, averaged across all $p_{\mathrm{T}}^{J/\psi}$ bins. The common contributions of integrated luminosity (1.8%) and track reconstruction (1%) are not shown. The average variation in the cross-sections due to the envelope of all possible spin-alignment scenarios is also shown ("upper" denotes the positive variation while "lower" denotes the negative variation).

Binning: $p_{\mathrm{T}}^{\chi_c}$	Fractional Uncertainty [%]			
	Prompt		Non-prompt	
	χ_{c1}	χ_{c2}	χ_{c1}	χ_{c2}
Muon reco. efficiency	1	1	1	1
Trigger efficiency	3	4	4	4
Converted-photon reco. efficiency	11	11	11	11
Conversion probability	4	4	4	4
Acceptance	2	2	2	2
Fit model	2	3	3	8
Total systematic	12	12	12	14
Spin-alignment envelope (upper)	29	31	29	31
Spin-alignment envelope (lower)	11	20	11	20

Table 3. The individual contributions to the systematic uncertainty on the cross-section measurements binned in $p_{\mathrm{T}}^{\chi_c}$, averaged across all $p_{\mathrm{T}}^{\chi_c}$ bins. The common contributions of integrated luminosity (1.8%) and track reconstruction (1%) are not shown. The average variation in the cross-sections due to the envelope of all possible spin-alignment scenarios is also shown ("upper" denotes the positive variation while "lower" denotes the negative variation).

6 Results and interpretation

The differential cross-sections of prompt and non-prompt χ_{c1} and χ_{c2} production are measured in bins of $p_{\mathrm{T}}^{J/\psi}$ and $p_{\mathrm{T}}^{\chi_c}$ within the rapidity region $|y^{J/\psi}| < 0.75$. The results measured as a function of $p_{\mathrm{T}}^{J/\psi}$ and $p_{\mathrm{T}}^{\chi_c}$ are presented within the regions $10 \leq p_{\mathrm{T}}^{J/\psi} < 30$ GeV and $12 \leq p_{\mathrm{T}}^{\chi_c} < 30$ GeV, respectively. The measurements of the prompt production of χ_{c1} and χ_{c2} as a function of $p_{\mathrm{T}}^{J/\psi}$ are combined with existing measurements [8] of prompt J/ψ production to determine the fraction of prompt J/ψ produced in χ_c decays. The production rate of χ_{c2} relative to χ_{c1} is measured for prompt and non-prompt χ_c as a function of $p_{\mathrm{T}}^{J/\psi}$. The fractions of χ_{c1} and χ_{c2} produced in the decays of b-hadrons are also presented as a function of $p_{\mathrm{T}}^{\chi_c}$. While the prompt and non-prompt χ_{c1} and χ_{c2} yields are necessarily extracted from separate fits, statistical correlations between the yields are taken into account in the calculation of the statistical uncertainties on the cross-section ratios and non-prompt fractions. Tabulated results for all of the measurements are included in appendix A.

The spin-alignment of the χ_c mesons produced at the LHC is unknown. All measurements are corrected for detector acceptance assuming isotropic angular distributions for the decay of the χ_c states. The total uncertainty in the measurements due to this assumption is obtained by comparing the acceptance calculated with the extreme χ_c spin-alignment scenarios discussed in section 4.1 to the central value, calculated with the isotropic scenario. The maximum uncertainty due to spin-alignment effects averaged over each measurement bin is shown in tables 2 and 3 and for each measurement bin in the tabulated results in appendix A. The uncertainty due to spin-alignment effects is not included in the total systematic uncertainty. Factors that can be used to scale the central cross-section values to any of the individual spin-alignment scenarios studied are also provided in table 13 of appendix A.

6.1 Differential cross-sections

Differential cross-sections for prompt χ_{c1} and χ_{c2} production are measured as a function of both $p_{\mathrm{T}}^{J/\psi}$ and $p_{\mathrm{T}}^{\chi_c}$ within the region $|y^{J/\psi}| < 0.75$. These results are corrected for acceptance assuming isotropic decay angular distributions for the χ_{c1} and χ_{c2} states and are shown in figures 3 and 4. The position along the p_{T} axis of each of the data points shown in these figures is adjusted to reflect the average value of the transverse momentum, $\langle p_{\mathrm{T}}^{J/\psi} \rangle$ or $\langle p_{\mathrm{T}}^{\chi_c} \rangle$, for the χ_c candidates within that p_{T} bin, after all acceptance and efficiency corrections have been applied. The measurements are compared with the predictions of next-to-leading-order (NLO) non-relativistic QCD (NRQCD) [19, 32, 33], the k_{T} factorisation approach [34, 35] and leading-order (LO) colour-singlet model (CSM) [36] calculations. The NRQCD factorisation approach separates the perturbative production of a heavy quark pair (in a colour-singlet or -octet state) from the non-perturbative evolution of a heavy quark pair into a quarkonium state [1]. The long-distance effects are described by matrix elements that are determined by fitting experimental data [2]. For the predictions shown, the NRQCD long-distance matrix elements are extracted from measurements of J/ψ and $\psi(2S)$ production at the Tevatron as described in ref. [33]. In the CSM, heavy quark pairs are produced directly in a colour-singlet state (described by perturbative QCD)

and a potential model is used to describe the formation of the bound state [37–40]. In the high p_T region studied, $gg \to \chi_{cJ}g$ processes constitute the dominant contribution to the CSM prediction. The k_T factorisation approach convolves a partonic cross-section from the CSM with an un-integrated gluon distribution that depends on both longitudinal and transverse momentum (as opposed to the collinear approximation, which neglects parton transverse momentum) to calculate the hadronic cross-section. The shaded uncertainty bands of the NRQCD and CSM predictions are derived from factorisation and renormalisation scale uncertainties, and the NRQCD uncertainty also includes a contribution from the extraction of NRQCD long distance matrix elements from data. Good agreement between the NRQCD calculation and the measurements is observed. The k_T factorisation approach predicts a cross-section significantly in excess of the measurement while the LO CSM prediction significantly underestimates the data. This suggests that higher-order corrections or colour-octet contributions to the cross-sections not included in either prediction may be numerically important.

Differential cross-sections are also measured for non-prompt χ_{c1} and χ_{c2} production as functions of both $p_\mathrm{T}^{J/\psi}$ and $p_\mathrm{T}^{\chi_c}$ within the region $|y^{J/\psi}| < 0.75$, assuming isotropic decay angular distributions. The results are shown in figure 5 and are compared to the fixed order next-to-leading-logarithm (FONLL) prediction for b-hadron production [6, 7]. These predictions are combined with measured momentum distributions of χ_{c1} and χ_{c2} in the $B^{\pm/0}$ rest frame for inclusive $B \to \chi_c X$ decays [41]. This prediction is scaled assuming all b-quarks hadronise into $B^{\pm/0}$ mesons. The current world average values for the branching fractions $\mathcal{B}\left(B^{\pm/0} \to \chi_{c1}X\right) = (3.86 \pm 0.27) \times 10^{-3}$ and $\mathcal{B}\left(B^{\pm/0} \to \chi_{c2}X\right) = (1.3 \pm 0.4) \times 10^{-3}$ are used [4]. The shaded uncertainty band on the FONLL predictions represents the theoretical uncertainty due to factorisation and renormalisation scales, quark masses and parton distribution functions combined with the uncertainty on the branching fractions used to scale the predictions. The measurements generally agree with the FONLL predictions, though the data tend to lie slightly below the predictions at high p_T.
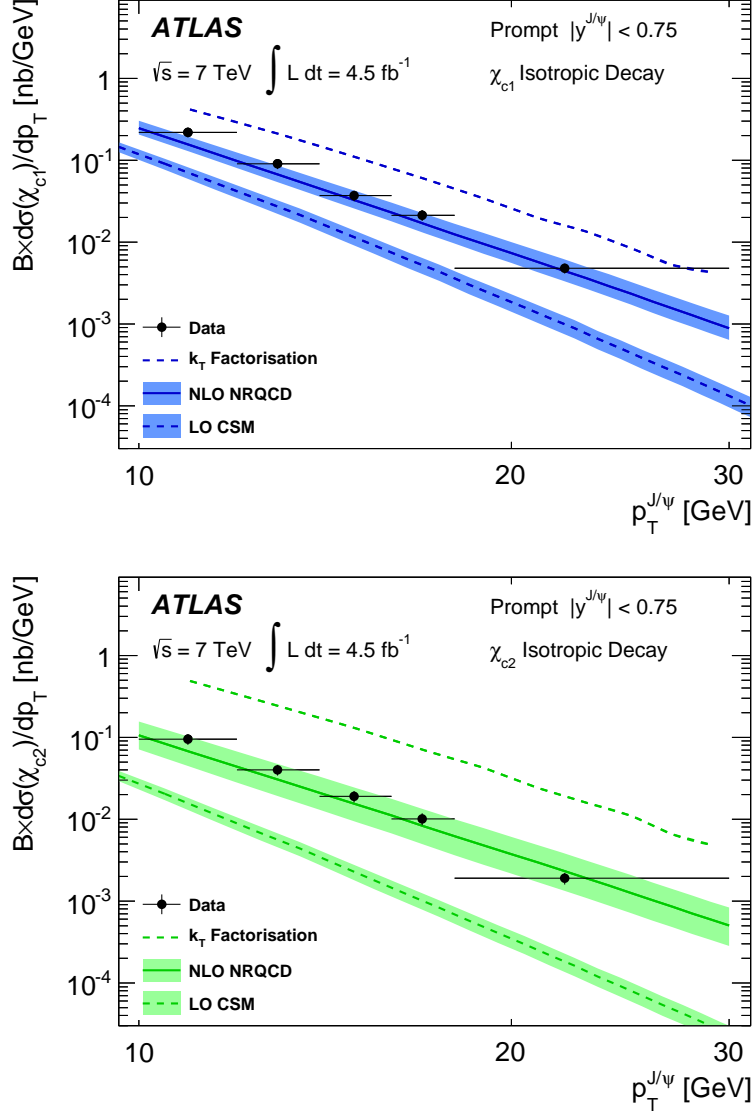
Figure 3. Differential cross-sections for prompt χ_{c1} (top) and χ_{c2} (bottom) production as a function of $p_T^{J/\psi}$. The predictions of NLO NRQCD, the k_T factorisation model and the LO CSM are compared to the measurements. The positions of the data points within each bin reflect the average $p_T^{J/\psi}$ of the χ_c candidates within the bin. The error bars represent the total uncertainty on the measurement, assuming isotropic decay angular distributions (in some cases, the error bar is smaller than the data point). The factor B denotes the product of branching fractions, $B = \mathcal{B}(\chi_{cJ} \to J/\psi\,\gamma) \cdot \mathcal{B}(J/\psi \to \mu^+\mu^-)$.
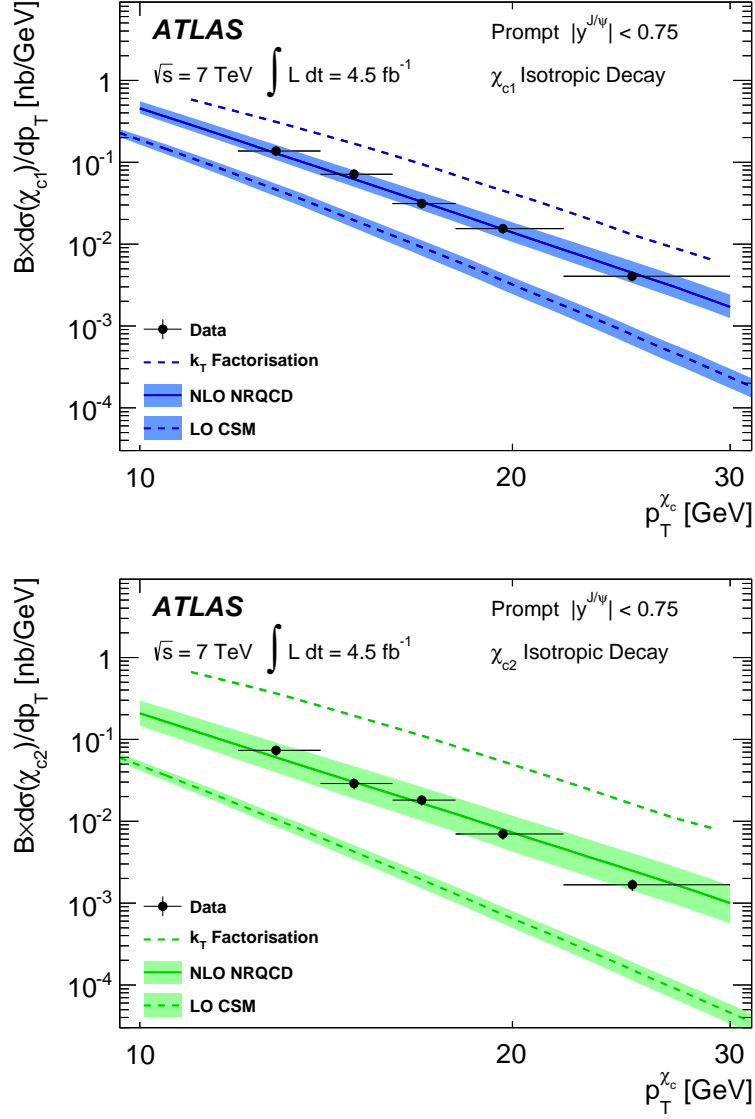
Figure 4. Differential cross-sections for prompt χ_{c1} (top) and χ_{c2} (bottom) production as a function of $p_T^{\chi_c}$. The predictions of NLO NRQCD, the k_T factorisation model and the LO CSM are compared to the measurements. The positions of the data points within each bin reflect the average $p_T^{\chi_c}$ of the χ_c candidates within the bin. The error bars represent the total uncertainty on the measurement, assuming isotropic decay angular distributions (in some cases, the error bar is smaller than the data point). The factor B denotes the product of branching fractions, $B = \mathcal{B}\left(\chi_{cJ} \to J/\psi\,\gamma\right) \cdot \mathcal{B}\left(J/\psi \to \mu^+\mu^-\right)$.
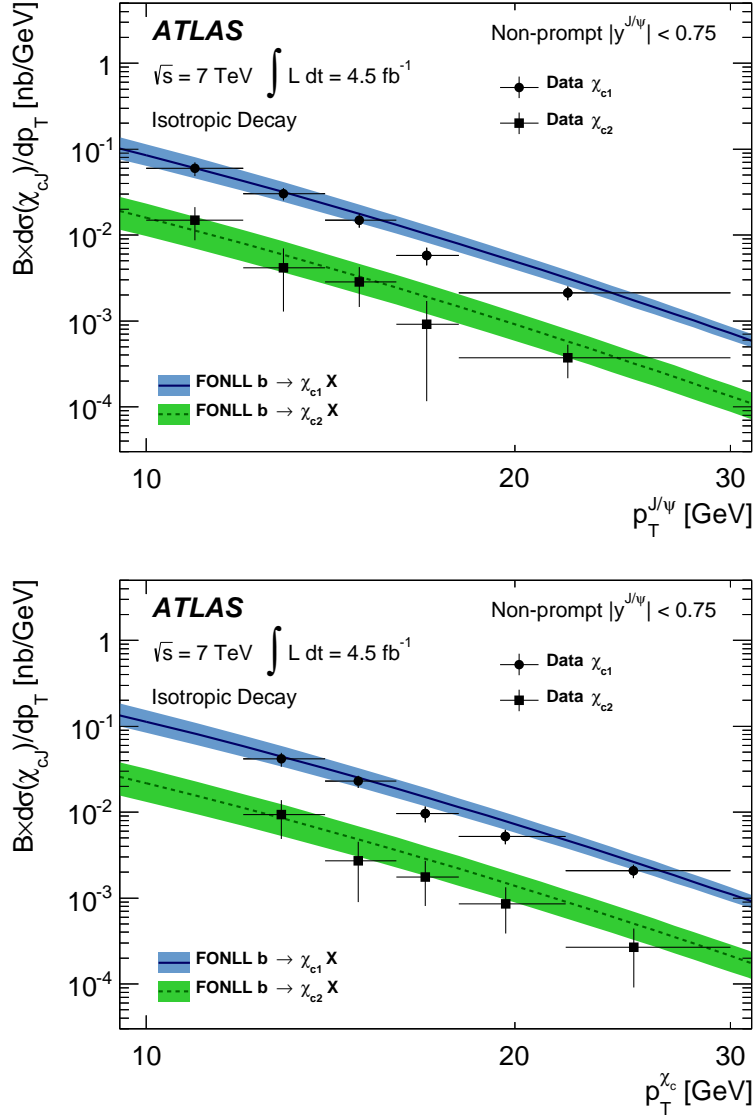
Figure 5. Differential cross-sections for non-prompt χ_{c1} and χ_{c2} production as a function of $p_T^{J/\psi}$ (top) and $p_T^{\chi_c}$ (bottom). The predictions of FONLL are compared to the measurements. The positions of the data points within each bin reflect the average $p_T^{J/\psi}$ and $p_T^{\chi_c}$ of the χ_c candidates within the bin. The error bars represent the total uncertainty on the measurement, assuming isotropic decay angular distributions. The factor B denotes the product of branching fractions, $B = \mathcal{B}\left(\chi_{cJ} \to J/\psi\,\gamma\right) \cdot \mathcal{B}\left(J/\psi \to \mu^+\mu^-\right)$.
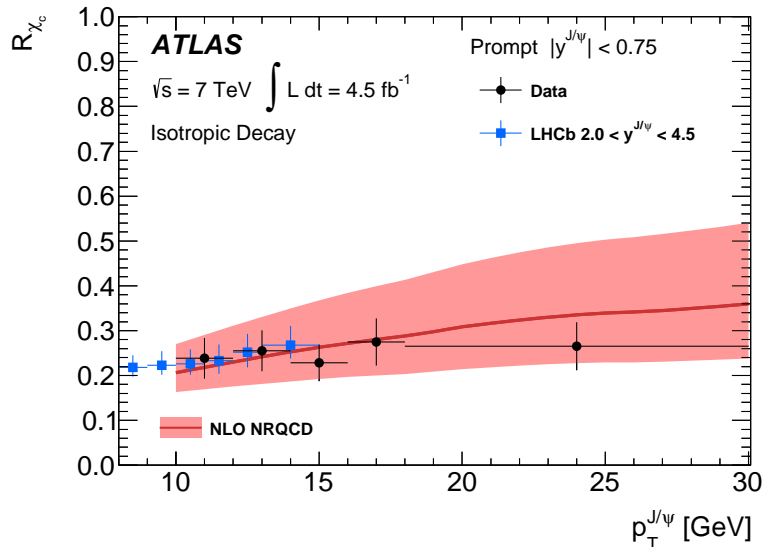
Figure 6. The fraction, R_{χ_c}, of prompt J/ψ produced in χ_c decays as a function of $p_T^{J/\psi}$. The measurements are compared to the prediction of NLO NRQCD. The measurement from LHCb [15] is also shown. The error bars represent the total uncertainty on the measurement, assuming isotropic decay angular distributions.

6.2 Fraction of prompt J/ψ produced in χ_c decays

The prompt χ_{c1} and χ_{c2} cross-sections are summed to provide their total contribution to the prompt J/ψ cross-section for each $p_T^{J/\psi}$ bin. The result is then divided by the prompt J/ψ cross-section measured by ATLAS [8] for each $p_T^{J/\psi}$ bin. The systematic uncertainties in the two measurements are treated as uncorrelated. This is motivated by the fact that the ATLAS measurement of the prompt J/ψ cross-section was performed with an independent data sample (recorded during the 2010 LHC run) and that the systematic uncertainties on the experimental efficiencies are evaluated using different methods and are all dominated by statistical effects. This provides a measurement of the fraction, R_{χ_c}, of J/ψ produced in feed-down from χ_c decays, neglecting the small contribution from radiative χ_{c0} decays, as a function of $p_T^{J/\psi}$. The measurements are shown in figure 6 and are compared to the predictions of NLO NRQCD and the LHCb measurement within the range $2.0 < y^{J/\psi} < 4.5$ [15]. The results show that between 20% and 30% of prompt J/ψ are produced in χ_c feed-down at high J/ψ transverse momentum. Motivated by recent measurements [42, 43], the spin-alignment envelope for this fraction given in table 9 in appendix A is calculated assuming no overall spin-alignment for promptly produced J/ψ.

6.3 Cross-section ratios

The production rates of χ_{c2} relative to χ_{c1} are measured for prompt and non-prompt χ_c as a function of $p_T^{J/\psi}$. The ratio of the prompt cross-sections is shown in figure 7. The measurements are compared to the NLO NRQCD and CSM predictions and to the measurements of
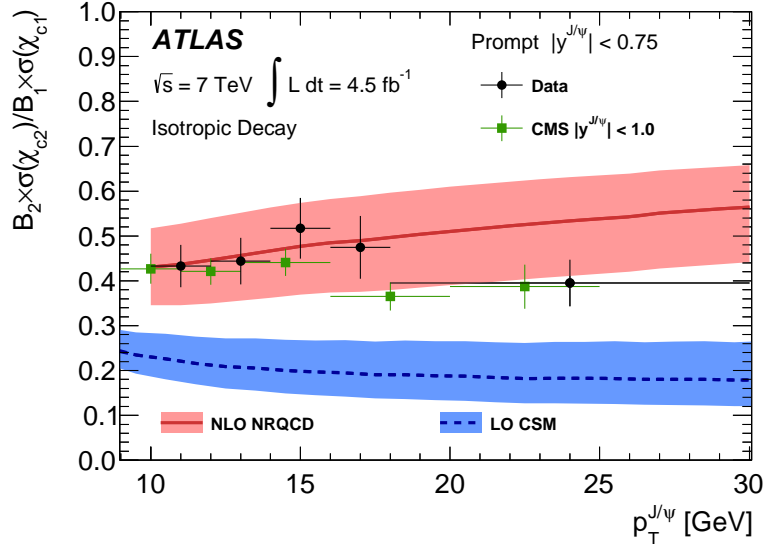
Figure 7. The production cross-section of prompt χ_{c2} relative to prompt χ_{c1} measured as a function of $p_T^{J/\psi}$. The measurements are compared to the predictions of NLO NRQCD and the LO CSM. The measurement from CMS [16] is also shown. The error bars represent the total uncertainty on the measurement, assuming isotropic decay angular distributions. The factors B_1 and B_2 denote the branching fractions $B_1 = \mathcal{B}\left(\chi_{c1} \to J/\psi\,\gamma\right)$ and $B_2 = \mathcal{B}\left(\chi_{c2} \to J/\psi\,\gamma\right)$, respectively.

CMS within the range $|y^{J/\psi}| < 1.0$ [16]. The NLO NRQCD prediction is in generally good agreement with the measurements, particularly at lower $p_T^{J/\psi}$ values. The cross-section ratio predicted by the CSM is consistently lower than the measurements. The ratio of the non-prompt cross-sections is shown in figure 8 and is compared to the measurement of CDF in $p\bar{p}$ collisions at $\sqrt{s} = 1.96$ TeV and for $p_T^{J/\psi} > 10$ GeV [18].

6.4 Non-prompt fractions

The prompt and non-prompt χ_{c1} and χ_{c2} cross-sections are used to calculate the fractions of inclusive χ_{c1} and χ_{c2} produced in the decays of b-hadrons, $f_{\text{non-prompt}}$. The non-prompt fraction is measured as a function of $p_T^{\chi_c}$ and is shown in figure 9. The combined non-prompt fraction is observed to increase as a function of $p_T^{\chi_c}$, as is observed in the J/ψ and $\psi(2S)$ systems. However, the inclusive production of χ_{c1} and χ_{c2} is dominated by prompt production in the kinematic region measured, contrary to what is observed in the J/ψ and $\psi(2S)$ systems for the same high-p_T region, where the inclusive cross-sections contain a larger component of feed-down from b-hadron decays [8, 9].
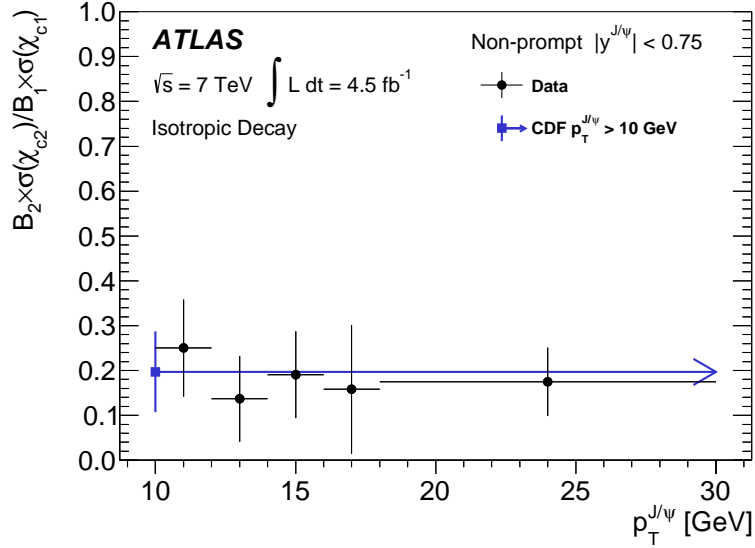
Figure 8. The production cross-section of non-prompt χ_{c2} relative to non-prompt χ_{c1}, $\mathcal{B}\left(\chi_{c2} \to J/\psi\,\gamma\right)\sigma\left(\chi_{c2}\right)/\mathcal{B}\left(\chi_{c1} \to J/\psi\,\gamma\right)\sigma\left(\chi_{c1}\right)$, measured as a function of $p_{\mathrm{T}}^{J/\psi}$. The measurement from CDF [18] is also shown. The error bars represent the total uncertainty on the measurement, assuming isotropic decay angular distributions. The factors B_1 and B_2 denote the branching fractions $B_1 = \mathcal{B}\left(\chi_{c1} \to J/\psi\,\gamma\right)$ and $B_2 = \mathcal{B}\left(\chi_{c2} \to J/\psi\,\gamma\right)$, respectively.
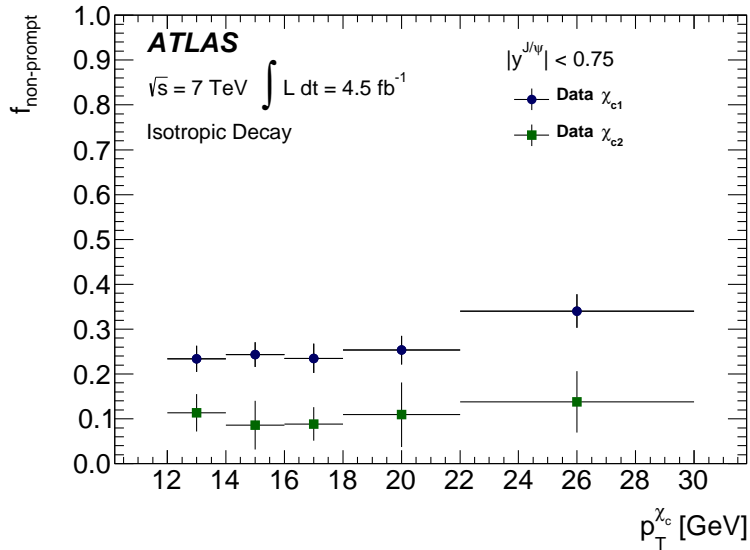
Figure 9. The fractions of χ_{c1} and χ_{c2} produced in the decays of b-hadrons, $f_{\mathrm{non\text{-}prompt}}$, as a function of $p_{\mathrm{T}}^{\chi_c}$. The error bars represent the total uncertainty on the measurement, assuming isotropic decay angular distributions.

7 Measurement of $\mathcal{B}\left(B^{\pm} \to \chi_{c1} K^{\pm}\right)$

The branching fraction $\mathcal{B}\left(B^{\pm} \to \chi_{c1} K^{\pm}\right)$ is measured using the decay $B^{\pm} \to J/\psi K^{\pm}$ as a reference channel (with $\chi_{c1} \to J/\psi\,\gamma$ and $J/\psi \to \mu^{+}\mu^{-}$ for both channels). The final states of both channels are identical apart from the photon.

The branching fraction $\mathcal{B}\left(B^{\pm} \to \chi_{c1} K^{\pm}\right)$ is measured from

$$\mathcal{B}\left(B^{\pm} \to \chi_{c1} K^{\pm}\right) = \mathcal{A}_B \cdot \frac{N^{B}_{\chi_{c1}}}{N^{B}_{J/\psi}} \cdot \frac{\mathcal{B}\left(B^{\pm} \to J/\psi K^{\pm}\right)}{\mathcal{B}\left(\chi_{c1} \to J/\psi\,\gamma\right)} \,,$$

where $\mathcal{A}_B$ is a factor to correct for the different detector acceptances of the two decays, and $N^{B}_{\chi_{c1}}$ and $N^{B}_{J/\psi}$ are the corrected yields for the signal and reference decay channels respectively. The current world-average values are used for the branching fractions: $\mathcal{B}\left(B^{\pm} \to J/\psi K^{\pm}\right) = (1.016 \pm 0.033) \times 10^{-3}$ and $\mathcal{B}\left(\chi_{c1} \to J/\psi\,\gamma\right) = 0.344 \pm 0.015$ [4]. Both decays are reconstructed within the region $10 \leq p_{\mathrm{T}}^{J/\psi} < 30$ GeV and $|y^{J/\psi}| < 0.75$.

The branching fraction $\mathcal{B}\left(B^{\pm} \to \chi_{c1} K^{\pm}\right)$ is measured using the same data sample and efficiency corrections used in the inclusive χ_c production measurements. The χ_{c1} and J/ψ candidate selections (with the photon being reconstructed from conversions) and fiducial region are kept as close to the inclusive χ_c measurement as possible.

7.1 Selection of $B^{\pm}$ decays

The selection of candidate $B^{\pm} \to \chi_{c1} K^{\pm}$ and $B^{\pm} \to J/\psi K^{\pm}$ decays begins by searching for χ_c and J/ψ candidates using the selection criteria described in the inclusive χ_c measurement. Charged particles with tracks consistent with originating from the $\mu^{+}\mu^{-}$ vertex are assigned the charged kaon mass and the $\mu^{+}\mu^{-}K^{\pm}$ vertex is fitted. The candidate charged kaon track is required to contain at least one silicon pixel hit and at least six SCT hits, transverse momentum $p_{\mathrm{T}} > 3$ GeV and pseudorapidity $|\eta| < 2.5$. Candidates with a vertex fit quality χ^2 per degree of freedom < 6 are retained. The L_{xy} of the $J/\psi \to \mu^{+}\mu^{-}$ candidate (as defined in section 4) is required to be greater than 0.3 mm to reject promptly produced J/ψ mesons. This cut rejects over 99% of the prompt J/ψ background and retains around 87% of the $B^{\pm}$ signal. Candidate $B^{\pm} \to \chi_{c1} K^{\pm} \to \mu^{+}\mu^{-}\gamma K^{\pm}$ decays are required to have $0.32 < m\left(\mu^{+}\mu^{-}\gamma\right) - m\left(\mu^{+}\mu^{-}\right) < 0.43$ GeV to select χ_{c1} decays and $4.65 < m\left(\mu^{+}\mu^{-}K^{\pm}\right) - m\left(\mu^{+}\mu^{-}\right) + m_{J/\psi} < 5.2$ GeV to reject backgrounds from $B^{\pm} \to J/\psi K^{\pm}$ decays.

7.2 Calculation of $\mathcal{A}_B$

The acceptance correction factor $\mathcal{A}_B$ is defined as the number of $B^{\pm} \to J/\psi K^{\pm}$ decays relative to the number of $B^{\pm} \to \chi_{c1} K^{\pm}$ decays that fall within their respective fiducial regions. The correction is derived from a large sample of generator-level MC simulation events that uses a fitted parameterisation of the ATLAS measurement of the $B^{\pm}$ differential cross-section [44] (in the $B^{\pm} \to J/\psi K^{\pm}$ mode) as an input. The simulation generates $B^{\pm} \to J/\psi K^{\pm}$ and $B^{\pm} \to \chi_{c1} K^{\pm}$ decays according to the measured spectrum. The angular distributions of the $B^{\pm}$ decay products are generated with helicity equal to zero for the charmonium state in the rest frame of the $B^{\pm}$ meson. This calculation gives $\mathcal{A}_B = 2.30\pm$

0.08 where the uncertainty is derived from the uncertainty in the fitted parameterisation of the measured $B^{\pm}$ cross-section. The difference in the values of $\mathcal{A}_B$ calculated with the nominal and alternative fit parameterisations is taken as an estimate of the systematic uncertainty.

7.3 Extraction of $N_{\chi_{c1}}^B$ and $N_{J/\psi}^B$

Candidate $B^{\pm} \to \chi_{c1} K^{\pm}$ and $B^{\pm} \to J/\psi K^{\pm}$ decays are weighted to correct for trigger efficiency, muon reconstruction efficiency and (for $B^{\pm} \to \chi_{c1} K^{\pm}$ decays) conversion probability and converted-photon reconstruction efficiency using the same corrections derived for the inclusive χ_c production measurement. Corrections are applied only for effects that are known not to fully cancel in the ratio $N_{\chi_{c1}}^B/N_{J/\psi}^B$. Trigger and muon reconstruction efficiencies are corrected since not all $J/\psi \to \mu^+\mu^-$ decays in the fiducial region studied fall within the efficiency plateau. Since the data are only partially corrected, the weighted yields are not representative of the true yields of $B^{\pm}$ mesons one would expect from the data sample and fiducial region used. The corrected yields $N_{\chi_{c1}}^B$ and $N_{J/\psi}^B$ are extracted from unbinned maximum likelihood fits to the $m\left(\mu^+\mu^-\gamma K^{\pm}\right) - m\left(\mu^+\mu^-\gamma\right) + m_{\chi_{c1}}$ and $m\left(\mu^+\mu^- K^{\pm}\right) - m\left(\mu^+\mu^-\right) + m_{J/\psi}$ distributions of selected $B^{\pm}$ decay candidates, where $m_{J/\psi}$ and $m_{\chi_{c1}}$ are the world-average values for the masses of the J/ψ and χ_{c1} states [4].

The mass distribution for candidate $B^{\pm} \to \chi_{c1} K^{\pm}$ decays is fitted with a $B^{\pm}$ signal modelled by a Gaussian pdf where both the mean value and width are free parameters in the fit. The background distribution is modelled with a template derived from MC simulation of inclusive $pp \to b\bar{b}X$ decays generated by PYTHIA 6 [21] and processed with the detector simulation. The Gaussian kernel estimation [45] procedure is applied to the background template from MC simulation to form a non-analytic background pdf. The mass distribution for candidate $B^{\pm} \to J/\psi K^{\pm}$ decays is modelled with a double-Gaussian signal pdf where the mean value (common to both Gaussian pdfs), both width parameters and the relative normalisation of both components are determined by the fit. The background contribution to the $B^{\pm} \to J/\psi K^{\pm}$ mass distribution from $B^{\pm} \to \chi_{c1,2} K^{\pm}$ and $B^{\pm/0} \to J/\psi (K\pi)^{\pm/0}$ decays (where only the J/ψ and charged kaon are reconstructed) is modelled by the sum of a Gaussian and a complementary error function [44]. The background contribution from $B^{\pm} \to J/\psi \pi^{\pm}$ decays where the kaon mass is wrongly assigned to the pion track is modelled with a CB function [44].

The results of the fits to the mass distributions of candidate $B^{\pm} \to \chi_{c1} K^{\pm}$ and $B^{\pm} \to J/\psi K^{\pm}$ decays are shown in figure 10.

7.4 Systematic uncertainties

Several sources of systematic uncertainty on the measurement are considered. The systematic uncertainties due to the efficiency corrections (trigger, conversion probability, and muon and conversion reconstruction) are quantified with the same methods used in the inclusive χ_c measurement. Several variations in both fit models are also tested to estimate the systematic uncertainty on $N_{\chi_{c1}}^B/N_{J/\psi}^B$ due to the fit models. The systematic uncertainty is taken as the maximum deviation of any single combination of alternative fit results from the average. The systematic uncertainty on $\mathcal{A}_B$ due to the fitted parameterisation of the
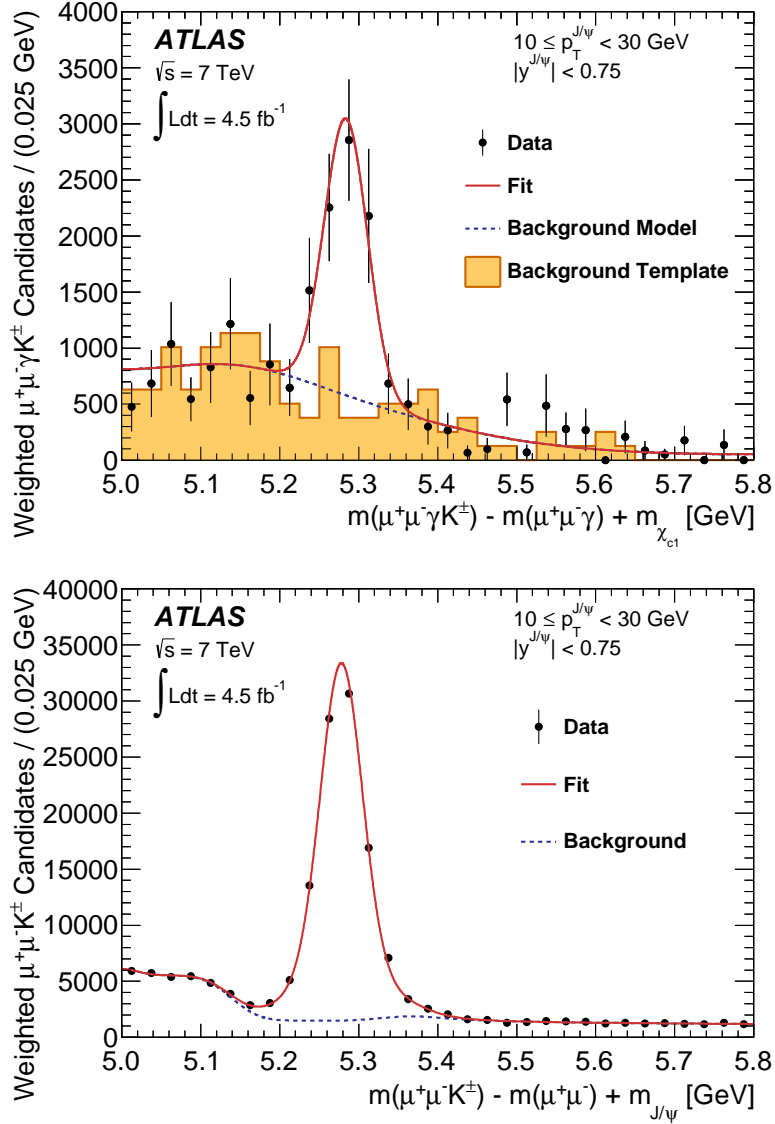
Figure 10. The results of fits to the $m\left(\mu^+\mu^-\gamma K^\pm\right)-m\left(\mu^+\mu^-\gamma\right)+m_{\chi_{c1}}$ (top) and $m\left(\mu^+\mu^- K^\pm\right)-m\left(\mu^+\mu^-\right)+m_{J/\psi}$ (bottom) distributions of selected $B^\pm$ decay candidates. The background template derived from MC simulation is shown as the shaded histogram in the top figure.

$B^\pm$ cross-section is also propagated into an uncertainty on $\mathcal{B}\left(B^\pm \to \chi_{c1}K^\pm\right)$. Table 4 shows a summary of the individual sources of systematic uncertainty considered.

7.5 Result

The measured branching fraction is $\mathcal{B}(B^\pm \to \chi_{c1}K^\pm) = (4.9\pm0.9\,(\text{stat.})\pm0.6\,(\text{syst.}))\times10^{-4}$. This value is in good agreement with the current world-average value of $(4.79 \pm 0.23) \times 10^{-4}$ [4] (dominated by measurements from Belle [46] and BaBar [47]), and supports the estimate of the conversion reconstruction efficiencies at the level of 19% (the total fractional

	Fractional Uncertainty [%]
Converted-photon reconstruction efficiency	10
Conversion probability	4
Muon reconstruction efficiency	1
Trigger efficiency	1
Acceptance	3
Fit model	6
Statistical	18
Systematic	13
Total	22

Table 4. Sources of systematic uncertainty on the measurement of $\mathcal{B}(B^\pm \to \chi_{c1} K^\pm)$.

uncertainty on the measurement, neglecting conversion-related systematic uncertainties). The precision of this measurement is significantly better than previous measurements from hadron collider experiments [4].

8 Conclusion

The cross-sections for prompt and non-prompt χ_{c1} and χ_{c2} production have been measured in $4.5\,\text{fb}^{-1}$ of pp collisions at $\sqrt{s} = 7$ TeV with the ATLAS detector at the LHC. The χ_c states are reconstructed from the radiative decay $\chi_c \to J/\psi\,\gamma$. The measurements are performed as a function of both $p_{\text{T}}^{J/\psi}$ and $p_{\text{T}}^{\chi_c}$ within the rapidity interval $|y^{J/\psi}| < 0.75$. The results, measured as a function of $p_{\text{T}}^{J/\psi}$ and $p_{\text{T}}^{\chi_c}$, are presented within the regions $10 \le p_{\text{T}}^{J/\psi} < 30$ GeV and $12 \le p_{\text{T}}^{\chi_c} < 30$ GeV, respectively. The production rate of the χ_{c2} state is measured relative to the χ_{c1} state for both prompt and non-prompt production as a function of $p_{\text{T}}^{J/\psi}$. The measurements of prompt χ_c are combined with existing ATLAS measurements of prompt J/ψ production to derive the fraction of prompt J/ψ produced in feed-down from χ_c decays. The fractions of χ_{c1} and χ_{c2} produced in the decays of b-hadrons are also presented as functions of $p_{\text{T}}^{\chi_c}$.

The measurements of prompt χ_c production are compared to the theoretical predictions of NLO NRQCD, the k_{T} factorisation approach and the Colour Singlet Model. The NRQCD predictions generally agree well with the data. The k_{T} factorisation approach predicts a cross-section significantly in excess of the measurement while the CSM prediction significantly underestimates the data. This suggests that higher-order corrections or colour-octet contributions to the cross-sections not included in either prediction may be numerically important. The measurements of non-prompt χ_c production generally agree well with predictions based upon the FONLL approach.

The branching fraction $\mathcal{B}(B^\pm \to \chi_{c1} K^\pm) = (4.9 \pm 0.9\,\text{(stat.)} \pm 0.6\,\text{(syst.)}) \times 10^{-4}$ is also measured with the same dataset and χ_c event selection. The measured value agrees well with the world average and supports the estimate of the conversion reconstruction efficiencies derived from simulation.

Acknowledgements

References

[1] G. T. Bodwin, E. Braaten, and G. P. Lepage, *Rigorous QCD analysis of inclusive annihilation and production of heavy quarkonium*, *Phys. Rev.* **D 51** (1995) 1125.

[2] N. Brambilla, et al., *Heavy quarkonium: progress, puzzles, and opportunities*, *Eur. Phys. J.* **C 71** (2011) 1534, [arXiv:1010.5827].

[3] M. Butenschoen and B. A. Kniehl, *World data of J/ψ production consolidate NRQCD factorization at NLO*, *Phys. Rev.* **D 84** (2011) 051501, [arXiv:1105.0820].

[4] **Particle Data Group**, J. Beringer et al., *Review of Particle Physics (RPP)*, *Phys. Rev.* **D 86** (2012) 010001.

[5] P. Faccioli, C. Lourenco, J. Seixas and H. K. Woehri, *Study of ψ′ and χ_c decays as feed-down sources of J/ψ hadro-production*, *JHEP* **10** (2008) 004, [arXiv:0809.2153].

[6] M. Cacciari et al., *Theoretical predictions for charm and bottom production at the LHC*, *JHEP* **10** (2012) 137, [arXiv:1205.6344].

[7] M. Cacciari, M. Greco, and P. Nason, *The p_T spectrum in heavy flavor hadroproduction*, *JHEP* **05** (1998) 007, [hep-ph/9803400].

[8] **ATLAS** Collaboration, *Measurement of the differential cross-sections of inclusive, prompt and non-prompt J/ψ production in proton-proton collisions at $\sqrt{s} = 7$ TeV*, *Nucl. Phys.* **B 850** (2011) 387, [arXiv:1104.3038].

[9] **CMS** Collaboration, *J/ψ and $\psi(2S)$ production in pp collisions at $\sqrt{s} = 7$ TeV*, *JHEP* **02** (2012) 011, [arXiv:1111.1557].

[10] **LHCb** Collaboration, R. Aaij et al., *Measurement of J/ψ production in pp collisions at $\sqrt{s} = 7$ TeV*, Eur. Phys. J. **C 71** (2011) 1645, [arXiv:1103.0423].

[11] **ALICE** Collaboration, B. Abelev et al., *J/ψ polarization in pp collisions at $\sqrt{s} = 7$ TeV*, *Phys. Rev. Lett.* **108** (2012) 082001, [arXiv:1111.1630]

[12] **ALICE** Collaboration, B. Abelev et al., *Measurement of prompt J/ψ and beauty hadron production cross sections at mid-rapidity in pp collisions at $\sqrt{s} = 7$ TeV*, *JHEP* **11** (2012) 065, [arXiv:1205.5880].

[13] **LHCb** Collaboration, R. Aaij et al., *Measurement of the cross-section ratio $\sigma(\chi_{c2})/\sigma(\chi_{c1})$ for prompt χ_c production at $\sqrt{s} = 7$ TeV* , *Phys. Lett.* **B 714** (2012) 215, [arXiv:1202.1080].

[14] **LHCb** Collaboration, R. Aaij et al., *Measurement of the relative rate of prompt χ_{c0}, χ_{c1} and χ_{c2} production at $\sqrt{s} = 7 TeV$*, *JHEP* **10** (2013) 115, [arXiv:1307.4285].

[15] **LHCb** Collaboration, R. Aaij et al., *Measurement of the ratio of prompt χ_c to J/ψ production in pp collisions at $\sqrt{s} = 7$ TeV*, *Phys. Lett.* **B 718** (2012) 431, [arXiv:1204.1462].

[16] **CMS** Collaboration, *Measurement of the relative prompt production rate of χ_{c2} and χ_{c1} in pp collisions at $\sqrt{s} = 7$ TeV*, *Eur. Phys. J.* **C 72** (2012) 2251, [arXiv:1210.0875].

[17] **CDF** Collaboration, F. Abe et al., *Production of J/ψ mesons from χ_c meson decays in $p\bar{p}$ collisions at $\sqrt{s} = 1.8$ TeV*, *Phys. Rev. Lett.* **79** (1997) 578.

[18] **CDF** Collaboration, A. Abulencia et al., *Measurement of $\sigma_{\chi_{c2}} \mathcal{B}(\chi_{c2} \to J/\psi\gamma)/\sigma_{\chi_{c1}} \mathcal{B}(\chi_{c1} \to J/\psi\gamma)$ in $p\bar{p}$ collisions at $\sqrt{s} = 1.96$ TeV*, *Phys. Rev. Lett.* **98** (2007) 232001, [hep-ex/0703028].

[19] Y.-Q. Ma, K. Wang, and K.-T. Chao, *QCD radiative corrections to χ_{cJ} production at hadron colliders*, *Phys. Rev.* **D 83** (2011) 111503, [arXiv:1002.3987].

[20] **ATLAS** Collaboration, *The ATLAS Experiment at the CERN Large Hadron Collider*, *JINST* **3** (2008) S08003.

[21] T. Sjöstrand, S. Mrenna, and P. Z. Skands, *PYTHIA 6.4 Physics and Manual*, *JHEP* **05** (2006) 026, [hep-ph/0603175].

[22] **ATLAS** Collaboration, *ATLAS tunes of PYTHIA 6 and Pythia 8 for MC11*, ATL-PHYS-PUB-2011-009, 2011.

[23] **GEANT4** Collaboration, S. Agostinelli et al., *GEANT4: A Simulation toolkit*, *Nucl. Instrum. Meth.* **A506** (2003) 250.

[24] **ATLAS** Collaboration, *The ATLAS Simulation Infrastructure*, *Eur. Phys. J.* **C 70** (2010) 823, [arXiv:1005.4568].

[25] P. Faccioli, C. Lourenco, J. Seixas, and H. K. Wohri, *Determination of χ_c and χ_b polarizations from dilepton angular distributions in radiative decays*, *Phys. Rev.* **D 83** (2011) 096001, [arXiv:1103.4882].

[26] **ATLAS** Collaboration, *Measurement of Upsilon production in 7 TeV pp collisions at ATLAS*, *Phys. Rev.* **D 87** (2013) 052004, [arXiv:1211.7255].

[27] **ATLAS** Collaboration, *A study of the material in the ATLAS inner detector using secondary hadronic interactions*, *JINST* **7** (2012) P01013, [arXiv:1110.6191].

[28] G. Punzi, *Comments on likelihood fits with variable resolution*, eConf C **030908** (2003) WELT002 [arXiv:physics/0401045].

[29] M. Oreglia, *A Study of the reactions $\psi' \to \gamma\gamma\psi$*. PhD thesis, Stanford University, 1980, SLAC-R-0236.
J. Gaiser, *Charmonium spectroscopy from radiative decays of the J/ψ and ψ'*. PhD thesis, Stanford University, 1982, SLAC-R-0255.
T. Skwarnicki, *A study of the radiative cascade transitions between the Υ' and Υ resonances*. PhD thesis, Institute of Nuclear Physics, Cracow, 1986, DESY-F31-86-02.

[30] **ATLAS** Collaboration, *Measurements of Higgs boson production and couplings in diboson final states with the ATLAS detector at the LHC*, Phys. Lett. **B 726** (2013) 88, [arXiv:1307.1427].

[31] **ATLAS** Collaboration, *Improved luminosity determination in pp collisions at $\sqrt{s} = 7$ TeV using the ATLAS detector at the LHC*, Eur. Phys. J. **C 73** (2013) 2518 [arXiv:1302.4393].

[32] H.-S. Shao, *HELAC-Onia: an automatic matrix element generator for heavy quarkonium physics*, Comput. Phys. Commun. **184** (2013) 2562, [arXiv:1212.5293].

[33] Y.-Q. Ma, K. Wang, and K.-T. Chao, *$J/\psi(\psi')$ production at the Tevatron and LHC at $\mathcal{O}(\alpha_s^4 v^4)$ in nonrelativistic QCD*, Phys. Rev. Lett. **106** (2011) 042002, [arXiv:1009.3655].

[34] S. Baranov, A. Lipatov, and N. Zotov, *Prompt J/ψ production at LHC: new evidence for the k_t-factorization*, Phys. Rev. **D 85** (2012) 014034, [arXiv:1108.2856].

[35] S. Baranov, *$\sigma(\chi_{c2})/\sigma(\chi_{c1})$ ratio in the k_T-factorization approach*, Phys. Rev. **D 83** (2011) 034035.

[36] L. A. Harland-Lang and W. J. Stirling, *CHIGEN: Monte Carlo Event Generator for inclusive χ_{cJ} production*, http://superchic.hepforge.org/chigen.html

[37] R. Baier and R. Rückl, *Hadronic Production of J/ψ and Υ: Transverse Momentum Distributions*, Phys. Lett. **B 102** (1981) 364.

[38] R. Baier and R. Rückl, *Hadronic Collisions: A Quarkonium Factory*, Z. Phys. **C 19** (1983) 251.

[39] E. L. Berger and D. L. Jones, *Inelastic Photoproduction of J/ψ and Υ by Gluons*, Phys. Rev. **D 23** (1981) 1521.

[40] C.-H. Chang, *Hadronic production of J/ψ associated with a gluon*, Nucl. Phys. **B 172** (1980) 425.

[41] **BaBar** Collaboration, B. Aubert et al., *Study of inclusive production of charmonium mesons in B decays*, Phys. Rev. **D 67** (2003) 032002, [hep-ex/0107025].

[42] **CMS** Collaboration, *Measurement of the prompt J/ψ and $\psi(2S)$ polarizations in pp collisions at $\sqrt{s} = 7$ TeV*, Phys. Lett. **B 727** (2013) 381, [arXiv:1307.6070].

[43] **LHCb** Collaboration, R. Aaij et al., *Measurement of J/ψ polarization in pp collisions at $\sqrt{s} = 7$ TeV*, *Eur. Phys. J.* **C 73** (2013) 2631, [arXiv:1307.6379].

[44] **ATLAS** Collaboration, *Measurement of the differential cross-section of B^+ meson production in pp collisions at $\sqrt{s} = 7$ TeV at ATLAS*, JHEP **10** (2013) 042, [arXiv:1307.0126].

[45] K. S. Cranmer, *Kernel estimation in high-energy physics*, *Comput. Phys. Commun.* **136** (2001) 198, [`hep-ex/0011057`].

[46] **Belle** Collaboration, V. Bhardwaj et al., *Observation of $X(3872) \to J/\psi\gamma$ and search for $X(3872) \to \psi'\gamma$ in B decays*, *Phys. Rev. Lett.* **107** (2011) 091803 [`arXiv:1105.0177`].

[47] **BaBar** Collaboration, B. Aubert et al., *Evidence for $X(3872) \to \psi(2S)\gamma$ in $B^{\pm} \to X(3872)K^{\pm}$ decays, and a study of $B \to c\bar{c}\gamma K$*, *Phys. Rev. Lett.* **102** (2009) 132001 [`arXiv:0809.0042`].

A   Tabulated results

The following tables show the results presented in section 6. Statistical and systematic uncertainties are shown for each measurement along with the uncertainty envelope associated with the unknown χ_c spin alignment.

$p_T^{J/\psi}$ [GeV]	$\langle p_T^{J/\psi} \rangle$ [GeV]	J	$\mathcal{B}\left(\chi_{cJ} \to J/\psi\,\gamma\right) \cdot \mathcal{B}\left(J/\psi \to \mu^+\mu^-\right) \cdot \frac{\mathrm{d}\sigma_J^{\mathrm{P}}}{\mathrm{d}p_T}$ [pb/GeV]
			Value	(stat.)	(syst.)	Spin-alignment envelope
10.0–12.0	11.0	1	218	±9	±28	+69 −28
	11.0	2	95	±6	±12	+34 −21
12.0–14.0	12.9	1	90	±4	±11	+31 −12
	12.9	2	40	±3	±5	+15 −10
14.0–16.0	14.9	1	37	±2	±5	+13 −5
	14.9	2	19	±2	±2	+7 −5
16.0–18.0	16.9	1	21	±1	±3	+7 −3
	16.9	2	10	±1	±1	+4 −2
18.0–30.0	22.1	1	4.8	±0.2	±0.6	+1.5 −0.6
	22.1	2	1.9	±0.2	±0.2	+0.6 −0.4

Table 5. Differential cross-section for prompt χ_{c1} and χ_{c2} production, measured in bins of $p_T^{J/\psi}$.

$p_T^{J/\psi}$ [GeV]	$\langle p_T^{J/\psi} \rangle$ [GeV]	J	$\mathcal{B}\left(\chi_{cJ} \to J/\psi\,\gamma\right) \cdot \mathcal{B}\left(J/\psi \to \mu^+\mu^-\right) \cdot \frac{\mathrm{d}\sigma_J^{\mathrm{NP}}}{\mathrm{d}p_T}$ [pb/GeV]
			Value	(stat.)	(syst.)	Spin-alignment envelope
10.0–12.0	11.0	1	60	±8	±8	+19 −8
	11.0	2	15	±6	±3	+5 −3
12.0–14.0	12.9	1	30	±3	±4	+10 −4
	12.9	2	4.1	±2.8	±0.7	+1.6 −1.0
14.0–16.0	14.9	1	15	±2	±2	+5 −2
	14.9	2	2.9	±1.3	±0.5	+1.1 −0.7
16.0–18.0	16.9	1	5.8	±1.1	±0.8	+1.9 −0.7
	16.9	2	0.9	±0.8	±0.2	+0.3 −0.2
18.0–30.0	22.1	1	2.1	±0.3	±0.3	+0.6 −0.2
	22.1	2	0.4	±0.1	±0.1	+0.1 −0.1

Table 6. Differential cross-section for non-prompt χ_{c1} and χ_{c2} production, measured in bins of $p_T^{J/\psi}$.

$p_{\mathrm{T}}^{\chi_c}$ [GeV]	$\langle p_{\mathrm{T}}^{\chi_c}\rangle$ [GeV]	J	$\mathcal{B}(\chi_{cJ}\to J/\psi\,\gamma)\cdot\mathcal{B}(J/\psi\to\mu^+\mu^-)\cdot\frac{\mathrm{d}\sigma_J^{\mathrm{P}}}{\mathrm{d}p_{\mathrm{T}}}$ [pb/GeV]			
			Value	(stat.)	(syst.)	Spin-alignment envelope
12.0–14.0	12.9	1	136	±7	±16	+41 −17
	12.9	2	73	±5	±9	+25 −15
14.0–16.0	14.9	1	71	±3	±9	+22 −8
	14.9	2	29	±2	±4	+10 −6
16.0–18.0	16.9	1	31	±2	±4	+10 −4
	16.9	2	18	±1	±2	+6 −4
18.0–22.0	19.6	1	15.4	±0.8	±1.8	+4.4 −1.8
	19.7	2	7.0	±0.6	±0.9	+2.1 −1.4
22.0–30.0	25.0	1	4.0	±0.2	±0.5	+1.0 −0.4
	25.0	2	1.7	±0.2	±0.2	+0.4 −0.3

Table 7. Differential cross-section for prompt χ_{c1} and χ_{c2} production, measured in bins of $p_{\mathrm{T}}^{\chi_c}$.

$p_{\mathrm{T}}^{\chi_c}$ [GeV]	$\langle p_{\mathrm{T}}^{\chi_c}\rangle$ [GeV]	J	$\mathcal{B}(\chi_{cJ}\to J/\psi\,\gamma)\cdot\mathcal{B}(J/\psi\to\mu^+\mu^-)\cdot\frac{\mathrm{d}\sigma_J^{\mathrm{NP}}}{\mathrm{d}p_{\mathrm{T}}}$ [pb/GeV]			
			Value	(stat.)	(syst.)	Spin-alignment envelope
12.0–14.0	12.9	1	42	±6	±5	+13 −5
	12.9	2	9	±4	±1	+3 −2
14.0–16.0	14.9	1	23	±2	±3	+7 −3
	14.9	2	2.7	±1.8	±0.4	+0.9 −0.6
16.0–18.0	16.9	1	10	±2	±1	+3 −1
	16.9	2	1.8	±0.9	±0.3	+0.6 −0.4
18.0–22.0	19.6	1	5.2	±0.8	±0.6	+1.5 −0.6
	19.7	2	0.9	±0.5	±0.1	+0.3 −0.2
22.0–30.0	25.0	1	2.1	±0.3	±0.3	+0.5 −0.2
	25.0	2	0.27	±0.17	±0.04	+0.07 −0.05

Table 8. Differential cross-section for non-prompt χ_{c1} and χ_{c2} production, measured in bins of $p_{\mathrm{T}}^{\chi_c}$.

	Prompt $R\chi_c$			
$p_{\mathrm{T}}^{J/\psi}$ [GeV]	Value	(stat.)	(syst.)	Spin-alignment envelope
10.0–12.0	0.24	± 0.02	± 0.04	$+0.08\ -0.04$
12.0–14.0	0.26	± 0.01	± 0.04	$+0.09\ -0.04$
14.0–16.0	0.23	± 0.02	± 0.04	$+0.08\ -0.04$
16.0–18.0	0.28	± 0.03	± 0.05	$+0.10\ -0.05$
18.0–30.0	0.27	± 0.03	± 0.05	$+0.09\ -0.04$

Table 9. Fraction of prompt J/ψ produced in feed-down from χ_c decays as a function of $p_{\mathrm{T}}^{J/\psi}$. The spin alignment envelope assumes that prompt J/ψ are produced unpolarised and represents the maximum uncertainty in the result due to the unknown χ_c spin alignment.

	Prompt $\frac{\sigma(\chi_{c2})\cdot\mathcal{B}(\chi_{c2}\to J/\psi\gamma)}{\sigma(\chi_{c1})\cdot\mathcal{B}(\chi_{c1}\to J/\psi\gamma)}$			
$p_{\mathrm{T}}^{J/\psi}$ [GeV]	Value	(stat.)	(syst.)	Spin-alignment envelope
10.0–12.0	0.43	± 0.04	± 0.03	$+0.24\ -0.18$
12.0–14.0	0.44	± 0.04	± 0.03	$+0.26\ -0.19$
14.0–16.0	0.52	± 0.06	± 0.04	$+0.30\ -0.23$
16.0–18.0	0.48	± 0.06	± 0.03	$+0.27\ -0.21$
18.0–30.0	0.40	± 0.04	± 0.03	$+0.20\ -0.16$

Table 10. Production rate of prompt χ_{c2} relative to prompt χ_{c1}, measured in bins of $p_{\mathrm{T}}^{J/\psi}$.

	Non-prompt $\frac{\sigma(\chi_{c2})\cdot\mathcal{B}(\chi_{c2}\to J/\psi\gamma)}{\sigma(\chi_{c1})\cdot\mathcal{B}(\chi_{c1}\to J/\psi\gamma)}$			
$p_{\mathrm{T}}^{J/\psi}$ [GeV]	Value	(stat.)	(syst.)	Spin-alignment envelope
10.0–12.0	0.25	± 0.10	± 0.03	$+0.14\ -0.10$
12.0–14.0	0.14	± 0.09	± 0.02	$+0.08\ -0.06$
14.0–16.0	0.19	± 0.09	± 0.02	$+0.11\ -0.08$
16.0–18.0	0.16	± 0.14	± 0.02	$+0.09\ -0.07$
18.0–30.0	0.18	± 0.07	± 0.02	$+0.09\ -0.07$

Table 11. Production rate of non-prompt χ_{c2} relative to non-prompt χ_{c1}, measured in bins of $p_{\mathrm{T}}^{J/\psi}$.

$p_\mathrm{T}^{\chi_c}$ [GeV]	J	Value	(stat.)	(syst.)	Spin-alignment envelope
				$f_\text{non-prompt}$	
12.0–14.0	1	0.23	±0.02	±0.02	+0.08 −0.07
	2	0.11	±0.04	±0.01	+0.07 −0.04
14.0–16.0	1	0.24	±0.02	±0.02	+0.08 −0.07
	2	0.09	±0.05	±0.01	+0.05 −0.03
16.0–18.0	1	0.2	±0.03	±0.02	+0.08 −0.06
	2	0.09	±0.04	±0.01	+0.05 −0.03
18.0–22.0	1	0.25	±0.03	±0.02	+0.08 −0.07
	2	0.11	±0.07	±0.01	+0.06 −0.04
22.0–30.0	1	0.34	±0.03	±0.03	+0.08 −0.07
	2	0.14	±0.07	±0.02	+0.06 −0.04

Table 12. Fraction of χ_{c1} and χ_{c2} produced in b-hadron decays as a function of $p_\mathrm{T}^{\chi_c}$.

Bin	Yield	Helicity 0	Helicity ±1	Helicity ±2	AZ+	AZ−
$10 \leq p_{\mathrm{T}}^{J/\psi} < 12$ GeV	P1	1.32	0.89	−	0.91	0.87
	P2	0.78	0.88	1.35	1.10	1.04
	NP1	1.31	0.89	−	0.91	0.87
	NP2	0.77	0.87	1.37	1.11	1.04
$12 \leq p_{\mathrm{T}}^{J/\psi} < 14$ GeV	P1	1.34	0.88	−	0.89	0.87
	P2	0.76	0.87	1.38	1.10	1.06
	NP1	1.33	0.88	−	0.89	0.87
	NP2	0.76	0.87	1.38	1.10	1.06
$14 \leq p_{\mathrm{T}}^{J/\psi} < 16$ GeV	P1	1.35	0.88	−	0.88	0.87
	P2	0.76	0.87	1.38	1.09	1.07
	NP1	1.34	0.88	−	0.89	0.87
	NP2	0.76	0.87	1.38	1.09	1.07
$16 \leq p_{\mathrm{T}}^{J/\psi} < 18$ GeV	P1	1.35	0.88	−	0.88	0.87
	P2	0.76	0.87	1.37	1.09	1.07
	NP1	1.33	0.88	−	0.88	0.87
	NP2	0.76	0.87	1.37	1.09	1.07
$18 \leq p_{\mathrm{T}}^{J/\psi} < 30$ GeV	P1	1.32	0.88	−	0.89	0.88
	P2	0.78	0.88	1.33	1.08	1.07
	NP1	1.30	0.89	−	0.89	0.88
	NP2	0.78	0.88	1.33	1.07	1.06
$12 \leq p_{\mathrm{T}}^{\chi_c} < 14$ GeV	P1	1.31	0.89	−	0.91	0.87
	P2	0.78	0.88	1.35	1.10	1.04
	NP1	1.31	0.89	−	0.91	0.87
	NP2	0.78	0.88	1.35	1.10	1.04
$14 \leq p_{\mathrm{T}}^{\chi_c} < 16$ GeV	P1	1.32	0.89	−	0.90	0.88
	P2	0.78	0.88	1.35	1.09	1.05
	NP1	1.32	0.89	−	0.90	0.88
	NP2	0.78	0.88	1.35	1.09	1.05
$16 \leq p_{\mathrm{T}}^{\chi_c} < 18$ GeV	P1	1.32	0.89	−	0.89	0.88
	P2	0.79	0.88	1.33	1.08	1.06
	NP1	1.32	0.89	−	0.89	0.88
	NP2	0.79	0.88	1.33	1.08	1.06
$18 \leq p_{\mathrm{T}}^{\chi_c} < 22$ GeV	P1	1.30	0.89	−	0.90	0.89
	P2	0.79	0.89	1.31	1.07	1.06
	NP1	1.30	0.89	−	0.90	0.89
	NP2	0.79	0.89	1.31	1.07	1.06
$22 \leq p_{\mathrm{T}}^{\chi_c} < 30$ GeV	P1	1.26	0.90	−	0.90	0.90
	P2	0.81	0.90	1.27	1.06	1.05
	NP1	1.26	0.90	−	0.90	0.90
	NP2	0.81	0.90	1.27	1.06	1.05

Table 13. Scale factors that modify the central cross-section values, evaluated assuming isotropic decay angular distributions, to a given spin alignment scenario. The different spin alignment scenarios are defined in table 1. The labels (N)P1 and (N)P2 correspond to (non-)prompt χ_{c1} and (non-)prompt χ_{c2} respectively.

The ATLAS Collaboration

G. Aad[48], T. Abajyan[21], B. Abbott[112], J. Abdallah[12], S. Abdel Khalek[116], O. Abdinov[11],
R. Aben[106], B. Abi[113], M. Abolins[89], O.S. AbouZeid[159], H. Abramowicz[154], H. Abreu[137],
Y. Abulaiti[147a,147b], B.S. Acharya[165a,165b,a], L. Adamczyk[38a], D.L. Adams[25], T.N. Addy[56],
J. Adelman[177], S. Adomeit[99], T. Adye[130], S. Aefsky[23], T. Agatonovic-Jovin[13b],
J.A. Aguilar-Saavedra[125f,125a], M. Agustoni[17], S.P. Ahlen[22], A. Ahmad[149],
F. Ahmadov[64,b], G. Aielli[134a,134b], T.P.A. Åkesson[80], G. Akimoto[156], A.V. Akimov[95],
M.A. Alam[76], J. Albert[170], S. Albrand[55], M.J. Alconada Verzini[70], M. Aleksa[30],
I.N. Aleksandrov[64], F. Alessandria[90a], C. Alexa[26a], G. Alexander[154], G. Alexandre[49],
T. Alexopoulos[10], M. Alhroob[165a,165c], M. Aliev[16], G. Alimonti[90a], L. Alio[84], J. Alison[31],
B.M.M. Allbrooke[18], L.J. Allison[71], P.P. Allport[73], S.E. Allwood-Spiers[53], J. Almond[83],
A. Aloisio[103a,103b], R. Alon[173], A. Alonso[36], F. Alonso[70], A. Altheimer[35],
B. Alvarez Gonzalez[89], M.G. Alviggi[103a,103b], K. Amako[65], Y. Amaral Coutinho[24a],
C. Amelung[23], V.V. Ammosov[129,*], S.P. Amor Dos Santos[125a,125c], A. Amorim[125a,125b],
S. Amoroso[48], N. Amram[154], G. Amundsen[23], C. Anastopoulos[30], L.S. Ancu[17],
N. Andari[30], T. Andeen[35], C.F. Anders[58b], G. Anders[58a], K.J. Anderson[31],
A. Andreazza[90a,90b], V. Andrei[58a], X.S. Anduaga[70], S. Angelidakis[9], P. Anger[44],
A. Angerami[35], F. Anghinolfi[30], A.V. Anisenkov[108], N. Anjos[125a], A. Annovi[47],
A. Antonaki[9], M. Antonelli[47], A. Antonov[97], J. Antos[145b], F. Anulli[133a], M. Aoki[102],
L. Aperio Bella[18], R. Apolle[119,c], G. Arabidze[89], I. Aracena[144], Y. Arai[65], A.T.H. Arce[45],
S. Arfaoui[149], J-F. Arguin[94], S. Argyropoulos[42], E. Arik[19a,*], M. Arik[19a],
A.J. Armbruster[88], O. Arnaez[82], V. Arnal[81], O. Arslan[21], A. Artamonov[96], G. Artoni[23],
S. Asai[156], N. Asbah[94], S. Ask[28], B. Åsman[147a,147b], L. Asquith[6], K. Assamagan[25],
R. Astalos[145a], A. Astbury[170], M. Atkinson[166], N.B. Atlay[142], B. Auerbach[6], E. Auge[116],
K. Augsten[127], M. Aurousseau[146b], G. Avolio[30], G. Azuelos[94,d], Y. Azuma[156],
M.A. Baak[30], C. Bacci[135a,135b], A.M. Bach[15], H. Bachacou[137], K. Bachas[155], M. Backes[30],
M. Backhaus[21], J. Backus Mayes[144], E. Badescu[26a], P. Bagiacchi[133a,133b],
P. Bagnaia[133a,133b], Y. Bai[33a], D.C. Bailey[159], T. Bain[35], J.T. Baines[130], O.K. Baker[177],
S. Baker[77], P. Balek[128], F. Balli[137], E. Banas[39], Sw. Banerjee[174], D. Banfi[30],
A. Bangert[151], V. Bansal[170], H.S. Bansil[18], L. Barak[173], S.P. Baranov[95], T. Barber[48],
E.L. Barberio[87], D. Barberis[50a,50b], M. Barbero[84], T. Barillari[100], M. Barisonzi[176],
T. Barklow[144], N. Barlow[28], B.M. Barnett[130], R.M. Barnett[15], A. Baroncelli[135a],
G. Barone[49], A.J. Barr[119], F. Barreiro[81], J. Barreiro Guimarães da Costa[57],
R. Bartoldus[144], A.E. Barton[71], P. Bartos[145a], V. Bartsch[150], A. Bassalat[116], A. Basye[166],
R.L. Bates[53], L. Batkova[145a], J.R. Batley[28], M. Battistin[30], F. Bauer[137], H.S. Bawa[144,e],
T. Beau[79], P.H. Beauchemin[162], R. Beccherle[50a], P. Bechtle[21], H.P. Beck[17], K. Becker[176],
S. Becker[99], M. Beckingham[139], A.J. Beddall[19c], A. Beddall[19c], S. Bedikian[177],
V.A. Bednyakov[64], C.P. Bee[84], L.J. Beemster[106], T.A. Beermann[176], M. Begel[25],
K. Behr[119], C. Belanger-Champagne[86], P.J. Bell[49], W.H. Bell[49], G. Bella[154],
L. Bellagamba[20a], A. Bellerive[29], M. Bellomo[30], A. Belloni[57], O.L. Beloborodova[108,f],
K. Belotskiy[97], O. Beltramello[30], O. Benary[154], D. Benchekroun[136a], K. Bendtz[147a,147b],
N. Benekos[166], Y. Benhammou[154], E. Benhar Noccioli[49], J.A. Benitez Garcia[160b],

D.P. Benjamin[45], J.R. Bensinger[23], K. Benslama[131], S. Bentvelsen[106], D. Berge[30],
E. Bergeaas Kuutmann[16], N. Berger[5], F. Berghaus[170], E. Berglund[106], J. Beringer[15],
C. Bernard[22], P. Bernat[77], R. Bernhard[48], C. Bernius[78], F.U. Bernlochner[170], T. Berry[76],
P. Berta[128], C. Bertella[84], F. Bertolucci[123a,123b], M.I. Besana[90a], G.J. Besjes[105],
O. Bessidskaia[147a,147b], N. Besson[137], S. Bethke[100], W. Bhimji[46], R.M. Bianchi[124],
L. Bianchini[23], M. Bianco[30], O. Biebel[99], S.P. Bieniek[77], K. Bierwagen[54], J. Biesiada[15],
M. Biglietti[135a], J. Bilbao De Mendizabal[49], H. Bilokon[47], M. Bindi[20a,20b], S. Binet[116],
A. Bingul[19c], C. Bini[133a,133b], B. Bittner[100], C.W. Black[151], J.E. Black[144], K.M. Black[22],
D. Blackburn[139], R.E. Blair[6], J.-B. Blanchard[137], T. Blazek[145a], I. Bloch[42], C. Blocker[23],
W. Blum[82,*], U. Blumenschein[54], G.J. Bobbink[106], V.S. Bobrovnikov[108], S.S. Bocchetta[80],
A. Bocci[45], C.R. Boddy[119], M. Boehler[48], J. Boek[176], T.T. Boek[176], N. Boelaert[36],
J.A. Bogaerts[30], A.G. Bogdanchikov[108], A. Bogouch[91,*], C. Bohm[147a], J. Bohm[126],
V. Boisvert[76], T. Bold[38a], V. Boldea[26a], A.S. Boldyrev[98], N.M. Bolnet[137], M. Bomben[79],
M. Bona[75], M. Boonekamp[137], S. Bordoni[79], C. Borer[17], A. Borisov[129], G. Borissov[71],
M. Borri[83], S. Borroni[42], J. Bortfeldt[99], V. Bortolotto[135a,135b], K. Bos[106],
D. Boscherini[20a], M. Bosman[12], H. Boterenbrood[106], J. Bouchami[94], J. Boudreau[124],
E.V. Bouhova-Thacker[71], D. Boumediene[34], C. Bourdarios[116], N. Bousson[84],
S. Boutouil[136d], A. Boveia[31], J. Boyd[30], I.R. Boyko[64], I. Bozovic-Jelisavcic[13b],
J. Bracinik[18], P. Branchini[135a], A. Brandt[8], G. Brandt[15], O. Brandt[58a], U. Bratzler[157],
B. Brau[85], J.E. Brau[115], H.M. Braun[176,*], S.F. Brazzale[165a,165c], B. Brelier[159],
K. Brendlinger[121], R. Brenner[167], S. Bressler[173], T.M. Bristow[46], D. Britton[53],
F.M. Brochu[28], I. Brock[21], R. Brock[89], F. Broggi[90a], C. Bromberg[89], J. Bronner[100],
G. Brooijmans[35], T. Brooks[76], W.K. Brooks[32b], J. Brosamer[15], E. Brost[115], G. Brown[83],
J. Brown[55], P.A. Bruckman de Renstrom[39], D. Bruncko[145b], R. Bruneliere[48], S. Brunet[60],
A. Bruni[20a], G. Bruni[20a], M. Bruschi[20a], L. Bryngemark[80], T. Buanes[14], Q. Buat[55],
F. Bucci[49], P. Buchholz[142], R.M. Buckingham[119], A.G. Buckley[53], S.I. Buda[26a],
I.A. Budagov[64], B. Budick[109], F. Buehrer[48], L. Bugge[118], M.K. Bugge[118], O. Bulekov[97],
A.C. Bundock[73], M. Bunse[43], H. Burckhart[30], S. Burdin[73], T. Burgess[14],
B. Burghgrave[107], S. Burke[130], I. Burmeister[43], E. Busato[34], V. Büscher[82], P. Bussey[53],
C.P. Buszello[167], B. Butler[57], J.M. Butler[22], A.I. Butt[3], C.M. Buttar[53],
J.M. Butterworth[77], W. Buttinger[28], A. Buzatu[53], M. Byszewski[10], S. Cabrera Urbán[168],
D. Caforio[20a,20b], O. Cakir[4a], P. Calafiura[15], G. Calderini[79], P. Calfayan[99], R. Calkins[107],
L.P. Caloba[24a], R. Caloi[133a,133b], D. Calvet[34], S. Calvet[34], R. Camacho Toro[49],
P. Camarri[134a,134b], D. Cameron[118], L.M. Caminada[15], R. Caminal Armadans[12],
S. Campana[30], M. Campanelli[77], V. Canale[103a,103b], F. Canelli[31], A. Canepa[160a],
J. Cantero[81], R. Cantrill[76], T. Cao[40], M.D.M. Capeans Garrido[30], I. Caprini[26a],
M. Caprini[26a], M. Capua[37a,37b], R. Caputo[82], R. Cardarelli[134a], T. Carli[30], G. Carlino[103a],
L. Carminati[90a,90b], S. Caron[105], E. Carquin[32a], G.D. Carrillo-Montoya[146c], A.A. Carter[75],
J.R. Carter[28], J. Carvalho[125a,125c], D. Casadei[77], M.P. Casado[12], C. Caso[50a,50b,*],
E. Castaneda-Miranda[146b], A. Castelli[106], V. Castillo Gimenez[168], N.F. Castro[125a],
P. Catastini[57], A. Catinaccio[30], J.R. Catmore[71], A. Cattai[30], G. Cattani[134a,134b],
S. Caughron[89], V. Cavaliere[166], D. Cavalli[90a], M. Cavalli-Sforza[12], V. Cavasinni[123a,123b],
F. Ceradini[135a,135b], B. Cerio[45], K. Cerny[128], A.S. Cerqueira[24b], A. Cerri[150], L. Cerrito[75],

F. Cerutti[15], A. Cervelli[17], S.A. Cetin[19b], A. Chafaq[136a], D. Chakraborty[107],
I. Chalupkova[128], K. Chan[3], P. Chang[166], B. Chapleau[86], J.D. Chapman[28],
D. Charfeddine[116], D.G. Charlton[18], V. Chavda[83], C.A. Chavez Barajas[30],
S. Cheatham[86], S. Chekanov[6], S.V. Chekulaev[160a], G.A. Chelkov[64], M.A. Chelstowska[88],
C. Chen[63], H. Chen[25], K. Chen[149], L. Chen[33d,g], S. Chen[33c], X. Chen[174], Y. Chen[35],
Y. Cheng[31], A. Cheplakov[64], R. Cherkaoui El Moursli[136e], V. Chernyatin[25,*], E. Cheu[7],
L. Chevalier[137], V. Chiarella[47], G. Chiefari[103a,103b], J.T. Childers[30], A. Chilingarov[71],
G. Chiodini[72a], A.S. Chisholm[18], R.T. Chislett[77], A. Chitan[26a], M.V. Chizhov[64],
S. Chouridou[9], B.K.B. Chow[99], I.A. Christidi[77], D. Chromek-Burckhart[30], M.L. Chu[152],
J. Chudoba[126], G. Ciapetti[133a,133b], A.K. Ciftci[4a], R. Ciftci[4a], D. Cinca[62], V. Cindro[74],
A. Ciocio[15], M. Cirilli[88], P. Cirkovic[13b], Z.H. Citron[173], M. Citterio[90a], M. Ciubancan[26a],
A. Clark[49], P.J. Clark[46], R.N. Clarke[15], W. Cleland[124], J.C. Clemens[84], B. Clement[55],
C. Clement[147a,147b], Y. Coadou[84], M. Cobal[165a,165c], A. Coccaro[139], J. Cochran[63],
S. Coelli[90a], L. Coffey[23], J.G. Cogan[144], J. Coggeshall[166], J. Colas[5], B. Cole[35], S. Cole[107],
A.P. Colijn[106], C. Collins-Tooth[53], J. Collot[55], T. Colombo[58c], G. Colon[85],
G. Compostella[100], P. Conde Muiño[125a,125b], E. Coniavitis[167], M.C. Conidi[12],
I.A. Connelly[76], S.M. Consonni[90a,90b], V. Consorti[48], S. Constantinescu[26a],
C. Conta[120a,120b], G. Conti[57], F. Conventi[103a,h], M. Cooke[15], B.D. Cooper[77],
A.M. Cooper-Sarkar[119], N.J. Cooper-Smith[76], K. Copic[15], T. Cornelissen[176],
M. Corradi[20a], F. Corriveau[86,i], A. Corso-Radu[164], A. Cortes-Gonzalez[12], G. Cortiana[100],
G. Costa[90a], M.J. Costa[168], D. Costanzo[140], D. Côté[8], G. Cottin[32a], L. Courneyea[170],
G. Cowan[76], B.E. Cox[83], K. Cranmer[109], G. Cree[29], S. Crépé-Renaudin[55], F. Crescioli[79],
M. Crispin Ortuzar[119], M. Cristinziani[21], G. Crosetti[37a,37b], C.-M. Cuciuc[26a],
C. Cuenca Almenar[177], T. Cuhadar Donszelmann[140], J. Cummings[177], M. Curatolo[47],
C. Cuthbert[151], H. Czirr[142], P. Czodrowski[44], Z. Czyczula[177], S. D'Auria[53],
M. D'Onofrio[73], A. D'Orazio[133a,133b], M.J. Da Cunha Sargedas De Sousa[125a,125b],
C. Da Via[83], W. Dabrowski[38a], A. Dafinca[119], T. Dai[88], F. Dallaire[94], C. Dallapiccola[85],
M. Dam[36], A.C. Daniells[18], M. Dano Hoffmann[36], V. Dao[105], G. Darbo[50a], G.L. Darlea[26c],
S. Darmora[8], J.A. Dassoulas[42], W. Davey[21], C. David[170], T. Davidek[128], E. Davies[119,c],
M. Davies[94], O. Davignon[79], A.R. Davison[77], Y. Davygora[58a], E. Dawe[143], I. Dawson[140],
R.K. Daya-Ishmukhametova[23], K. De[8], R. de Asmundis[103a], S. De Castro[20a,20b],
S. De Cecco[79], J. de Graat[99], N. De Groot[105], P. de Jong[106], C. De La Taille[116],
H. De la Torre[81], F. De Lorenzi[63], L. De Nooij[106], D. De Pedis[133a], A. De Salvo[133a],
U. De Sanctis[165a,165c], A. De Santo[150], J.B. De Vivie De Regie[116], G. De Zorzi[133a,133b],
W.J. Dearnaley[71], R. Debbe[25], C. Debenedetti[46], B. Dechenaux[55], D.V. Dedovich[64],
J. Degenhardt[121], J. Del Peso[81], T. Del Prete[123a,123b], T. Delemontex[55], F. Deliot[137],
M. Deliyergiyev[74], A. Dell'Acqua[30], L. Dell'Asta[22], M. Della Pietra[103a,h], D. della Volpe[49],
M. Delmastro[5], P.A. Delsart[55], C. Deluca[106], S. Demers[177], M. Demichev[64], A. Demilly[79],
B. Demirkoz[12,j], S.P. Denisov[129], D. Derendarz[39], J.E. Derkaoui[136d], F. Derue[79],
P. Dervan[73], K. Desch[21], P.O. Deviveiros[106], A. Dewhurst[130], B. DeWilde[149],
S. Dhaliwal[106], R. Dhullipudi[78,k], A. Di Ciaccio[134a,134b], L. Di Ciaccio[5],
A. Di Domenico[133a,133b], C. Di Donato[103a,103b], A. Di Girolamo[30], B. Di Girolamo[30],
A. Di Mattia[153], B. Di Micco[135a,135b], R. Di Nardo[47], A. Di Simone[48], R. Di Sipio[20a,20b],

D. Di Valentino[29], M.A. Diaz[32a], E.B. Diehl[88], J. Dietrich[42], T.A. Dietzsch[58a], S. Diglio[87],
K. Dindar Yagci[40], J. Dingfelder[21], C. Dionisi[133a,133b], P. Dita[26a], S. Dita[26a], F. Dittus[30],
F. Djama[84], T. Djobava[51b], M.A.B. do Vale[24c], A. Do Valle Wemans[125a,125g],
T.K.O. Doan[5], D. Dobos[30], E. Dobson[77], J. Dodd[35], C. Doglioni[49], T. Doherty[53],
T. Dohmae[156], J. Dolejsi[128], Z. Dolezal[128], B.A. Dolgoshein[97,*], M. Donadelli[24d],
S. Donati[123a,123b], P. Dondero[120a,120b], J. Donini[34], J. Dopke[30], A. Doria[103a],
A. Dos Anjos[174], A. Dotti[123a,123b], M.T. Dova[70], A.T. Doyle[53], M. Dris[10], J. Dubbert[88],
S. Dube[15], E. Dubreuil[34], E. Duchovni[173], G. Duckeck[99], O.A. Ducu[26a], D. Duda[176],
A. Dudarev[30], F. Dudziak[63], L. Duflot[116], L. Duguid[76], M. Dührssen[30], M. Dunford[58a],
H. Duran Yildiz[4a], M. Düren[52], M. Dwuznik[38a], J. Ebke[99], W. Edson[2], C.A. Edwards[76],
N.C. Edwards[46], W. Ehrenfeld[21], T. Eifert[144], G. Eigen[14], K. Einsweiler[15],
E. Eisenhandler[75], T. Ekelof[167], M. El Kacimi[136c], M. Ellert[167], S. Elles[5], F. Ellinghaus[82],
K. Ellis[75], N. Ellis[30], J. Elmsheuser[99], M. Elsing[30], D. Emeliyanov[130], Y. Enari[156],
O.C. Endner[82], M. Endo[117], R. Engelmann[149], J. Erdmann[177], A. Ereditato[17],
D. Eriksson[147a], G. Ernis[176], J. Ernst[2], M. Ernst[25], J. Ernwein[137], D. Errede[166],
S. Errede[166], E. Ertel[82], M. Escalier[116], H. Esch[43], C. Escobar[124], X. Espinal Curull[12],
B. Esposito[47], F. Etienne[84], A.I. Etienvre[137], E. Etzion[154], D. Evangelakou[54], H. Evans[60],
L. Fabbri[20a,20b], G. Facini[30], R.M. Fakhrutdinov[129], S. Falciano[133a], Y. Fang[33a],
M. Fanti[90a,90b], A. Farbin[8], A. Farilla[135a], T. Farooque[159], S. Farrell[164],
S.M. Farrington[171], P. Farthouat[30], F. Fassi[168], P. Fassnacht[30], D. Fassouliotis[9],
B. Fatholahzadeh[159], A. Favareto[50a,50b], L. Fayard[116], P. Federic[145a], O.L. Fedin[122],
W. Fedorko[169], M. Fehling-Kaschek[48], L. Feligioni[84], C. Feng[33d], E.J. Feng[6], H. Feng[88],
A.B. Fenyuk[129], W. Fernando[6], S. Ferrag[53], J. Ferrando[53], V. Ferrara[42], A. Ferrari[167],
P. Ferrari[106], R. Ferrari[120a], D.E. Ferreira de Lima[53], A. Ferrer[168], D. Ferrere[49],
C. Ferretti[88], A. Ferretto Parodi[50a,50b], M. Fiascaris[31], F. Fiedler[82], A. Filipčič[74],
M. Filipuzzi[42], F. Filthaut[105], M. Fincke-Keeler[170], K.D. Finelli[45],
M.C.N. Fiolhais[125a,125c,l], L. Fiorini[168], A. Firan[40], J. Fischer[176], M.J. Fisher[110],
E.A. Fitzgerald[23], M. Flechl[48], I. Fleck[142], P. Fleischmann[175], S. Fleischmann[176],
G.T. Fletcher[140], G. Fletcher[75], T. Flick[176], A. Floderus[80], L.R. Flores Castillo[174],
A.C. Florez Bustos[160b], M.J. Flowerdew[100], T. Fonseca Martin[17], A. Formica[137],
A. Forti[83], D. Fortin[160a], D. Fournier[116], H. Fox[71], P. Francavilla[12], M. Franchini[20a,20b],
S. Franchino[30], D. Francis[30], M. Franklin[57], S. Franz[61], M. Fraternali[120a,120b],
S. Fratina[121], S.T. French[28], C. Friedrich[42], F. Friedrich[44], D. Froidevaux[30], J.A. Frost[28],
C. Fukunaga[157], E. Fullana Torregrosa[128], B.G. Fulsom[144], J. Fuster[168], C. Gabaldon[55],
O. Gabizon[173], A. Gabrielli[20a,20b], A. Gabrielli[133a,133b], S. Gadatsch[106], T. Gadfort[25],
S. Gadomski[49], G. Gagliardi[50a,50b], P. Gagnon[60], C. Galea[99], B. Galhardo[125a,125c],
E.J. Gallas[119], V. Gallo[17], B.J. Gallop[130], P. Gallus[127], G. Galster[36], K.K. Gan[110],
R.P. Gandrajula[62], J. Gao[33b,g], Y.S. Gao[144,e], F.M. Garay Walls[46], F. Garberson[177],
C. García[168], J.E. García Navarro[168], M. Garcia-Sciveres[15], R.W. Gardner[31],
N. Garelli[144], V. Garonne[30], C. Gatti[47], G. Gaudio[120a], B. Gaur[142], L. Gauthier[94],
P. Gauzzi[133a,133b], I.L. Gavrilenko[95], C. Gay[169], G. Gaycken[21], E.N. Gazis[10], P. Ge[33d,m],
Z. Gecse[169], C.N.P. Gee[130], D.A.A. Geerts[106], Ch. Geich-Gimbel[21], K. Gellerstedt[147a,147b],
C. Gemme[50a], A. Gemmell[53], M.H. Genest[55], S. Gentile[133a,133b], M. George[54],

S. George[76], D. Gerbaudo[164], A. Gershon[154], H. Ghazlane[136b], N. Ghodbane[34],
B. Giacobbe[20a], S. Giagu[133a,133b], V. Giangiobbe[12], P. Giannetti[123a,123b], F. Gianotti[30],
B. Gibbard[25], S.M. Gibson[76], M. Gilchriese[15], T.P.S. Gillam[28], D. Gillberg[30],
A.R. Gillman[130], D.M. Gingrich[3,d], N. Giokaris[9], M.P. Giordani[165c], R. Giordano[103a,103b],
F.M. Giorgi[16], P. Giovannini[100], P.F. Giraud[137], D. Giugni[90a], C. Giuliani[48], M. Giunta[94],
B.K. Gjelsten[118], I. Gkialas[155,n], L.K. Gladilin[98], C. Glasman[81], J. Glatzer[21], A. Glazov[42],
G.L. Glonti[64], M. Goblirsch-Kolb[100], J.R. Goddard[75], J. Godfrey[143], J. Godlewski[30],
C. Goeringer[82], S. Goldfarb[88], T. Golling[177], D. Golubkov[129], A. Gomes[125a,125b,125d],
L.S. Gomez Fajardo[42], R. Gonçalo[76], J. Goncalves Pinto Firmino Da Costa[42],
L. Gonella[21], S. González de la Hoz[168], G. Gonzalez Parra[12], M.L. Gonzalez Silva[27],
S. Gonzalez-Sevilla[49], J.J. Goodson[149], L. Goossens[30], P.A. Gorbounov[96], H.A. Gordon[25],
I. Gorelov[104], G. Gorfine[176], B. Gorini[30], E. Gorini[72a,72b], A. Gorišek[74], E. Gornicki[39],
A.T. Goshaw[6], C. Gössling[43], M.I. Gostkin[64], M. Gouighri[136a], D. Goujdami[136c],
M.P. Goulette[49], A.G. Goussiou[139], C. Goy[5], S. Gozpinar[23], H.M.X. Grabas[137],
L. Graber[54], I. Grabowska-Bold[38a], P. Grafström[20a,20b], K-J. Grahn[42], J. Gramling[49],
E. Gramstad[118], F. Grancagnolo[72a], S. Grancagnolo[16], V. Grassi[149], V. Gratchev[122],
H.M. Gray[30], J.A. Gray[149], E. Graziani[135a], O.G. Grebenyuk[122], Z.D. Greenwood[78,k],
K. Gregersen[36], I.M. Gregor[42], P. Grenier[144], J. Griffiths[8], N. Grigalashvili[64],
A.A. Grillo[138], K. Grimm[71], S. Grinstein[12,o], Ph. Gris[34], Y.V. Grishkevich[98],
J.-F. Grivaz[116], J.P. Grohs[44], A. Grohsjean[42], E. Gross[173], J. Grosse-Knetter[54],
G.C. Grossi[134a,134b], J. Groth-Jensen[173], Z.J. Grout[150], K. Grybel[142], F. Guescini[49],
D. Guest[177], O. Gueta[154], C. Guicheney[34], E. Guido[50a,50b], T. Guillemin[116], S. Guindon[2],
U. Gul[53], C. Gumpert[44], J. Gunther[127], J. Guo[35], S. Gupta[119], P. Gutierrez[112],
N.G. Gutierrez Ortiz[53], C. Gutschow[77], N. Guttman[154], C. Guyot[137], C. Gwenlan[119],
C.B. Gwilliam[73], A. Haas[109], C. Haber[15], H.K. Hadavand[8], P. Haefner[21], S. Hageboeck[21],
Z. Hajduk[39], H. Hakobyan[178], M. Haleem[41], D. Hall[119], G. Halladjian[89], K. Hamacher[176],
P. Hamal[114], K. Hamano[87], M. Hamer[54], A. Hamilton[146a,p], S. Hamilton[162], L. Han[33b],
K. Hanagaki[117], K. Hanawa[156], M. Hance[15], P. Hanke[58a], J.R. Hansen[36], J.B. Hansen[36],
J.D. Hansen[36], P.H. Hansen[36], P. Hansson[144], K. Hara[161], A.S. Hard[174], T. Harenberg[176],
S. Harkusha[91], D. Harper[88], R.D. Harrington[46], O.M. Harris[139], P.F. Harrison[171],
F. Hartjes[106], A. Harvey[56], S. Hasegawa[102], Y. Hasegawa[141], S. Hassani[137], S. Haug[17],
M. Hauschild[30], R. Hauser[89], M. Havranek[21], C.M. Hawkes[18], R.J. Hawkings[30],
A.D. Hawkins[80], T. Hayashi[161], D. Hayden[89], C.P. Hays[119], H.S. Hayward[73],
S.J. Haywood[130], S.J. Head[18], T. Heck[82], V. Hedberg[80], L. Heelan[8], S. Heim[121],
B. Heinemann[15], S. Heisterkamp[36], J. Hejbal[126], L. Helary[22], C. Heller[99], M. Heller[30],
S. Hellman[147a,147b], D. Hellmich[21], C. Helsens[30], J. Henderson[119], R.C.W. Henderson[71],
A. Henrichs[177], A.M. Henriques Correia[30], S. Henrot-Versille[116], C. Hensel[54],
G.H. Herbert[16], C.M. Hernandez[8], Y. Hernández Jiménez[168], R. Herrberg-Schubert[16],
G. Herten[48], R. Hertenberger[99], L. Hervas[30], G.G. Hesketh[77], N.P. Hessey[106],
R. Hickling[75], E. Higón-Rodriguez[168], J.C. Hill[28], K.H. Hiller[42], S. Hillert[21], S.J. Hillier[18],
I. Hinchliffe[15], E. Hines[121], M. Hirose[117], D. Hirschbuehl[176], J. Hobbs[149], N. Hod[106],
M.C. Hodgkinson[140], P. Hodgson[140], A. Hoecker[30], M.R. Hoeferkamp[104], J. Hoffman[40],
D. Hoffmann[84], J.I. Hofmann[58a], M. Hohlfeld[82], T.R. Holmes[15], T.M. Hong[121],

L. Hooft van Huysduynen[109], J-Y. Hostachy[55], S. Hou[152], A. Hoummada[136a],
J. Howard[119], J. Howarth[83], M. Hrabovsky[114], I. Hristova[16], J. Hrivnac[116], T. Hryn'ova[5],
P.J. Hsu[82], S.-C. Hsu[139], D. Hu[35], X. Hu[25], Y. Huang[146c], Z. Hubacek[30], F. Hubaut[84],
F. Huegging[21], A. Huettmann[42], T.B. Huffman[119], E.W. Hughes[35], G. Hughes[71],
M. Huhtinen[30], T.A. Hülsing[82], M. Hurwitz[15], N. Huseynov[64,b], J. Huston[89], J. Huth[57],
G. Iacobucci[49], G. Iakovidis[10], I. Ibragimov[142], L. Iconomidou-Fayard[116], J. Idarraga[116],
E. Ideal[177], P. Iengo[103a], O. Igonkina[106], T. Iizawa[172], Y. Ikegami[65], K. Ikematsu[142],
M. Ikeno[65], D. Iliadis[155], N. Ilic[159], Y. Inamaru[66], T. Ince[100], P. Ioannou[9], M. Iodice[135a],
K. Iordanidou[9], V. Ippolito[133a,133b], A. Irles Quiles[168], C. Isaksson[167], M. Ishino[67],
M. Ishitsuka[158], R. Ishmukhametov[110], C. Issever[119], S. Istin[19a], A.V. Ivashin[129],
W. Iwanski[39], H. Iwasaki[65], J.M. Izen[41], V. Izzo[103a], B. Jackson[121], J.N. Jackson[73],
M. Jackson[73], P. Jackson[1], M.R. Jaekel[30], V. Jain[2], K. Jakobs[48], S. Jakobsen[36],
T. Jakoubek[126], J. Jakubek[127], D.O. Jamin[152], D.K. Jana[112], E. Jansen[77], H. Jansen[30],
J. Janssen[21], M. Janus[171], R.C. Jared[174], G. Jarlskog[80], L. Jeanty[57], G.-Y. Jeng[151],
I. Jen-La Plante[31], D. Jennens[87], P. Jenni[48,q], J. Jentzsch[43], C. Jeske[171], S. Jézéquel[5],
M.K. Jha[20a], H. Ji[174], W. Ji[82], J. Jia[149], Y. Jiang[33b], M. Jimenez Belenguer[42], S. Jin[33a],
A. Jinaru[26a], O. Jinnouchi[158], M.D. Joergensen[36], D. Joffe[40], K.E. Johansson[147a],
P. Johansson[140], K.A. Johns[7], K. Jon-And[147a,147b], G. Jones[171], R.W.L. Jones[71],
T.J. Jones[73], P.M. Jorge[125a,125b], K.D. Joshi[83], J. Jovicevic[148], X. Ju[174], C.A. Jung[43],
R.M. Jungst[30], P. Jussel[61], A. Juste Rozas[12,o], M. Kaci[168], A. Kaczmarska[39],
P. Kadlecik[36], M. Kado[116], H. Kagan[110], M. Kagan[144], E. Kajomovitz[45], S. Kalinin[176],
S. Kama[40], N. Kanaya[156], M. Kaneda[30], S. Kaneti[28], T. Kanno[158], V.A. Kantserov[97],
J. Kanzaki[65], B. Kaplan[109], A. Kapliy[31], D. Kar[53], K. Karakostas[10], N. Karastathis[10],
M. Karnevskiy[82], S.N. Karpov[64], K. Karthik[109], V. Kartvelishvili[71], A.N. Karyukhin[129],
L. Kashif[174], G. Kasieczka[58b], R.D. Kass[110], A. Kastanas[14], Y. Kataoka[156], A. Katre[49],
J. Katzy[42], V. Kaushik[7], K. Kawagoe[69], T. Kawamoto[156], G. Kawamura[54], S. Kazama[156],
V.F. Kazanin[108], M.Y. Kazarinov[64], R. Keeler[170], P.T. Keener[121], R. Kehoe[40], M. Keil[54],
J.S. Keller[139], H. Keoshkerian[5], O. Kepka[126], B.P. Kerševan[74], S. Kersten[176],
K. Kessoku[156], J. Keung[159], F. Khalil-zada[11], H. Khandanyan[147a,147b], A. Khanov[113],
D. Kharchenko[64], A. Khodinov[97], A. Khomich[58a], T.J. Khoo[28], G. Khoriauli[21],
A. Khoroshilov[176], V. Khovanskiy[96], E. Khramov[64], J. Khubua[51b], H. Kim[147a,147b],
S.H. Kim[161], N. Kimura[172], O. Kind[16], B.T. King[73], M. King[66], R.S.B. King[119],
S.B. King[169], J. Kirk[130], A.E. Kiryunin[100], T. Kishimoto[66], D. Kisielewska[38a],
T. Kitamura[66], T. Kittelmann[124], K. Kiuchi[161], E. Kladiva[145b], M. Klein[73], U. Klein[73],
K. Kleinknecht[82], P. Klimek[147a,147b], A. Klimentov[25], R. Klingenberg[43], J.A. Klinger[83],
E.B. Klinkby[36], T. Klioutchnikova[30], P.F. Klok[105], E.-E. Kluge[58a], P. Kluit[106],
S. Kluth[100], E. Kneringer[61], E.B.F.G. Knoops[84], A. Knue[54], T. Kobayashi[156], M. Kobel[44],
M. Kocian[144], P. Kodys[128], S. Koenig[82], P. Koevesarki[21], T. Koffas[29], E. Koffeman[106],
L.A. Kogan[119], S. Kohlmann[176], Z. Kohout[127], T. Kohriki[65], T. Koi[144], H. Kolanoski[16],
I. Koletsou[5], J. Koll[89], A.A. Komar[95,*], Y. Komori[156], T. Kondo[65], K. Köneke[48],
A.C. König[105], T. Kono[65,r], R. Konoplich[109,s], N. Konstantinidis[77], R. Kopeliansky[153],
S. Koperny[38a], L. Köpke[82], A.K. Kopp[48], K. Korcyl[39], K. Kordas[155], A. Korn[46],
A.A. Korol[108], I. Korolkov[12], E.V. Korolkova[140], V.A. Korotkov[129], O. Kortner[100],

S. Kortner[100], V.V. Kostyukhin[21], S. Kotov[100], V.M. Kotov[64], A. Kotwal[45],
C. Kourkoumelis[9], V. Kouskoura[155], A. Koutsman[160a], R. Kowalewski[170],
T.Z. Kowalski[38a], W. Kozanecki[137], A.S. Kozhin[129], V. Kral[127], V.A. Kramarenko[98],
G. Kramberger[74], M.W. Krasny[79], A. Krasznahorkay[109], J.K. Kraus[21], A. Kravchenko[25],
S. Kreiss[109], J. Kretzschmar[73], K. Kreutzfeldt[52], N. Krieger[54], P. Krieger[159],
K. Kroeninger[54], H. Kroha[100], J. Kroll[121], J. Kroseberg[21], J. Krstic[13a], U. Kruchonak[64],
H. Krüger[21], T. Kruker[17], N. Krumnack[63], Z.V. Krumshteyn[64], A. Kruse[174],
M.C. Kruse[45], M. Kruskal[22], T. Kubota[87], S. Kuday[4a], S. Kuehn[48], A. Kugel[58c],
T. Kuhl[42], V. Kukhtin[64], Y. Kulchitsky[91], S. Kuleshov[32b], M. Kuna[133a,133b], J. Kunkle[121],
A. Kupco[126], H. Kurashige[66], M. Kurata[161], Y.A. Kurochkin[91], R. Kurumida[66],
V. Kus[126], E.S. Kuwertz[148], M. Kuze[158], J. Kvita[143], R. Kwee[16], A. La Rosa[49],
L. La Rotonda[37a,37b], L. Labarga[81], S. Lablak[136a], C. Lacasta[168], F. Lacava[133a,133b],
J. Lacey[29], H. Lacker[16], D. Lacour[79], V.R. Lacuesta[168], E. Ladygin[64], R. Lafaye[5],
B. Laforge[79], T. Lagouri[177], S. Lai[48], H. Laier[58a], E. Laisne[55], L. Lambourne[77],
C.L. Lampen[7], W. Lampl[7], E. Lançon[137], U. Landgraf[48], M.P.J. Landon[75], V.S. Lang[58a],
C. Lange[42], A.J. Lankford[164], F. Lanni[25], K. Lantzsch[30], A. Lanza[120a], S. Laplace[79],
C. Lapoire[21], J.F. Laporte[137], T. Lari[90a], A. Larner[119], M. Lassnig[30], P. Laurelli[47],
V. Lavorini[37a,37b], W. Lavrijsen[15], P. Laycock[73], B.T. Le[55], O. Le Dortz[79],
E. Le Guirriec[84], E. Le Menedeu[12], T. LeCompte[6], F. Ledroit-Guillon[55], C.A. Lee[152],
H. Lee[106], J.S.H. Lee[117], S.C. Lee[152], L. Lee[177], G. Lefebvre[79], M. Lefebvre[170],
F. Legger[99], C. Leggett[15], A. Lehan[73], M. Lehmacher[21], G. Lehmann Miotto[30], X. Lei[7],
A.G. Leister[177], M.A.L. Leite[24d], R. Leitner[128], D. Lellouch[173], B. Lemmer[54],
V. Lendermann[58a], K.J.C. Leney[146c], T. Lenz[106], G. Lenzen[176], B. Lenzi[30], R. Leone[7],
K. Leonhardt[44], S. Leontsinis[10], C. Leroy[94], J-R. Lessard[170], C.G. Lester[28],
C.M. Lester[121], J. Levêque[5], D. Levin[88], L.J. Levinson[173], A. Lewis[119], G.H. Lewis[109],
A.M. Leyko[21], M. Leyton[16], B. Li[33b,t], B. Li[84], H. Li[149], H.L. Li[31], S. Li[45], X. Li[88],
Z. Liang[119,u], H. Liao[34], B. Liberti[134a], P. Lichard[30], K. Lie[166], J. Liebal[21], W. Liebig[14],
C. Limbach[21], A. Limosani[87], M. Limper[62], S.C. Lin[152,v], F. Linde[106], B.E. Lindquist[149],
J.T. Linnemann[89], E. Lipeles[121], A. Lipniacka[14], M. Lisovyi[42], T.M. Liss[166], D. Lissauer[25],
A. Lister[169], A.M. Litke[138], B. Liu[152], D. Liu[152], J.B. Liu[33b], K. Liu[33b,w], L. Liu[88],
M. Liu[45], M. Liu[33b], Y. Liu[33b], M. Livan[120a,120b], S.S.A. Livermore[119], A. Lleres[55],
J. Llorente Merino[81], S.L. Lloyd[75], F. Lo Sterzo[152], E. Lobodzinska[42], P. Loch[7],
W.S. Lockman[138], T. Loddenkoetter[21], F.K. Loebinger[83], A.E. Loevschall-Jensen[36],
A. Loginov[177], C.W. Loh[169], T. Lohse[16], K. Lohwasser[48], M. Lokajicek[126],
V.P. Lombardo[5], J.D. Long[88], R.E. Long[71], L. Lopes[125a], D. Lopez Mateos[57],
B. Lopez Paredes[140], J. Lorenz[99], N. Lorenzo Martinez[116], M. Losada[163], P. Loscutoff[15],
M.J. Losty[160a,*], X. Lou[41], A. Lounis[116], J. Love[6], P.A. Love[71], A.J. Lowe[144,e], F. Lu[33a],
H.J. Lubatti[139], C. Luci[133a,133b], A. Lucotte[55], D. Ludwig[42], I. Ludwig[48], F. Luehring[60],
W. Lukas[61], L. Luminari[133a], E. Lund[118], J. Lundberg[147a,147b], O. Lundberg[147a,147b],
B. Lund-Jensen[148], M. Lungwitz[82], D. Lynn[25], R. Lysak[126], E. Lytken[80], H. Ma[25],
L.L. Ma[33d], G. Maccarrone[47], A. Macchiolo[100], B. Maček[74], J. Machado Miguens[125a,125b],
D. Macina[30], R. Mackeprang[36], R. Madar[48], R.J. Madaras[15], H.J. Maddocks[71],
W.F. Mader[44], A. Madsen[167], M. Maeno[8], T. Maeno[25], L. Magnoni[164], E. Magradze[54],

K. Mahboubi[48], J. Mahlstedt[106], S. Mahmoud[73], G. Mahout[18], C. Maiani[137],
C. Maidantchik[24a], A. Maio[125a,125b,125d], S. Majewski[115], Y. Makida[65], N. Makovec[116],
P. Mal[137,x], B. Malaescu[79], Pa. Malecki[39], V.P. Maleev[122], F. Malek[55], U. Mallik[62],
D. Malon[6], C. Malone[144], S. Maltezos[10], V.M. Malyshev[108], S. Malyukov[30],
J. Mamuzic[13b], L. Mandelli[90a], I. Mandić[74], R. Mandrysch[62], J. Maneira[125a,125b],
A. Manfredini[100], L. Manhaes de Andrade Filho[24b], J.A. Manjarres Ramos[137], A. Mann[99],
P.M. Manning[138], A. Manousakis-Katsikakis[9], B. Mansoulie[137], R. Mantifel[86],
L. Mapelli[30], L. March[168], J.F. Marchand[29], F. Marchese[134a,134b], G. Marchiori[79],
M. Marcisovsky[126], C.P. Marino[170], C.N. Marques[125a], F. Marroquim[24a], Z. Marshall[15],
L.F. Marti[17], S. Marti-Garcia[168], B. Martin[30], B. Martin[89], J.P. Martin[94], T.A. Martin[171],
V.J. Martin[46], B. Martin dit Latour[49], H. Martinez[137], M. Martinez[12,o],
S. Martin-Haugh[130], A.C. Martyniuk[170], M. Marx[139], F. Marzano[133a], A. Marzin[112],
L. Masetti[82], T. Mashimo[156], R. Mashinistov[95], J. Masik[83], A.L. Maslennikov[108],
I. Massa[20a,20b], N. Massol[5], P. Mastrandrea[149], A. Mastroberardino[37a,37b],
T. Masubuchi[156], H. Matsunaga[156], T. Matsushita[66], P. Mättig[176], S. Mättig[42],
J. Mattmann[82], C. Mattravers[119,c], J. Maurer[84], S.J. Maxfield[73], D.A. Maximov[108,f],
R. Mazini[152], L. Mazzaferro[134a,134b], M. Mazzanti[90a], G. Mc Goldrick[159], S.P. Mc Kee[88],
A. McCarn[88], R.L. McCarthy[149], T.G. McCarthy[29], N.A. McCubbin[130],
K.W. McFarlane[56,*], J.A. Mcfayden[140], G. Mchedlidze[51b], T. Mclaughlan[18],
S.J. McMahon[130], R.A. McPherson[170,i], A. Meade[85], J. Mechnich[106], M. Mechtel[176],
M. Medinnis[42], S. Meehan[31], R. Meera-Lebbai[112], S. Mehlhase[36], A. Mehta[73],
K. Meier[58a], C. Meineck[99], B. Meirose[80], C. Melachrinos[31], B.R. Mellado Garcia[146c],
F. Meloni[90a,90b], L. Mendoza Navas[163], A. Mengarelli[20a,20b], S. Menke[100], E. Meoni[162],
K.M. Mercurio[57], S. Mergelmeyer[21], N. Meric[137], P. Mermod[49], L. Merola[103a,103b],
C. Meroni[90a], F.S. Merritt[31], H. Merritt[110], A. Messina[30,y], J. Metcalfe[25], A.S. Mete[164],
C. Meyer[82], C. Meyer[31], J-P. Meyer[137], J. Meyer[30], J. Meyer[54], S. Michal[30],
R.P. Middleton[130], S. Migas[73], L. Mijović[137], G. Mikenberg[173], M. Mikestikova[126],
M. Mikuž[74], D.W. Miller[31], C. Mills[57], A. Milov[173], D.A. Milstead[147a,147b], D. Milstein[173],
A.A. Minaenko[129], M. Miñano Moya[168], I.A. Minashvili[64], A.I. Mincer[109], B. Mindur[38a],
M. Mineev[64], Y. Ming[174], L.M. Mir[12], G. Mirabelli[133a], T. Mitani[172], J. Mitrevski[138],
V.A. Mitsou[168], S. Mitsui[65], P.S. Miyagawa[140], J.U. Mjörnmark[80], T. Moa[147a,147b],
V. Moeller[28], S. Mohapatra[149], W. Mohr[48], S. Molander[147a,147b], R. Moles-Valls[168],
A. Molfetas[30], K. Mönig[42], C. Monini[55], J. Monk[36], E. Monnier[84], J. Montejo Berlingen[12],
F. Monticelli[70], S. Monzani[20a,20b], R.W. Moore[3], C. Mora Herrera[49], A. Moraes[53],
N. Morange[62], J. Morel[54], D. Moreno[82], M. Moreno Llácer[168], P. Morettini[50a],
M. Morgenstern[44], M. Morii[57], S. Moritz[82], A.K. Morley[148], G. Mornacchi[30],
J.D. Morris[75], L. Morvaj[102], H.G. Moser[100], M. Mosidze[51b], J. Moss[110], R. Mount[144],
E. Mountricha[25], S.V. Mouraviev[95,*], E.J.W. Moyse[85], R.D. Mudd[18], F. Mueller[58a],
J. Mueller[124], K. Mueller[21], T. Mueller[28], T. Mueller[82], D. Muenstermann[49],
Y. Munwes[154], J.A. Murillo Quijada[18], W.J. Murray[130], I. Mussche[106], E. Musto[153],
A.G. Myagkov[129,z], M. Myska[126], O. Nackenhorst[54], J. Nadal[54], K. Nagai[61], R. Nagai[158],
Y. Nagai[84], K. Nagano[65], A. Nagarkar[110], Y. Nagasaka[59], M. Nagel[100], A.M. Nairz[30],
Y. Nakahama[30], K. Nakamura[65], T. Nakamura[156], I. Nakano[111], H. Namasivayam[41],

G. Nanava[21], A. Napier[162], R. Narayan[58b], M. Nash[77,c], T. Nattermann[21], T. Naumann[42],
G. Navarro[163], H.A. Neal[88], P.Yu. Nechaeva[95], T.J. Neep[83], A. Negri[120a,120b], G. Negri[30],
M. Negrini[20a], S. Nektarijevic[49], A. Nelson[164], T.K. Nelson[144], S. Nemecek[126],
P. Nemethy[109], A.A. Nepomuceno[24a], M. Nessi[30,aa], M.S. Neubauer[166], M. Neumann[176],
A. Neusiedl[82], R.M. Neves[109], P. Nevski[25], F.M. Newcomer[121], P.R. Newman[18],
D.H. Nguyen[6], V. Nguyen Thi Hong[137], R.B. Nickerson[119], R. Nicolaidou[137],
B. Nicquevert[30], J. Nielsen[138], N. Nikiforou[35], A. Nikiforov[16], V. Nikolaenko[129,z],
I. Nikolic-Audit[79], K. Nikolics[49], K. Nikolopoulos[18], P. Nilsson[8], Y. Ninomiya[156],
A. Nisati[133a], R. Nisius[100], T. Nobe[158], L. Nodulman[6], M. Nomachi[117], I. Nomidis[155],
S. Norberg[112], M. Nordberg[30], J. Novakova[128], M. Nozaki[65], L. Nozka[114], K. Ntekas[10],
A.-E. Nuncio-Quiroz[21], G. Nunes Hanninger[87], T. Nunnemann[99], E. Nurse[77],
B.J. O'Brien[46], F. O'grady[7], D.C. O'Neil[143], V. O'Shea[53], L.B. Oakes[99],
F.G. Oakham[29,d], H. Oberlack[100], J. Ocariz[79], A. Ochi[66], M.I. Ochoa[77], S. Oda[69],
S. Odaka[65], H. Ogren[60], A. Oh[83], S.H. Oh[45], C.C. Ohm[30], T. Ohshima[102],
W. Okamura[117], H. Okawa[25], Y. Okumura[31], T. Okuyama[156], A. Olariu[26a],
A.G. Olchevski[64], S.A. Olivares Pino[46], M. Oliveira[125a,125c,l], D. Oliveira Damazio[25],
E. Oliver Garcia[168], D. Olivito[121], A. Olszewski[39], J. Olszowska[39], A. Onofre[125a,125e],
P.U.E. Onyisi[31,ab], C.J. Oram[160a], M.J. Oreglia[31], Y. Oren[154], D. Orestano[135a,135b],
N. Orlando[72a,72b], C. Oropeza Barrera[53], R.S. Orr[159], B. Osculati[50a,50b], R. Ospanov[121],
G. Otero y Garzon[27], H. Otono[69], M. Ouchrif[136d], E.A. Ouellette[170], F. Ould-Saada[118],
A. Ouraou[137], K.P. Oussoren[106], Q. Ouyang[33a], A. Ovcharova[15], M. Owen[83], S. Owen[140],
V.E. Ozcan[19a], N. Ozturk[8], K. Pachal[119], A. Pacheco Pages[12], C. Padilla Aranda[12],
S. Pagan Griso[15], E. Paganis[140], C. Pahl[100], F. Paige[25], P. Pais[85], K. Pajchel[118],
G. Palacino[160b], S. Palestini[30], D. Pallin[34], A. Palma[125a,125b], J.D. Palmer[18], Y.B. Pan[174],
E. Panagiotopoulou[10], J.G. Panduro Vazquez[76], P. Pani[106], N. Panikashvili[88],
S. Panitkin[25], D. Pantea[26a], Th.D. Papadopoulou[10], K. Papageorgiou[155,n],
A. Paramonov[6], D. Paredes Hernandez[34], M.A. Parker[28], F. Parodi[50a,50b], J.A. Parsons[35],
U. Parzefall[48], S. Pashapour[54], E. Pasqualucci[133a], S. Passaggio[50a], A. Passeri[135a],
F. Pastore[135a,135b,*], Fr. Pastore[76], G. Pásztor[49,ac], S. Pataraia[176], N.D. Patel[151],
J.R. Pater[83], S. Patricelli[103a,103b], T. Pauly[30], J. Pearce[170], M. Pedersen[118],
S. Pedraza Lopez[168], R. Pedro[125a,125b], S.V. Peleganchuk[108], D. Pelikan[167], H. Peng[33b],
B. Penning[31], J. Penwell[60], D.V. Perepelitsa[35], T. Perez Cavalcanti[42],
E. Perez Codina[160a], M.T. Pérez García-Estañ[168], V. Perez Reale[35], L. Perini[90a,90b],
H. Pernegger[30], R. Perrino[72a], R. Peschke[42], V.D. Peshekhonov[64], K. Peters[30],
R.F.Y. Peters[54,ad], B.A. Petersen[30], J. Petersen[30], T.C. Petersen[36], E. Petit[5],
A. Petridis[147a,147b], C. Petridou[155], E. Petrolo[133a], F. Petrucci[135a,135b], M. Petteni[143],
R. Pezoa[32b], P.W. Phillips[130], G. Piacquadio[144], E. Pianori[171], A. Picazio[49], E. Piccaro[75],
M. Piccinini[20a,20b], S.M. Piec[42], R. Piegaia[27], D.T. Pignotti[110], J.E. Pilcher[31],
A.D. Pilkington[77], J. Pina[125a,125b,125d], M. Pinamonti[165a,165c,ae], A. Pinder[119],
J.L. Pinfold[3], A. Pingel[36], B. Pinto[125a], C. Pizio[90a,90b], M.-A. Pleier[25], V. Pleskot[128],
E. Plotnikova[64], P. Plucinski[147a,147b], S. Poddar[58a], F. Podlyski[34], R. Poettgen[82],
L. Poggioli[116], D. Pohl[21], M. Pohl[49], G. Polesello[120a], A. Policicchio[37a,37b], R. Polifka[159],
A. Polini[20a], C.S. Pollard[45], V. Polychronakos[25], D. Pomeroy[23], K. Pommès[30],

L. Pontecorvo[133a], B.G. Pope[89], G.A. Popeneciu[26b], D.S. Popovic[13a], A. Poppleton[30],
X. Portell Bueso[12], G.E. Pospelov[100], S. Pospisil[127], K. Potamianos[15], I.N. Potrap[64],
C.J. Potter[150], C.T. Potter[115], G. Poulard[30], J. Poveda[60], V. Pozdnyakov[64], R. Prabhu[77],
P. Pralavorio[84], A. Pranko[15], S. Prasad[30], R. Pravahan[8], S. Prell[63], D. Price[83], J. Price[73],
L.E. Price[6], D. Prieur[124], M. Primavera[72a], M. Proissl[46], K. Prokofiev[109], F. Prokoshin[32b],
E. Protopapadaki[137], S. Protopopescu[25], J. Proudfoot[6], X. Prudent[44], M. Przybycien[38a],
H. Przysiezniak[5], S. Psoroulas[21], E. Ptacek[115], E. Pueschel[85], D. Puldon[149],
M. Purohit[25,af], P. Puzo[116], Y. Pylypchenko[62], J. Qian[88], A. Quadt[54], D.R. Quarrie[15],
W.B. Quayle[146c], D. Quilty[53], V. Radeka[25], V. Radescu[42], S.K. Radhakrishnan[149],
P. Radloff[115], F. Ragusa[90a,90b], G. Rahal[179], S. Rajagopalan[25], M. Rammensee[48],
M. Rammes[142], A.S. Randle-Conde[40], C. Rangel-Smith[79], K. Rao[164], F. Rauscher[99],
T.C. Rave[48], T. Ravenscroft[53], M. Raymond[30], A.L. Read[118], D.M. Rebuzzi[120a,120b],
A. Redelbach[175], G. Redlinger[25], R. Reece[138], K. Reeves[41], A. Reinsch[115], H. Reisin[27],
I. Reisinger[43], M. Relich[164], C. Rembser[30], Z.L. Ren[152], A. Renaud[116], M. Rescigno[133a],
S. Resconi[90a], B. Resende[137], P. Reznicek[99], R. Rezvani[94], R. Richter[100], M. Ridel[79],
P. Rieck[16], M. Rijssenbeek[149], A. Rimoldi[120a,120b], L. Rinaldi[20a], E. Ritsch[61], I. Riu[12],
G. Rivoltella[90a,90b], F. Rizatdinova[113], E. Rizvi[75], S.H. Robertson[86,i],
A. Robichaud-Veronneau[119], D. Robinson[28], J.E.M. Robinson[83], A. Robson[53],
J.G. Rocha de Lima[107], C. Roda[123a,123b], D. Roda Dos Santos[126], L. Rodrigues[30],
S. Roe[30], O. Røhne[118], S. Rolli[162], A. Romaniouk[97], M. Romano[20a,20b], G. Romeo[27],
E. Romero Adam[168], N. Rompotis[139], L. Roos[79], E. Ros[168], S. Rosati[133a], K. Rosbach[49],
A. Rose[150], M. Rose[76], P.L. Rosendahl[14], O. Rosenthal[142], V. Rossetti[147a,147b],
E. Rossi[103a,103b], L.P. Rossi[50a], R. Rosten[139], M. Rotaru[26a], I. Roth[173], J. Rothberg[139],
D. Rousseau[116], C.R. Royon[137], A. Rozanov[84], Y. Rozen[153], X. Ruan[146c], F. Rubbo[12],
I. Rubinskiy[42], V.I. Rud[98], C. Rudolph[44], M.S. Rudolph[159], F. Rühr[7],
A. Ruiz-Martinez[63], L. Rumyantsev[64], Z. Rurikova[48], N.A. Rusakovich[64], A. Ruschke[99],
J.P. Rutherfoord[7], N. Ruthmann[48], P. Ruzicka[126], Y.F. Ryabov[122], M. Rybar[128],
G. Rybkin[116], N.C. Ryder[119], A.F. Saavedra[151], S. Sacerdoti[27], A. Saddique[3], I. Sadeh[154],
H.F-W. Sadrozinski[138], R. Sadykov[64], F. Safai Tehrani[133a], H. Sakamoto[156], Y. Sakurai[172],
G. Salamanna[75], A. Salamon[134a], M. Saleem[112], D. Salek[106], P.H. Sales De Bruin[139],
D. Salihagic[100], A. Salnikov[144], J. Salt[168], B.M. Salvachua Ferrando[6], D. Salvatore[37a,37b],
F. Salvatore[150], A. Salvucci[105], A. Salzburger[30], D. Sampsonidis[155], A. Sanchez[103a,103b],
J. Sánchez[168], V. Sanchez Martinez[168], H. Sandaker[14], H.G. Sander[82], M.P. Sanders[99],
M. Sandhoff[176], T. Sandoval[28], C. Sandoval[163], R. Sandstroem[100], D.P.C. Sankey[130],
A. Sansoni[47], C. Santoni[34], R. Santonico[134a,134b], H. Santos[125a], I. Santoyo Castillo[150],
K. Sapp[124], A. Sapronov[64], J.G. Saraiva[125a,125d], E. Sarkisyan-Grinbaum[8], B. Sarrazin[21],
G. Sartisohn[176], O. Sasaki[65], Y. Sasaki[156], N. Sasao[67], I. Satsounkevitch[91], G. Sauvage[5,*],
E. Sauvan[5], J.B. Sauvan[116], P. Savard[159,d], V. Savinov[124], D.O. Savu[30], C. Sawyer[119],
L. Sawyer[78,k], D.H. Saxon[53], J. Saxon[121], C. Sbarra[20a], A. Sbrizzi[3], T. Scanlon[30],
D.A. Scannicchio[164], M. Scarcella[151], J. Schaarschmidt[173], P. Schacht[100], D. Schaefer[121],
A. Schaelicke[46], S. Schaepe[21], S. Schaetzel[58b], U. Schäfer[82], A.C. Schaffer[116], D. Schaile[99],
R.D. Schamberger[149], V. Scharf[58a], V.A. Schegelsky[122], D. Scheirich[88], M. Schernau[164],
M.I. Scherzer[35], C. Schiavi[50a,50b], J. Schieck[99], C. Schillo[48], M. Schioppa[37a,37b],

S. Schlenker[30], E. Schmidt[48], K. Schmieden[30], C. Schmitt[82], C. Schmitt[99], S. Schmitt[58b],
B. Schneider[17], Y.J. Schnellbach[73], U. Schnoor[44], L. Schoeffel[137], A. Schoening[58b],
B.D. Schoenrock[89], A.L.S. Schorlemmer[54], M. Schott[82], D. Schouten[160a],
J. Schovancova[25], M. Schram[86], S. Schramm[159], M. Schreyer[175], C. Schroeder[82],
N. Schroer[58c], N. Schuh[82], M.J. Schultens[21], H.-C. Schultz-Coulon[58a], H. Schulz[16],
M. Schumacher[48], B.A. Schumm[138], Ph. Schune[137], A. Schwartzman[144], Ph. Schwegler[100],
Ph. Schwemling[137], R. Schwienhorst[89], J. Schwindling[137], T. Schwindt[21], M. Schwoerer[5],
F.G. Sciacca[17], E. Scifo[116], G. Sciolla[23], W.G. Scott[130], F. Scutti[21], J. Searcy[88],
G. Sedov[42], E. Sedykh[122], S.C. Seidel[104], A. Seiden[138], F. Seifert[127], J.M. Seixas[24a],
G. Sekhniaidze[103a], S.J. Sekula[40], K.E. Selbach[46], D.M. Seliverstov[122], G. Sellers[73],
M. Seman[145b], N. Semprini-Cesari[20a,20b], C. Serfon[30], L. Serin[116], L. Serkin[54], T. Serre[84],
R. Seuster[160a], H. Severini[112], F. Sforza[100], A. Sfyrla[30], E. Shabalina[54], M. Shamim[115],
L.Y. Shan[33a], J.T. Shank[22], Q.T. Shao[87], M. Shapiro[15], P.B. Shatalov[96], K. Shaw[165a,165c],
P. Sherwood[77], S. Shimizu[66], M. Shimojima[101], T. Shin[56], M. Shiyakova[64], A. Shmeleva[95],
M.J. Shochet[31], D. Short[119], S. Shrestha[63], E. Shulga[97], M.A. Shupe[7], S. Shushkevich[42],
P. Sicho[126], D. Sidorov[113], A. Sidoti[133a], F. Siegert[48], Dj. Sijacki[13a], O. Silbert[173],
J. Silva[125a,125d], Y. Silver[154], D. Silverstein[144], S.B. Silverstein[147a], V. Simak[127],
O. Simard[5], Lj. Simic[13a], S. Simion[116], E. Simioni[82], B. Simmons[77], R. Simoniello[90a,90b],
M. Simonyan[36], P. Sinervo[159], N.B. Sinev[115], V. Sipica[142], G. Siragusa[175], A. Sircar[78],
A.N. Sisakyan[64,*], S.Yu. Sivoklokov[98], J. Sjölin[147a,147b], T.B. Sjursen[14], L.A. Skinnari[15],
H.P. Skottowe[57], K.Yu. Skovpen[108], P. Skubic[112], M. Slater[18], T. Slavicek[127], K. Sliwa[162],
V. Smakhtin[173], B.H. Smart[46], L. Smestad[118], S.Yu. Smirnov[97], Y. Smirnov[97],
L.N. Smirnova[98,ag], O. Smirnova[80], K.M. Smith[53], M. Smizanska[71], K. Smolek[127],
A.A. Snesarev[95], G. Snidero[75], J. Snow[112], S. Snyder[25], R. Sobie[170,i], F. Socher[44],
J. Sodomka[127], A. Soffer[154], D.A. Soh[152,u], C.A. Solans[30], M. Solar[127], J. Solc[127],
E.Yu. Soldatov[97], U. Soldevila[168], E. Solfaroli Camillocci[133a,133b], A.A. Solodkov[129],
O.V. Solovyanov[129], V. Solovyev[122], N. Soni[1], A. Sood[15], V. Sopko[127], B. Sopko[127],
M. Sosebee[8], R. Soualah[165a,165c], P. Soueid[94], A.M. Soukharev[108], D. South[42],
S. Spagnolo[72a,72b], F. Spanò[76], W.R. Spearman[57], R. Spighi[20a], G. Spigo[30],
M. Spousta[128], T. Spreitzer[159], B. Spurlock[8], R.D. St. Denis[53], J. Stahlman[121],
R. Stamen[58a], E. Stanecka[39], R.W. Stanek[6], C. Stanescu[135a], M. Stanescu-Bellu[42],
M.M. Stanitzki[42], S. Stapnes[118], E.A. Starchenko[129], J. Stark[55], P. Staroba[126],
P. Starovoitov[42], R. Staszewski[39], P. Stavina[145a,*], G. Steele[53], P. Steinbach[44],
P. Steinberg[25], I. Stekl[127], B. Stelzer[143], H.J. Stelzer[89], O. Stelzer-Chilton[160a],
H. Stenzel[52], S. Stern[100], G.A. Stewart[30], J.A. Stillings[21], M.C. Stockton[86], M. Stoebe[86],
K. Stoerig[48], G. Stoicea[26a], S. Stonjek[100], A.R. Stradling[8], A. Straessner[44],
J. Strandberg[148], S. Strandberg[147a,147b], A. Strandlie[118], E. Strauss[144], M. Strauss[112],
P. Strizenec[145b], R. Ströhmer[175], D.M. Strom[115], R. Stroynowski[40], S.A. Stucci[17],
B. Stugu[14], I. Stumer[25,*], J. Stupak[149], P. Sturm[176], N.A. Styles[42], D. Su[144], J. Su[124],
HS. Subramania[3], R. Subramaniam[78], A. Succurro[12], Y. Sugaya[117], C. Suhr[107],
M. Suk[127], V.V. Sulin[95], S. Sultansoy[4c], T. Sumida[67], X. Sun[55], J.E. Sundermann[48],
K. Suruliz[140], G. Susinno[37a,37b], M.R. Sutton[150], Y. Suzuki[65], M. Svatos[126], S. Swedish[169],
M. Swiatlowski[144], I. Sykora[145a], T. Sykora[128], D. Ta[89], K. Tackmann[42], J. Taenzer[159],

A. Taffard[164], R. Tafirout[160a], N. Taiblum[154], Y. Takahashi[102], H. Takai[25],
R. Takashima[68], H. Takeda[66], T. Takeshita[141], Y. Takubo[65], M. Talby[84],
A.A. Talyshev[108,f], J.Y.C. Tam[175], M.C. Tamsett[78,ah], K.G. Tan[87], J. Tanaka[156],
R. Tanaka[116], S. Tanaka[132], S. Tanaka[65], A.J. Tanasijczuk[143], K. Tani[66], N. Tannoury[84],
S. Tapprogge[82], S. Tarem[153], F. Tarrade[29], G.F. Tartarelli[90a], P. Tas[128], M. Tasevsky[126],
T. Tashiro[67], E. Tassi[37a,37b], A. Tavares Delgado[125a,125b], Y. Tayalati[136d], C. Taylor[77],
F.E. Taylor[93], G.N. Taylor[87], W. Taylor[160b], F.A. Teischinger[30],
M. Teixeira Dias Castanheira[75], P. Teixeira-Dias[76], K.K. Temming[48], H. Ten Kate[30],
P.K. Teng[152], S. Terada[65], K. Terashi[156], J. Terron[81], S. Terzo[100], M. Testa[47],
R.J. Teuscher[159,i], J. Therhaag[21], T. Theveneaux-Pelzer[34], S. Thoma[48], J.P. Thomas[18],
E.N. Thompson[35], P.D. Thompson[18], P.D. Thompson[159], A.S. Thompson[53],
L.A. Thomsen[36], E. Thomson[121], M. Thomson[28], W.M. Thong[87], R.P. Thun[88,*],
F. Tian[35], M.J. Tibbetts[15], T. Tic[126], V.O. Tikhomirov[95,ai], Yu.A. Tikhonov[108,f],
S. Timoshenko[97], E. Tiouchichine[84], P. Tipton[177], S. Tisserant[84], T. Todorov[5],
S. Todorova-Nova[128], B. Toggerson[164], J. Tojo[69], S. Tokár[145a], K. Tokushuku[65],
K. Tollefson[89], L. Tomlinson[83], M. Tomoto[102], L. Tompkins[31], K. Toms[104],
N.D. Topilin[64], E. Torrence[115], H. Torres[143], E. Torró Pastor[168], J. Toth[84,ac],
F. Touchard[84], D.R. Tovey[140], H.L. Tran[116], T. Trefzger[175], L. Tremblet[30], A. Tricoli[30],
I.M. Trigger[160a], S. Trincaz-Duvoid[79], M.F. Tripiana[70], N. Triplett[25], W. Trischuk[159],
B. Trocmé[55], C. Troncon[90a], M. Trottier-McDonald[143], M. Trovatelli[135a,135b], P. True[89],
M. Trzebinski[39], A. Trzupek[39], C. Tsarouchas[30], J.C-L. Tseng[119], P.V. Tsiareshka[91],
D. Tsionou[137], G. Tsipolitis[10], N. Tsirintanis[9], S. Tsiskaridze[12], V. Tsiskaridze[48],
E.G. Tskhadadze[51a], I.I. Tsukerman[96], V. Tsulaia[15], J.-W. Tsung[21], S. Tsuno[65],
D. Tsybychev[149], A. Tua[140], A. Tudorache[26a], V. Tudorache[26a], A.N. Tuna[121],
S.A. Tupputi[20a,20b], S. Turchikhin[98,ag], D. Turecek[127], I. Turk Cakir[4d], R. Turra[90a,90b],
P.M. Tuts[35], A. Tykhonov[74], M. Tylmad[147a,147b], M. Tyndel[130], K. Uchida[21], I. Ueda[156],
R. Ueno[29], M. Ughetto[84], M. Ugland[14], M. Uhlenbrock[21], F. Ukegawa[161], G. Unal[30],
A. Undrus[25], G. Unel[164], F.C. Ungaro[48], Y. Unno[65], D. Urbaniec[35], P. Urquijo[21],
G. Usai[8], A. Usanova[61], L. Vacavant[84], V. Vacek[127], B. Vachon[86], N. Valencic[106],
S. Valentinetti[20a,20b], A. Valero[168], L. Valery[34], S. Valkar[128], E. Valladolid Gallego[168],
S. Vallecorsa[49], J.A. Valls Ferrer[168], R. Van Berg[121], P.C. Van Der Deijl[106],
R. van der Geer[106], H. van der Graaf[106], R. Van Der Leeuw[106], D. van der Ster[30],
N. van Eldik[30], P. van Gemmeren[6], J. Van Nieuwkoop[143], I. van Vulpen[106],
M.C. van Woerden[30], M. Vanadia[100], W. Vandelli[30], A. Vaniachine[6], P. Vankov[42],
F. Vannucci[79], G. Vardanyan[178], R. Vari[133a], E.W. Varnes[7], T. Varol[85], D. Varouchas[15],
A. Vartapetian[8], K.E. Varvell[151], V.I. Vassilakopoulos[56], F. Vazeille[34],
T. Vazquez Schroeder[54], J. Veatch[7], F. Veloso[125a,125c], S. Veneziano[133a], A. Ventura[72a,72b],
D. Ventura[85], M. Venturi[48], N. Venturi[159], A. Venturini[23], V. Vercesi[120a], M. Verducci[139],
W. Verkerke[106], J.C. Vermeulen[106], A. Vest[44], M.C. Vetterli[143,d], O. Viazlo[80],
I. Vichou[166], T. Vickey[146c,aj], O.E. Vickey Boeriu[146c], G.H.A. Viehhauser[119], S. Viel[169],
R. Vigne[30], M. Villa[20a,20b], M. Villaplana Perez[168], E. Vilucchi[47], M.G. Vincter[29],
V.B. Vinogradov[64], J. Virzi[15], O. Vitells[173], M. Viti[42], I. Vivarelli[150], F. Vives Vaque[3],
S. Vlachos[10], D. Vladoiu[99], M. Vlasak[127], A. Vogel[21], P. Vokac[127], G. Volpi[47], M. Volpi[87],

G. Volpini[90a], H. von der Schmitt[100], H. von Radziewski[48], E. von Toerne[21], V. Vorobel[128], M. Vos[168], R. Voss[30], J.H. Vossebeld[73], N. Vranjes[137], M. Vranjes Milosavljevic[106], V. Vrba[126], M. Vreeswijk[106], T. Vu Anh[48], R. Vuillermet[30], I. Vukotic[31], Z. Vykydal[127], W. Wagner[176], P. Wagner[21], S. Wahrmund[44], J. Wakabayashi[102], S. Walch[88], J. Walder[71], R. Walker[99], W. Walkowiak[142], R. Wall[177], P. Waller[73], B. Walsh[177], C. Wang[45], H. Wang[15], H. Wang[40], J. Wang[152], J. Wang[33a], K. Wang[86], R. Wang[104], S.M. Wang[152], T. Wang[21], X. Wang[177], A. Warburton[86], C.P. Ward[28], D.R. Wardrope[77], M. Warsinsky[48], A. Washbrook[46], C. Wasicki[42], I. Watanabe[66], P.M. Watkins[18], A.T. Watson[18], I.J. Watson[151], M.F. Watson[18], G. Watts[139], S. Watts[83], A.T. Waugh[151], B.M. Waugh[77], S. Webb[83], M.S. Weber[17], S.W. Weber[175], J.S. Webster[31], A.R. Weidberg[119], P. Weigell[100], J. Weingarten[54], C. Weiser[48], H. Weits[106], P.S. Wells[30], T. Wenaus[25], D. Wendland[16], Z. Weng[152,u], T. Wengler[30], S. Wenig[30], N. Wermes[21], M. Werner[48], P. Werner[30], M. Wessels[58a], J. Wetter[162], K. Whalen[29], A. White[8], M.J. White[1], R. White[32b], S. White[123a,123b], D. Whiteson[164], D. Whittington[60], D. Wicke[176], F.J. Wickens[130], W. Wiedenmann[174], M. Wielers[80,c], P. Wienemann[21], C. Wiglesworth[36], L.A.M. Wiik-Fuchs[21], P.A. Wijeratne[77], A. Wildauer[100], M.A. Wildt[42,ak], H.G. Wilkens[30], J.Z. Will[99], H.H. Williams[121], S. Williams[28], W. Willis[35,*], S. Willocq[85], J.A. Wilson[18], A. Wilson[88], I. Wingerter-Seez[5], S. Winkelmann[48], F. Winklmeier[115], M. Wittgen[144], T. Wittig[43], J. Wittkowski[99], S.J. Wollstadt[82], M.W. Wolter[39], H. Wolters[125a,125c], W.C. Wong[41], B.K. Wosiek[39], J. Wotschack[30], M.J. Woudstra[83], K.W. Wozniak[39], K. Wraight[53], M. Wright[53], S.L. Wu[174], X. Wu[49], Y. Wu[88], E. Wulf[35], T.R. Wyatt[83], B.M. Wynne[46], S. Xella[36], M. Xiao[137], C. Xu[33b,al], D. Xu[33a], L. Xu[33b,am], B. Yabsley[151], S. Yacoob[146b,an], M. Yamada[65], H. Yamaguchi[156], Y. Yamaguchi[156], A. Yamamoto[65], K. Yamamoto[63], S. Yamamoto[156], T. Yamamura[156], T. Yamanaka[156], K. Yamauchi[102], Y. Yamazaki[66], Z. Yan[22], H. Yang[33e], H. Yang[174], U.K. Yang[83], Y. Yang[110], S. Yanush[92], L. Yao[33a], Y. Yasu[65], E. Yatsenko[42], K.H. Yau Wong[21], J. Ye[40], S. Ye[25], A.L. Yen[57], E. Yildirim[42], M. Yilmaz[4b], R. Yoosoofmiya[124], K. Yorita[172], R. Yoshida[6], K. Yoshihara[156], C. Young[144], C.J.S. Young[30], S. Youssef[22], D.R. Yu[15], J. Yu[8], J. Yu[113], L. Yuan[66], A. Yurkewicz[107], B. Zabinski[39], R. Zaidan[62], A.M. Zaitsev[129,z], A. Zaman[149], S. Zambito[23], L. Zanello[133a,133b], D. Zanzi[100], A. Zaytsev[25], C. Zeitnitz[176], M. Zeman[127], A. Zemla[38a], K. Zengel[23], O. Zenin[129], T. Ženiš[145a], D. Zerwas[116], G. Zevi della Porta[57], D. Zhang[88], H. Zhang[89], J. Zhang[6], L. Zhang[152], X. Zhang[33d], Z. Zhang[116], Z. Zhao[33b], A. Zhemchugov[64], J. Zhong[119], B. Zhou[88], L. Zhou[35], N. Zhou[164], C.G. Zhu[33d], H. Zhu[33a], J. Zhu[88], Y. Zhu[33b], X. Zhuang[33a], A. Zibell[99], D. Zieminska[60], N.I. Zimine[64], C. Zimmermann[82], R. Zimmermann[21], S. Zimmermann[21], S. Zimmermann[48], Z. Zinonos[54], M. Ziolkowski[142], R. Zitoun[5], G. Zobernig[174], A. Zoccoli[20a,20b], M. zur Nedden[16], G. Zurzolo[103a,103b], V. Zutshi[107], L. Zwalinski[30].

[1] School of Chemistry and Physics, University of Adelaide, Adelaide, Australia
[2] Physics Department, SUNY Albany, Albany NY, United States of America
[3] Department of Physics, University of Alberta, Edmonton AB, Canada
[4] (a) Department of Physics, Ankara University, Ankara; (b) Department of Physics, Gazi

University, Ankara; [c] Division of Physics, TOBB University of Economics and Technology, Ankara; [d] Turkish Atomic Energy Authority, Ankara, Turkey

[5] LAPP, CNRS/IN2P3 and Université de Savoie, Annecy-le-Vieux, France

[6] High Energy Physics Division, Argonne National Laboratory, Argonne IL, United States of America

[7] Department of Physics, University of Arizona, Tucson AZ, United States of America

[8] Department of Physics, The University of Texas at Arlington, Arlington TX, United States of America

[9] Physics Department, University of Athens, Athens, Greece

[10] Physics Department, National Technical University of Athens, Zografou, Greece

[11] Institute of Physics, Azerbaijan Academy of Sciences, Baku, Azerbaijan

[12] Institut de Física d'Altes Energies and Departament de Física de la Universitat Autònoma de Barcelona, Barcelona, Spain

[13] [a] Institute of Physics, University of Belgrade, Belgrade; [b] Vinca Institute of Nuclear Sciences, University of Belgrade, Belgrade, Serbia

[14] Department for Physics and Technology, University of Bergen, Bergen, Norway

[15] Physics Division, Lawrence Berkeley National Laboratory and University of California, Berkeley CA, United States of America

[16] Department of Physics, Humboldt University, Berlin, Germany

[17] Albert Einstein Center for Fundamental Physics and Laboratory for High Energy Physics, University of Bern, Bern, Switzerland

[18] School of Physics and Astronomy, University of Birmingham, Birmingham, United Kingdom

[19] [a] Department of Physics, Bogazici University, Istanbul; [b] Department of Physics, Dogus University, Istanbul; [c] Department of Physics Engineering, Gaziantep University, Gaziantep, Turkey

[20] [a] INFN Sezione di Bologna; [b] Dipartimento di Fisica e Astronomia, Università di Bologna, Bologna, Italy

[21] Physikalisches Institut, University of Bonn, Bonn, Germany

[22] Department of Physics, Boston University, Boston MA, United States of America

[23] Department of Physics, Brandeis University, Waltham MA, United States of America

[24] [a] Universidade Federal do Rio De Janeiro COPPE/EE/IF, Rio de Janeiro; [b] Federal University of Juiz de Fora (UFJF), Juiz de Fora; [c] Federal University of Sao Joao del Rei (UFSJ), Sao Joao del Rei; [d] Instituto de Fisica, Universidade de Sao Paulo, Sao Paulo, Brazil

[25] Physics Department, Brookhaven National Laboratory, Upton NY, United States of America

[26] [a] National Institute of Physics and Nuclear Engineering, Bucharest; [b] National Institute for Research and Development of Isotopic and Molecular Technologies, Physics Department, Cluj Napoca; [c] University Politehnica Bucharest, Bucharest; [d] West University in Timisoara, Timisoara, Romania

[27] Departamento de Física, Universidad de Buenos Aires, Buenos Aires, Argentina

[28] Cavendish Laboratory, University of Cambridge, Cambridge, United Kingdom

[29] Department of Physics, Carleton University, Ottawa ON, Canada

[30] CERN, Geneva, Switzerland

[31] Enrico Fermi Institute, University of Chicago, Chicago IL, United States of America

[32] [a] Departamento de Física, Pontificia Universidad Católica de Chile, Santiago; [b] Departamento de Física, Universidad Técnica Federico Santa María, Valparaíso, Chile

[33] [a] Institute of High Energy Physics, Chinese Academy of Sciences, Beijing; [b] Department of Modern Physics, University of Science and Technology of China, Anhui; [c] Department of Physics, Nanjing University, Jiangsu; [d] School of Physics, Shandong University, Shandong; [e] Physics Department, Shanghai Jiao Tong University, Shanghai, China

[34] Laboratoire de Physique Corpusculaire, Clermont Université and Université Blaise Pascal and CNRS/IN2P3, Clermont-Ferrand, France

[35] Nevis Laboratory, Columbia University, Irvington NY, United States of America

[36] Niels Bohr Institute, University of Copenhagen, Kobenhavn, Denmark

[37] [a] INFN Gruppo Collegato di Cosenza; [b] Dipartimento di Fisica, Università della Calabria, Rende, Italy

[38] [a] AGH University of Science and Technology, Faculty of Physics and Applied Computer Science, Krakow; [b] Marian Smoluchowski Institute of Physics, Jagiellonian University, Krakow, Poland

[39] The Henryk Niewodniczanski Institute of Nuclear Physics, Polish Academy of Sciences, Krakow, Poland

[40] Physics Department, Southern Methodist University, Dallas TX, United States of America

[41] Physics Department, University of Texas at Dallas, Richardson TX, United States of America

[42] DESY, Hamburg and Zeuthen, Germany

[43] Institut für Experimentelle Physik IV, Technische Universität Dortmund, Dortmund, Germany

[44] Institut für Kern- und Teilchenphysik, Technische Universität Dresden, Dresden, Germany

[45] Department of Physics, Duke University, Durham NC, United States of America

[46] SUPA - School of Physics and Astronomy, University of Edinburgh, Edinburgh, United Kingdom

[47] INFN Laboratori Nazionali di Frascati, Frascati, Italy

[48] Fakultät für Mathematik und Physik, Albert-Ludwigs-Universität, Freiburg, Germany

[49] Section de Physique, Université de Genève, Geneva, Switzerland

[50] [a] INFN Sezione di Genova; [b] Dipartimento di Fisica, Università di Genova, Genova, Italy

[51] [a] E. Andronikashvili Institute of Physics, Iv. Javakhishvili Tbilisi State University, Tbilisi; [b] High Energy Physics Institute, Tbilisi State University, Tbilisi, Georgia

[52] II Physikalisches Institut, Justus-Liebig-Universität Giessen, Giessen, Germany

[53] SUPA - School of Physics and Astronomy, University of Glasgow, Glasgow, United Kingdom

[54] II Physikalisches Institut, Georg-August-Universität, Göttingen, Germany

[55] Laboratoire de Physique Subatomique et de Cosmologie, Université Joseph Fourier and CNRS/IN2P3 and Institut National Polytechnique de Grenoble, Grenoble, France

[56] Department of Physics, Hampton University, Hampton VA, United States of America

[57] Laboratory for Particle Physics and Cosmology, Harvard University, Cambridge MA, United States of America

[58] [a] Kirchhoff-Institut für Physik, Ruprecht-Karls-Universität Heidelberg, Heidelberg; [b] Physikalisches Institut, Ruprecht-Karls-Universität Heidelberg, Heidelberg; [c] ZITI Institut für technische Informatik, Ruprecht-Karls-Universität Heidelberg, Mannheim, Germany

[59] Faculty of Applied Information Science, Hiroshima Institute of Technology, Hiroshima, Japan

[60] Department of Physics, Indiana University, Bloomington IN, United States of America

[61] Institut für Astro- und Teilchenphysik, Leopold-Franzens-Universität, Innsbruck, Austria

[62] University of Iowa, Iowa City IA, United States of America

[63] Department of Physics and Astronomy, Iowa State University, Ames IA, United States of America

[64] Joint Institute for Nuclear Research, JINR Dubna, Dubna, Russia

[65] KEK, High Energy Accelerator Research Organization, Tsukuba, Japan

[66] Graduate School of Science, Kobe University, Kobe, Japan

[67] Faculty of Science, Kyoto University, Kyoto, Japan

[68] Kyoto University of Education, Kyoto, Japan

[69] Department of Physics, Kyushu University, Fukuoka, Japan

[70] Instituto de Física La Plata, Universidad Nacional de La Plata and CONICET, La Plata, Argentina

[71] Physics Department, Lancaster University, Lancaster, United Kingdom

[72] [a] INFN Sezione di Lecce; [b] Dipartimento di Matematica e Fisica, Università del Salento, Lecce, Italy

[73] Oliver Lodge Laboratory, University of Liverpool, Liverpool, United Kingdom

[74] Department of Physics, Jožef Stefan Institute and University of Ljubljana, Ljubljana, Slovenia

[75] School of Physics and Astronomy, Queen Mary University of London, London, United Kingdom

[76] Department of Physics, Royal Holloway University of London, Surrey, United Kingdom

[77] Department of Physics and Astronomy, University College London, London, United Kingdom

[78] Louisiana Tech University, Ruston LA, United States of America

[79] Laboratoire de Physique Nucléaire et de Hautes Energies, UPMC and Université Paris-Diderot and CNRS/IN2P3, Paris, France

[80] Fysiska institutionen, Lunds universitet, Lund, Sweden

[81] Departamento de Fisica Teorica C-15, Universidad Autonoma de Madrid, Madrid, Spain

[82] Institut für Physik, Universität Mainz, Mainz, Germany

[83] School of Physics and Astronomy, University of Manchester, Manchester, United Kingdom

[84] CPPM, Aix-Marseille Université and CNRS/IN2P3, Marseille, France

[85] Department of Physics, University of Massachusetts, Amherst MA, United States of America

[86] Department of Physics, McGill University, Montreal QC, Canada

[87] School of Physics, University of Melbourne, Victoria, Australia

[88] Department of Physics, The University of Michigan, Ann Arbor MI, United States of America

[89] Department of Physics and Astronomy, Michigan State University, East Lansing MI, United States of America

[90] [a] INFN Sezione di Milano; [b] Dipartimento di Fisica, Università di Milano, Milano, Italy

[91] B.I. Stepanov Institute of Physics, National Academy of Sciences of Belarus, Minsk, Republic of Belarus

[92] National Scientific and Educational Centre for Particle and High Energy Physics, Minsk, Republic of Belarus

[93] Department of Physics, Massachusetts Institute of Technology, Cambridge MA, United States of America

[94] Group of Particle Physics, University of Montreal, Montreal QC, Canada

[95] P.N. Lebedev Institute of Physics, Academy of Sciences, Moscow, Russia

[96] Institute for Theoretical and Experimental Physics (ITEP), Moscow, Russia

[97] Moscow Engineering and Physics Institute (MEPhI), Moscow, Russia

[98] D.V.Skobeltsyn Institute of Nuclear Physics, M.V.Lomonosov Moscow State University, Moscow, Russia

[99] Fakultät für Physik, Ludwig-Maximilians-Universität München, München, Germany

[100] Max-Planck-Institut für Physik (Werner-Heisenberg-Institut), München, Germany

[101] Nagasaki Institute of Applied Science, Nagasaki, Japan

[102] Graduate School of Science and Kobayashi-Maskawa Institute, Nagoya University, Nagoya, Japan

[103] [a] INFN Sezione di Napoli; [b] Dipartimento di Scienze Fisiche, Università di Napoli, Napoli, Italy

[104] Department of Physics and Astronomy, University of New Mexico, Albuquerque NM, United States of America

[105] Institute for Mathematics, Astrophysics and Particle Physics, Radboud University Nijmegen/Nikhef, Nijmegen, Netherlands

[106] Nikhef National Institute for Subatomic Physics and University of Amsterdam, Amsterdam, Netherlands

[107] Department of Physics, Northern Illinois University, DeKalb IL, United States of America

[108] Budker Institute of Nuclear Physics, SB RAS, Novosibirsk, Russia

[109] Department of Physics, New York University, New York NY, United States of America

[110] Ohio State University, Columbus OH, United States of America

[111] Faculty of Science, Okayama University, Okayama, Japan

[112] Homer L. Dodge Department of Physics and Astronomy, University of Oklahoma, Norman OK, United States of America

[113] Department of Physics, Oklahoma State University, Stillwater OK, United States of America

[114] Palacký University, RCPTM, Olomouc, Czech Republic

[115] Center for High Energy Physics, University of Oregon, Eugene OR, United States of America

[116] LAL, Université Paris-Sud and CNRS/IN2P3, Orsay, France

[117] Graduate School of Science, Osaka University, Osaka, Japan

[118] Department of Physics, University of Oslo, Oslo, Norway

[119] Department of Physics, Oxford University, Oxford, United Kingdom

[120] [a] INFN Sezione di Pavia; [b] Dipartimento di Fisica, Università di Pavia, Pavia, Italy

[121] Department of Physics, University of Pennsylvania, Philadelphia PA, United States of America

[122] Petersburg Nuclear Physics Institute, Gatchina, Russia

[123] [a] INFN Sezione di Pisa; [b] Dipartimento di Fisica E. Fermi, Università di Pisa, Pisa, Italy

[124] Department of Physics and Astronomy, University of Pittsburgh, Pittsburgh PA, United States of America

[125] [a] Laboratorio de Instrumentacao e Fisica Experimental de Particulas - LIP, Lisboa; [b] Faculdade de Ciências, Universidade de Lisboa, Lisboa; [c] Department of Physics, University of Coimbra, Coimbra; [d] Centro de Física Nuclear da Universidade de Lisboa, Lisboa; [e] Departamento de Fisica, Universidade do Minho, Braga, Portugal; [f] Departamento de Fisica Teorica y del Cosmos and CAFPE, Universidad de Granada, Granada, Spain; [g] Dep Fisica and CEFITEC of Faculdade de Ciencias e Tecnologia, Universidade Nova de Lisboa, Caparica, Portugal

[126] Institute of Physics, Academy of Sciences of the Czech Republic, Praha, Czech Republic

[127] Czech Technical University in Prague, Praha, Czech Republic

[128] Faculty of Mathematics and Physics, Charles University in Prague, Praha, Czech Republic

[129] State Research Center Institute for High Energy Physics, Protvino, Russia

[130] Particle Physics Department, Rutherford Appleton Laboratory, Didcot, United Kingdom

[131] Physics Department, University of Regina, Regina SK, Canada

[132] Ritsumeikan University, Kusatsu, Shiga, Japan

[133] [a] INFN Sezione di Roma I; [b] Dipartimento di Fisica, Università La Sapienza, Roma, Italy

[134] [a] INFN Sezione di Roma Tor Vergata; [b] Dipartimento di Fisica, Università di Roma Tor Vergata, Roma, Italy

[135] [a] INFN Sezione di Roma Tre; [b] Dipartimento di Matematica e Fisica, Università

Roma Tre, Roma, Italy

[136] [a] Faculté des Sciences Ain Chock, Réseau Universitaire de Physique des Hautes Energies - Université Hassan II, Casablanca; [b] Centre National de l'Energie des Sciences Techniques Nucleaires, Rabat; [c] Faculté des Sciences Semlalia, Université Cadi Ayyad, LPHEA-Marrakech; [d] Faculté des Sciences, Université Mohamed Premier and LPTPM, Oujda; [e] Faculté des sciences, Université Mohammed V-Agdal, Rabat, Morocco

[137] DSM/IRFU (Institut de Recherches sur les Lois Fondamentales de l'Univers), CEA Saclay (Commissariat à l'Energie Atomique et aux Energies Alternatives), Gif-sur-Yvette, France

[138] Santa Cruz Institute for Particle Physics, University of California Santa Cruz, Santa Cruz CA, United States of America

[139] Department of Physics, University of Washington, Seattle WA, United States of America

[140] Department of Physics and Astronomy, University of Sheffield, Sheffield, United Kingdom

[141] Department of Physics, Shinshu University, Nagano, Japan

[142] Fachbereich Physik, Universität Siegen, Siegen, Germany

[143] Department of Physics, Simon Fraser University, Burnaby BC, Canada

[144] SLAC National Accelerator Laboratory, Stanford CA, United States of America

[145] [a] Faculty of Mathematics, Physics & Informatics, Comenius University, Bratislava; [b] Department of Subnuclear Physics, Institute of Experimental Physics of the Slovak Academy of Sciences, Kosice, Slovak Republic

[146] [a] Department of Physics, University of Cape Town, Cape Town; [b] Department of Physics, University of Johannesburg, Johannesburg; [c] School of Physics, University of the Witwatersrand, Johannesburg, South Africa

[147] [a] Department of Physics, Stockholm University; [b] The Oskar Klein Centre, Stockholm, Sweden

[148] Physics Department, Royal Institute of Technology, Stockholm, Sweden

[149] Departments of Physics & Astronomy and Chemistry, Stony Brook University, Stony Brook NY, United States of America

[150] Department of Physics and Astronomy, University of Sussex, Brighton, United Kingdom

[151] School of Physics, University of Sydney, Sydney, Australia

[152] Institute of Physics, Academia Sinica, Taipei, Taiwan

[153] Department of Physics, Technion: Israel Institute of Technology, Haifa, Israel

[154] Raymond and Beverly Sackler School of Physics and Astronomy, Tel Aviv University, Tel Aviv, Israel

[155] Department of Physics, Aristotle University of Thessaloniki, Thessaloniki, Greece

[156] International Center for Elementary Particle Physics and Department of Physics, The University of Tokyo, Tokyo, Japan

[157] Graduate School of Science and Technology, Tokyo Metropolitan University, Tokyo, Japan

[158] Department of Physics, Tokyo Institute of Technology, Tokyo, Japan

[159] Department of Physics, University of Toronto, Toronto ON, Canada

[160] [a] TRIUMF, Vancouver BC; [b] Department of Physics and Astronomy, York University, Toronto ON, Canada

[161] Faculty of Pure and Applied Sciences, University of Tsukuba, Tsukuba, Japan

[162] Department of Physics and Astronomy, Tufts University, Medford MA, United States of America

[163] Centro de Investigaciones, Universidad Antonio Narino, Bogota, Colombia

[164] Department of Physics and Astronomy, University of California Irvine, Irvine CA, United States of America

[165] [a] INFN Gruppo Collegato di Udine; [b] ICTP, Trieste; [c] Dipartimento di Chimica, Fisica e Ambiente, Università di Udine, Udine, Italy

[166] Department of Physics, University of Illinois, Urbana IL, United States of America

[167] Department of Physics and Astronomy, University of Uppsala, Uppsala, Sweden

[168] Instituto de Física Corpuscular (IFIC) and Departamento de Física Atómica, Molecular y Nuclear and Departamento de Ingeniería Electrónica and Instituto de Microelectrónica de Barcelona (IMB-CNM), University of Valencia and CSIC, Valencia, Spain

[169] Department of Physics, University of British Columbia, Vancouver BC, Canada

[170] Department of Physics and Astronomy, University of Victoria, Victoria BC, Canada

[171] Department of Physics, University of Warwick, Coventry, United Kingdom

[172] Waseda University, Tokyo, Japan

[173] Department of Particle Physics, The Weizmann Institute of Science, Rehovot, Israel

[174] Department of Physics, University of Wisconsin, Madison WI, United States of America

[175] Fakultät für Physik und Astronomie, Julius-Maximilians-Universität, Würzburg, Germany

[176] Fachbereich C Physik, Bergische Universität Wuppertal, Wuppertal, Germany

[177] Department of Physics, Yale University, New Haven CT, United States of America

[178] Yerevan Physics Institute, Yerevan, Armenia

[179] Centre de Calcul de l'Institut National de Physique Nucléaire et de Physique des Particules (IN2P3), Villeurbanne, France

[a] Also at Department of Physics, King's College London, London, United Kingdom

[b] Also at Institute of Physics, Azerbaijan Academy of Sciences, Baku, Azerbaijan

[c] Also at Particle Physics Department, Rutherford Appleton Laboratory, Didcot, United Kingdom

[d] Also at TRIUMF, Vancouver BC, Canada

[e] Also at Department of Physics, California State University, Fresno CA, United States of America

[f] Also at Novosibirsk State University, Novosibirsk, Russia

[g] Also at CPPM, Aix-Marseille Université and CNRS/IN2P3, Marseille, France

[h] Also at Università di Napoli Parthenope, Napoli, Italy

[i] Also at Institute of Particle Physics (IPP), Canada

[j] Also at Department of Physics, Middle East Technical University, Ankara, Turkey

[k] Also at Louisiana Tech University, Ruston LA, United States of America

[l] Also at Department of Physics, University of Coimbra, Coimbra, Portugal

[m] Also at Department of Physics and Astronomy, Michigan State University, East Lansing MI, United States of America

[n] Also at Department of Financial and Management Engineering, University of the Aegean, Chios, Greece

[o] Also at Institucio Catalana de Recerca i Estudis Avancats, ICREA, Barcelona, Spain

[p] Also at Department of Physics, University of Cape Town, Cape Town, South Africa

[q] Also at CERN, Geneva, Switzerland

[r] Also at Ochadai Academic Production, Ochanomizu University, Tokyo, Japan

[s] Also at Manhattan College, New York NY, United States of America

[t] Also at Institute of Physics, Academia Sinica, Taipei, Taiwan

[u] Also at School of Physics and Engineering, Sun Yat-sen University, Guangzhou, China

[v] Also at Academia Sinica Grid Computing, Institute of Physics, Academia Sinica, Taipei, Taiwan

[w] Also at Laboratoire de Physique Nucléaire et de Hautes Energies, UPMC and Université Paris-Diderot and CNRS/IN2P3, Paris, France

[x] Also at School of Physical Sciences, National Institute of Science Education and Research, Bhubaneswar, India

[y] Also at Dipartimento di Fisica, Università La Sapienza, Roma, Italy

[z] Also at Moscow Institute of Physics and Technology State University, Dolgoprudny, Russia

[aa] Also at Section de Physique, Université de Genève, Geneva, Switzerland

[ab] Also at Department of Physics, The University of Texas at Austin, Austin TX, United States of America

[ac] Also at Institute for Particle and Nuclear Physics, Wigner Research Centre for Physics, Budapest, Hungary

[ad] Also at DESY, Hamburg and Zeuthen, Germany

[ae] Also at International School for Advanced Studies (SISSA), Trieste, Italy

[af] Also at Department of Physics and Astronomy, University of South Carolina, Columbia SC, United States of America

[ag] Also at Faculty of Physics, M.V.Lomonosov Moscow State University, Moscow, Russia

[ah] Also at Physics Department, Brookhaven National Laboratory, Upton NY, United States of America

[ai] Also at Moscow Engineering and Physics Institute (MEPhI), Moscow, Russia

[aj] Also at Department of Physics, Oxford University, Oxford, United Kingdom

[ak] Also at Institut für Experimentalphysik, Universität Hamburg, Hamburg, Germany

[al] Also at DSM/IRFU (Institut de Recherches sur les Lois Fondamentales de l'Univers), CEA Saclay (Commissariat à l'Energie Atomique et aux Energies Alternatives), Gif-sur-Yvette, France

[am] Also at Department of Physics, The University of Michigan, Ann Arbor MI, United States of America

[an] Also at Discipline of Physics, University of KwaZulu-Natal, Durban, South Africa

* Deceased